Intrinsic Geometry in Screw Algebra and Derivative Jacobian and Their Uses in the Metamorphic Hand

Sun, Jie

Awarding institution:
King's College London

Intrinsic Geometry in Screw Algebra and Derivative Jacobian and Their Uses in the Metamorphic Hand

Jie Sun

A thesis submitted in fulfillment of the requirements

for the degree of Doctor of Philosophy

King's College London, University of London

Abstract

Line geometry is a foundation of screw algebra in line coordinates that were created by Plücker as ray coordinates taking a line as a ray between two points and axis coordinates taking a line as the intersection of two planes. This Thesis reveals the geometrical meaning and intrinsic relationship between these ray coordinates and axis coordinates, leading to an in-depth understanding of conformability and duality of these two sets of screw coordinates, and their related vector space and dual vector space.

Based on the study of screw algebra, the resultant twist of a serial manipulator is presented geometrically by an assembly of unit joint screws with the corresponding velocity amplitudes. This leads to the geometrical interpretation for the resultant twist with its instantaneous screw axis (ISA) that is formulated by a combination of weighted position vectors of joint screws. The screw-based Jacobian is then derived after recognizing the resultant twist of a serial manipulator. The case leads to a revelation for the first time the relationship of a Jacobian matrix acquired by using screw algebra and a derivative Jacobian matrix using differential functions, and to an in-depth investigation of transformation between these two Jacobians.

To extend the application of screw algebra and this derivative Jacobian, kinematics analysis of a novel reconfigurable base-integrated parallel mechanism is proposed and its screw-based Jacobian is derived, leading to its equivalent model, the Metamorphic hand with a reconfigurable palm. The method is then applied to the investigation of the

Metamorphic Hand, while manipulating an object, based on the product sub-manifolds and the exponential method. Evaluation of the functionality of the Metamorphic hand is further analysed, with the Anthropomorphism Index (AI) and palmar shape modulation as the criteria, evaluating performance enhancement of the Metamorphic hand in comparison to other robotic hands with a fixed palm.

The Thesis presents novel discoveries in the intrinsic geometry of screw coordinates and the coherent connection between Jacobian formed by screw algebra and the Jacobian using the derivative method. This intrinsic geometry insight is then used to investigate for the first time the parallel mechanism with a reconfigurable base, paving a way for an in-depth investigation of the Metamorphic hand on its reconfigurability and grasp affordability and for the first time using Anthropomorphic Index to evaluate the Metamorphic hand. The Thesis presents a foundation in the study of the Metamorphic hand.

Acknowledgement

I would like to express my sincere gratitude to Prof. Jian S. Dai for his continuous supports and instructions being a supervisor, and I feel lucky and flattered to be a PhD student supervised by such an elegant and knowledgeable mentor.

Prof. Dai is a world-class scientist with over 30 years lasting impact in the fields of mechanisms and robotics. Prof. Dai always tries to solve problems in robotics with appropriate mathematical methods, in such an elegant way to link robotics with mathematics, and further with art. This is a philosophy I learn from him beyond my PhD study. In every talk and meeting with Prof. Dai, I can feel his strong passion and firm belief to overcome any difficulties on the road of scientific research, which encourage me all the time during my PhD study and, for sure, every minute in the rest of my life.

There were so many unforgettable moments over the last few years with Prof. Dai. I couldn't forget the first time I met him in ROBIO 2011 in Tianjin, China, when I was an undergraduate and I felt horned and nervous to get the acquaintance of such a famous scholar. And then one month later, we met again in Washington D.C., USA, when I attended the student robotics competition in ASME 2011 IDETC. I won the first place award and received his warm congratulations. At that time, I made up my mind to pursue my PhD under his supervision. The next stories were Prof. Dai gave me great supports for applying for a scholarship at King's, guided me carrying out research, offered me so many opportunities to attend summer schools and conferences, assisted

me in writing and revising papers, etc. I would like to thank Prof. Dai again for all these good memories and his great help and guidance not only in research but also every aspect of my life.

I also want to thank Dr. Guowu Wei and Dr. Ketao Zhang. I had great experiences working with Guowu and Ketao in TOMSY project and SQUIRREL project. As former research assistants, they gave unlimited help to new students like me, created a favorable atmosphere in my group, and provided detailed orientation. I enjoyed every moment discussing and working with them. Now Guowu is a lecturer in Salford Universiy and Ketao leaves for Imperial College for another research position. Though I cannot meet them very often, memories always stay.

I must thank Mr. Xinsheng Zhang, who are not only a colleague in my group but also the closest friend to me in London. Xinsheng has a solid theoretical background and deep understanding in screw theory, lie group and lie algebra. We always study and discuss together, and recently when the SQUIRREL project brings him in, we work together as well. I appreciate very much for having such a loyal friend and the friendship he gives me.

I also want to give my thanks to Dr. Chen Qiu, Dr. Evangelos Emmanouil, and Dr. Vahid Aminzadeh, with whom I work in my PhD study. Chen has keen senses of smell on research and always works hard. He generates very good results during his PhD and is a model I need to learn from. Vahid guided me to the lab when I entered the group and answered all my questions regarding equipment and resources in the lab. I took

over Evangelos's work in SQUIRREL project when he graduated, and he gave me instructions patiently.

Apart from my supervisor and colleagues, I would like to thank other researchers in the Centre for Robotics Research, particularly Dr. Peng Qi, Dr. Shan Luo, Mr. Xiaozhan Yang, and faculty members in Department of Informatics, particularly Dr. Hongbin Liu, Dr. Matthew Howard, Dr. Helge Wurdemann who is a lecturer in University College of London, and Prof. Kaspar Althoefer who moves to Queen Mary University of London recently. Also thank my friends Mr. Liqiang Fan, Mr. Dabo Chen, Ms. Yile Wu, and Ms. Zhen He for all the friendships and love.

I must give my sincere thanks to King's College London who accepts me as a PhD candidate and provides me the full scholarship, King's China Award, to cover my tuition fee and living costs for three years of my PhD study.

I also want to acknowledge the support during writing-up from the European Commission 7th Framework Project SQUIRREL "*Clearing Clutter Bit by Bit*" under Grant No. 610532.

At last, special thanks must be given to my parents Mr. Jiuwen Sun and Mrs. Yuhua Liu, who always support and encourage me at my back unconditionally, and the love from family is always the greatest motivation for me to move forward.

Table of Contents

Abstract ..... **iii**
Acknowledgement ..... **v**
Table of Contents ..... **viii**
List of Figures ..... **xiii**
List of Tables ..... **xv**
List of Symbols ..... **xvi**
Chapter 1 Introduction **1**
1.1 State of the Problem 1
1.2 Aims and Objectives 3
1.3 Organization of the Thesis 4
Chapter 2 Background **8**
2.1 Introduction 8
2.2 Line Geometry and Screw Coordinates 8
2.3 Methodologies on First-Order Kinematics Analysis 10
2.4 Reconfigurable Base-Integrated Parallel Robots 12
2.5 Metamorphic Hand with a Reconfigurable Palm 14
2.5.1 The Dexterous Hands 15
2.5.2 Dexterous Hands with a Reconfigurable Palm 17
2.5.3 The Metamorphic Hands 18
2.5.4 Grasping Affordance 19
2.6 Conclusions 20
Chapter 3 Geometry of Screw Coordinates **22**
3.1 Introduction 22
3.2 Position Vectors and Their Triangular Resultant for Ray Coordinates 23
3.3 Projected Triangle for Axis Coordinates with Weighted Plane Normals 27
3.3.1 Duality in Point-Plane Representations of a Line 27
3.3.2 Algebraic Derivation of Axis Coordinates 30
3.3.3 Geometrical Presentation of Axis Coordinates 32
3.4 Conclusions 34
Chapter 4 Geometrically Intrinsic Connections of Screw Coordinates **36**

4.1 Introduction 36
4.2 Form and Geometry Conformability of Two Sets of Coordinates 36
4.3 Correlated Ratio Relationships 39
4.4 Correlation Coefficient and Correlation Operator 42
4.5 Duality and Conformability 45
4.6 Conclusions 47
Chapter 5 Geometrical Meaning of a Twist Based on Screw Algebra 49
5.1 Introduction 49
5.2 Homogenous Coordinates of Screws as 6-Dimensional Vector 50
5.2.1 Homogenous Screw Coordinates 50
5.2.2 Screw System of n^{th} Order 52
5.3 The Helicoidal Velocity Field 52
5.4 Linear Velocity from a Twist 54
5.4.1 Point on a Rigid Body Coincident with the Reference Point 54
5.4.2 Geometrical Meaning of Secondary Part of a Screw 56
5.4.3 Position Vector of the Resultant Twist 59
5.4.4 Coordinated ISA of the End-Effector of a Serial Manipulator 60
5.5 Screw based Jacobian Derivation of Serial Robots 62
5.5.1 Jacobian Matrix of a Planar Serial Manipulator 62
5.5.2 Resultant Twist of a Spatial Serial Manipulator 64
5.6 Conclusions 65
Chapter 6 Geometrical Interpretation of the Transformation between Robot Jacobian and Screw Jacobian 66
6.1 Introduction 66
6.2 Derivative Method based Jacobian of a 3R Planar Serial Manipulator 67
6.2.1 Linear Velocity of a 3R Planar Serial Manipulator 67
6.2.2 Jacobian Generation based on the Derivative Method 68
6.3 Reconciliation of the Jacobian based on Screw Algebra and Derivative Method 69
6.3.1 Transformation Using a Skew-Symmetric Matrix 69
6.3.2 Reconciliation of the Jacobian of a 3R Serial Manipulator 71
6.4 Reconciliation of Jacobian Matrices a Spatial Serial Manipulator 73
6.4.1 Screw Algebra based Jacobian for a Spatial Serial Manipulator 73
6.4.2 Transformation Matrices of a Spatial Serial Manipulator 76
6.4.3 Derivative Method based Jacobian for a Spatial Serial Manipulator 78

6.5 Conclusions 80

Chapter 7 Screw Jacobian Analysis of a Reconfigurable Platform-Based Parallel Mechanism 81

7.1 Introduction 81

7.2 A Spherical-Base Integrated Parallel Mechanism 82

7.2.1 From Manipulation with a Metamorphic Hand to a Parallel Mechanism with a Reconfigurable Base 82

7.2.2 Structure of the Spherical-Base Integrated Parallel Mechanism 83

7.3 Mechanism Decomposition and Geometric Constraints of the Spherical-Base Integrated Parallel Mechanism 84

7.3.1 Constraint Equations of the Reconfigurable Base 85

7.3.2 Position of the 3-RRS Parallel Mechanism in a Particular Configuration of the Reconfigurable Base 90

7.3.3 Forward Kinematics of the Spherical-base Integrated Parallel Mechanism 91

7.4 Inverse Kinematics of the Spherical-Base Integrated Parallel Mechanism .. 95

7.5 Screw Theory based Jacobian Analysis 100

7.5.1 Jacobian Analysis for the Reconfigurable Base 100

7.5.2 Screw-based Jacobian Analysis for the Spherical-Base Integrated Parallel Mechanism 101

7.5.3 Velocity of the Spherical-Base Integrated Parallel Mechanism 104

7.6 Conclusions 107

Chapter 8 Screw Embedded Jacobian and Exponential Mapping of Grasp Affordability with a Reconfigurable Palm 109

8.1 Introduction 109

8.2 Structure of a Mobile Manipulator with a Metamorphic Robotic Hand 110

8.3 Kinematics of the Metamorphic Hand and the Serial Manipulator 112

8.3.1 Geometry and Kinematics of the Articulated Reconfigurable Palm ... 113

8.3.2 Kinematics of the 7-DOF Serial Robot 115

8.3.3 Palm Integrated Kinematics of the Metamorphic Hand and the Manipulator 119

8.4 Metamorphic Hand based Grasp Constraints 121

8.4.1 Form of Grasp Map and Grasp Constraints 122

8.4.2 Grasp Constraints of the Metamorphic Hand 123

8.5 Grasp Affordance Related to the Manipulator Kinematics and Grasp Constraints 127

8.5.1 Grasp Affordance based on Object Models 127

8.5.2 Relation of Grasp Affordance to the Manipulator Kinematics and Grasp Constraints 129
8.6 Conclusions 131
Chapter 9 Geometric Topology with Product Submanifolds on Metamorphic Hand Grasping 132
9.1 Introduction 132
9.2 Product Submanifolds and its Tangent Space 133
9.2.1 Product Submanifolds of *SE*(3) 133
9.2.2 Tangent Spaces of Product Submanifolds 135
9.2.3 10 Lie Subgroups of *SE*(3) 137
9.3 Operation of Lie Group for Metamorphic Hand Grasping 138
9.3.1 Topology Diagram for the Metamorphic Hand 138
9.3.2 Lie Group Operations on Hand-Object Model 139
9.4 Conclusions 143
Chapter 10 Geometry Variation Entailed Metamorphic Hand Benchmarking and Anthropomorphism Index 144
10.1 Introduction 144
10.2 Kinematic Transverse Arch of the Metamorphic Palm 145
10.2.1 The Kinematic Transverse Arch of Human Hands 145
10.2.2 Transverse Arch Inspired Palm Geometry Variation Analysis 147
10.2.3 The Palm Geometry Variation related Actuation Constraints 148
10.2.4 Geometric Constraints of the Metamorphic Palm 150
10.3 Arch Measurement of the Metamorphic Palm 152
10.4 Palm Geometry Variation based Workspace of the Metamorphic Hand 155
10.5 Hand Model Generation and Simplification for Benchmarking 160
10.5.1 Hand Model Generation 160
10.5.2 Hand Model Simplification 161
10.6 Measurement Indexes and Criteria 162
10.6.1 Projection based Measurement Indexes 162
10.6.2 Evaluation of the Metamorphic Hand based on AI 163
10.6.3 The Improvement of AI with the Reconfigurable Palm 163
10.7 Comparison of the Metamorphic Hand with Selected Robotic hands 165
10.7.1 The Effect of Number of DODs 165
10.7.2 The Effect of Distribution of DOFs 166
10.7.3 The Influence of Sampling Density on AI 167
10.7.4 AI Analysis According to Different Palm Configurations 168

10.8 Conclusions 169
Chapter 11 Conclusions 171
11.1 General Conclusions 171
11.2 Contributions and Main Achievements of the Thesis 174
11.3 Future Works 177
List of Publications 179
References 181
Appendix A 195
Appendix B 196
Appendix C 198

List of Figures

Figure 3.1 A line with two position vectors 23
Figure 3.2 Geometrical interpretation of Plücker coordinates in ray order of a line... 25
Figure 3.3 A line as the intersection of two planes 28
Figure 3.4 Geometrical interpretation of the axis coordinates 33
Figure 4.1 Integrated geometrical presentations of ray and axis coordinates 37
Figure 4.2 Conformability graph 45
Figure 5.1 Instantaneous screw axis and the helicoidal velocity field 53
Figure 5.2 A Twist modeled by a revolute joint of a rigid body 55
Figure 5.3 Geometry representation of a resultant twist in a serial manipulator..... 56
Figure 5.4 A 3R planar serial manipulator 63
Figure 6.1 Screw coordinates with respect to the global reference frame of A RRPRR spatial serial manipulator 74
Figure 6.2 A spatial 5-DOF RRPRR serial manipulator 76
Figure 7.1 Object manipulated by a three-fingered metamorphic hand 83
Figure 7.2 Structure of the spherical-base integrated parallel mechanism 84
Figure 7.3 The reconfigurable base of the spherical-base integrated parallel mechanism 86
Figure 7.4 Kinematic analysis for limb 2 of the spherical-base integrated parallel mechanism 94
Figure 7.5 Motion screw of the spherical-base integrated parallel mechanism 102
Figure 7.6 Motion screw of closed-loop mechanism decomposed from the parallel mechanism 105
Figure 8.1 Structure of a mobile manipulator with a metamorphic robotic hand 111
Figure 8.2 The articulated reconfigurable palm and its geometry..... 113
Figure 8.3 Geometry of the mobile manipulator in the reference position. 116
Figure 8.4 Grasp a disk with the three-fingered Metamorphic hand..... 119
Figure 8.5 Relations of grasp affordance, manipulator kinematics and grasp constraint 130

Figure 9.1 The relationship among the complex, submanifold, and subgroup of SE(3) 134
Figure 9.2 A commutative diagram for the product submanifold, the submanifolds, and the related tangent spaces 136
Figure 9.3 Lie group built-in topology diagram for the hand-object system with a reconfigurable base 139
Figure 9.4 A simplified topology diagram by merging the subgroups of finger 2 and 3 141
Figure 9.5 A simplified topology diagram by merging all the subgroups of finger 1, 2 and 3 142
Figure 9.6 The final deducted topology diagram of the Metamorphic hand with grasped object 143
Figure 10.1 Arches of human hand, (a) Human palm arches, (b) The kinematic transverse arches 146
Figure 10.2 The kinematic transverse arch of the metamorphic palm 147
Figure 10.3 The Metamorphic hand with a reconfigurable palm 149
Figure 10.4 The range of θ_1 with respect to the changes of θ_5 152
Figure 10.5 The contributions of the thenar arch, hypothenar arch in kinematic transverse arches at the change of θ_1 when $\theta_5 = 120°$ 153
Figure 10.6 The kinematic transverse arch of the reconfigurable palm 154
Figure 10.7 The workspace of the thumb and other fingers processed with Delaunay triangulation method. (a) The workspace of index finger, middle finger, ring finger and little finger. (b) The workspace of the thumb 156
Figure 10.8 The workspace of the whole hand with two palm actuation angles as $\theta_5=\pi/2$, $\theta_1=-2\pi/3$ 157
Figure 10.9 The functional workspace of each finger 158
Figure 10.10 The functional workspace with different θ_1 when $\theta_0 = \pi/2$, $2\pi/3$ and $5\pi/6$ 159
Figure 10.11 The model of the Metamorphic hand 161
Figure 10.12 Projection of the Metamorphic hand to the latent space. (a) The projection of the Metamorphic hand with the reconfigurable palm; (b) The projection of the Metamorphic hand with the freezed reconfigurable palm ($\theta_3 = \theta_4 = 0$) 164
Figure 10.13 The value of AI with fixed sample size and various sampling density 168
Figure 10.14 The value of AI with different palm configurations 169

List of Tables

Table 4.1 Duality and conformability 46
Table 8.1 Joint twists of the 7-DOF serial robot 117
Table 9.1 Proper lie subgroups of $SE(3)$ with motion types..... 137
Table 10.1 The AI of four robotic hands evaluated by the toolbox 166

List of Symbols

$\boldsymbol{L}$	A line vector
$\boldsymbol{l}^{\mathrm{T}}$	The primary part of a line vector
$\boldsymbol{l}_0{}^{\mathrm{T}}$	The secondary part of a line vector
Δ	The correlation operator
$se(3)$	Lie algebra of the special Euclidean group of 3-dimensional Euclidean space
$\boldsymbol{S}_i$	Screw associated with the ith joint
$\boldsymbol{S}_{ij}$	Screw associated with the jth joint in the ith limb
$\boldsymbol{s}_i$	The direction vector of a screw associated with the ith joint
$\boldsymbol{s}_0$	The secondary part of a screw
h	The pitch of a screw
ε	Dual unit of dual vector
$\mathbb{R}^3$	3-dimensional affine space
$\mathbb{P}^3$	3-dimensional projective space
$\mathbf{V}^6$	6-dimensional vector space
$\mathbb{S}_n$	Screw system of order n
$\boldsymbol{T}_i$	The twist of associated the ith joint
$\mathbf{J}_{\mathrm{s}}$	Screw-based Jacobian matrix
$\mathbf{J}_{\mathrm{D}}$	Derivative method-based Jacobian matrix
$\mathbf{J}_{\mathrm{h}}$	Hand Jacobian matrix
${}^{i}\mathbf{T}_j$	Transformation matrix from the ith coordinate frame to the jth coordinate frame

$\mathbf{R}(x_i,\varphi_i)$	A 3×3 rotation matrix that represents a rotation about x_i-axis by φ_i
$\boldsymbol{P}_{\mathrm{A}}$	Position vector of point A in the global coordinate frame
${}^{\mathrm{F}}\boldsymbol{P}_{\mathrm{C}i}$	The position vector of point C_i (i = 1, 2 and 3) with respect to global coordinate frame F
$\dot{\boldsymbol{\theta}}_a$	The velocity vector of active joints
$\dot{\theta}_i$	The change rate of the ith joint
$SE(3)$	The special Euclidean group of 3-dimensional Euclidean space
$SO(3)$	The special orthogonal group of 3-dimensional Euclidean space
$[\boldsymbol{d}\times]$	Skew-symmetric matrix of vector $\boldsymbol{d}$
Ad_g	Adjoint transformation associated with g
$e^{[\boldsymbol{S}_1]\theta_1}$	Exponential map from Lie algebra to Lie group
$\mathcal{T}(\boldsymbol{u})$	Lie subgroups of $SE(3)$
$\mathcal{M}$	Product submanifold of $SE(3)$
$\mathbf{B}_{ci}$	The wrench basis corresponding to different contact types
$\boldsymbol{V}_{po}^{b}$	The body velocity of the object expressed in a global reference frame
$\mathbf{G}_i$	Grasp matrix of the ith finger
x_{T_g}	A grasp executed by the Metamorphic hand
α_i	The angle of the ith link in the palm of the Metamorphic hand
MW	Workspace of fingers in the Metamorphic hand
FW	Functional workspace of the Metamorphic hand

Chapter 1 Introduction

1.1 State of the Problem

Line geometry is a foundation for screw theory. Homogenous coordinates can be used to present a line in space, known as a line vector. Line coordinates are then extended by Plücker to ray coordinates and axis coordinates, namely a line as a ray between two points and a line as the intersection of two planes. A screw is formed by adding the primary part with a scalar known as a pitch to the secondary part of a line vector. As a geometrical entity, a screw in the form of six coordinates can carry a twist by associating a velocity amplitude or carry a force by a force intensity, in such ways to obtain the physical meanings in mechanism and robot analysis.

Though Plücker coordinates in ray order are well received, their counterpart in axis order is relatively not well known and, in particular, the geometrical meaning of ray coordinates and axis coordinates are not well revealed. Moreover, the duality and intrinsic relationship between ray coordinates and axis coordinates still remain unclear. The explicit relation between the relevant vector space and dual vector space needs to be investigated for acquiring the geometrical interpretation between the two set of Plücker.

Based on line geometry, screw theory is developed and plays a key role in mechanics and mechanisms. As a twist can be regarded as a unit screw associating a velocity

amplitude, the kinematics analysis of mechanisms is closely linked to the application of screw algebra. In particular, the twist of the end-effector of a serial manipulator is the assembly of unit joint screws with the corresponding joint changing rates. In a different way, the Denavit-Hartenberg method is also well-known to formulate the position of the end-effector, as well as the first-order kinematics by taking its time derivative. The relation of velocities and Jacobian matrices acquired by the derivative method and screw algebra is not well presented, and the transformation between the two Jacobian needs to be further investigated.

There have been substantial interests in kinematics analysis of multifingered hands. The metamorphic hand is developed to achieve higher performance and graspability by involving a reconfigurable palm. Instead of considering the hand kinematics in isolation, an equivalent transformation to map the hand-object system to a parallel mechanism integrated with a reconfigurable base is conducted through treating the non-sliding contact between a fingertip and the grasped object as a spherical pair. In such a way, the Metamorphic hand with a grasped object is regarded as a typical parallel mechanism with a reconfigurable base. Then the methodologies to study parallel mechanism can be migrated to understanding the motion of the grasped object. Screw theory is adopted to formulating the base geometry variation of the reconfigurable parallel mechanism, and the influence of reconfigurable base on the moving platform also needs to be studied by Jacobian analysis.

The grasping matrix of the metamorphic hand needs to be explored to establish a mathematics model for the further study of grasping affordance. Product-of-exponential mapping and topology based product submanifolds are also appropriate tools to build

the mathematical model and highlight the enhancement of the integrated flexible palm in terms of grasping and manipulation.

Furthermore, evaluation of the performance of the Metamorphic hand has to be considered to demonstrate the improvement of dexterity by involving this reconfigurable palm. Comparison and reconciliation between the human palm and the reconfigurable palm are crucial to reveal the intrinsic advancement of this flexible palm. To assess the palmar shape modulation through transverse metacarpal arch inspired by human hands, the favorable palm configuration can be found for the best fit of finger grasping positions. The Anthropomorphism Index is also proposed to compare different hand constructions in such a way to verify the advantages of a robotic hand with a flexible palm.

1.2 Aims and Objectives

The thesis emphasizes the intrinsic geometry connection of screw coordinates and the formulation of Jacobians with different methods, followed by their relation and transformation. The thesis also applies these mathematical tools to analyzing the grasp matrix of the Metamorphic hand and evaluating its performance.

The objectives of this thesis are listed as follows,

a) Reveal the interrelation of the line coordinates and give the intrinsic geometrical interpretation of the correlation operator widely used in screw algebra.
b) Study the duality and conformability of the screw coordinates, as well as the insight of its representation in vector space and dual vector space.

c) Explore the geometrical meaning of a twist and the transformation between the screw-based Jacobian and derivative method-based Jacobian.
d) Investigate kinematics of the reconfigurable platform based-parallel mechanism and the Jacobian analysis by means of screw algebra.
e) Develop the grasping matrix and grasping affordance of the Metamorphic hand with the product-of-exponential method.
f) Present the topological evolution of the Metamorphic hand with grasped object model with product submanifolds operations.
g) Evaluate the performance of the Metamorphic hand by a nonlinear data reduction model and a palmar shape modulation migrated from human palm variation.

1.3 Organization of the Thesis

This thesis is organized into 11 chapters, and brief introduction and construction of each chapter is presented as follows,

Chapter 1 is the introduction of this thesis where the state of problems, aims and objectives, and its organization are described.

Chapter 2 covers the background of this thesis, state-of-the-art and the problems going to be investigated in the following chapters. The background includes a brief introduction to line geometry and screw coordinates, the mathematical methods to study the first-order kinematics of a robot, the typical parallel robots, and reconfigurable base-integrated parallel robots, and the development of dexterous robotic hands and the Metamorphic hand with a reconfigurable palm.

Chapter 3 introduces screw coordinates and their geometrical interpretation. In order to reveal the geometrical insight in Euclidean 3-space, homogeneous coordinates of a point and a plane are converting to a set of homogeneous coordinates with the last component as 1, using ratios of homogeneous coordinates. A line joined by two points, which produces ray coordinates, and a line intersected by two planes, which produces axis coordinates, are formulated, and the geometrical meaning of each single component in these two sets of coordinates is given.

Chapter 4 reveals the intrinsic connection between ray coordinates and axis coordinates. The interrelation of the two sets of coordinates and their conformability are investigated through their geometrical representation. Further, the correlated ratio relationships and a corresponding correlation coefficient of the coordinates are studied, followed by a correlation operator to link the vector space with dual vector space in where the two sets of coordinates are formed. The intrinsic relation of the ray coordinates and axis coordinates are summarized in a duality and conformability table.

Chapter 5 presents the geometrical meaning of a twist and the geometrical representation of a resultant twist assembled by unit joint screws with their corresponding velocity amplitudes. The instantaneous screw axis of the resultant twist is coordinated, and its position vector is obtained. The Jacobian matrix of a planar serial manipulator is derived followed by the generation of a resultant twist of a spatial serial manipulator.

Chapter 6 derives the transformation between the screw-based Jacobian matrix and the derivative method-based Jacobian matrix of a serial manipulator. Through the investigation of the linear velocity of a serial manipulator, reconciliation of the Jacobians based on screw algebra and derivative method is formulated with their geometrical interpretation. At last, a spatial serial manipulator is exampled to verify the proposed transformation method.

Chapter 7 proposes a parallel mechanism with a reconfigurable base for the first time. The base of this parallel mechanism is formed by a spherical five-bar linkage mechanism, which provides augmented motion for each limb. Structure design of the proposed spherical-base integrated parallel mechanism is introduced, and geometry and kinematics of the mechanism are investigated leading to closed-form solutions of kinematics. Screw theory-based Jacobian is then presented in the form of partitioned matrix followed by the velocity analysis.

Chapter 8 presents the construction of the mathematical model of the Metamorphic hand grasping an object. The kinematics of a 7-DOF serial manipulator is also proposed with its last link attached the Metamorphic hand. The grasping matrix of the hand is established with the screw embedded Jacobian and product-of-exponential method. The preliminary study of grasping affordance of the hand is also presented with its relation to the manipulator kinematics.

Chapter 9 presents the grasping model of the Metamorphic hand manipulating an object. Apart from introducing the 10 corresponding Lie subgroups, product submanifolds of Lie group $SE(3)$ and Lie subgroup built-in topology diagram are defined with operation

rules. Based on the topological model of the hand-object system, the operation of Lie group is implemented to simplify the topology diagram of the Metamorphic hand by merging the product submanifolds of two adjacent fingers in a recursive way.

Chapter 10 uses a nonlinear dimension reduction model, Gaussian Process Latent Variable Model (GPLVM), to project the high dimension fingertip data to a 2D latent plane in such a way to evaluate robotic hands and carry out the comparison among different hands. A different way relates the Metamorphic palm to the human palm with transverse metacarpal arch, which acts as a new approach to evaluate a robotic hand with palmar shape modulations. Then the functional workspace, as an indicator evaluating the precise manipulation of the metamorphic hand, is extended to show the impact of palm arch on graspability.

Chapter 2 Background

2.1 Introduction

This chapter states the background of the thesis, including state-of-the-art and the problems going to be investigated in the following chapters. A brief introduction to line geometry and screw coordinates is presented in Section 2.2 with its connection to screw theory and screw coordinates. Following this, the application of screw algebra, as well as the derivative method, to study the first-order kinematics of a robot is described in Section 2.3, as the mathematical foundation. Then in Section 2.4, the development of typical parallel robots and the latest reconfigurable base-integrated parallel robots are in introduced in Section 2.4. Finally, state-of-the-art in the field of dexterous hands, and the development of Metamorphic hand are presented in Section 2.5.

2.2 Line Geometry and Screw Coordinates

It has long been known that a line can be presented in a parametric equation and it was Cayley [1] and Plücker [2] who for the first time created six coordinates to present a straight line in space. By taking a line as an intersection of two planes and utilizing the homogeneous coordinates, algebraic derivations give six coordinates to define a line vector. This gives Plücker coordinates in axis order [3,4]. In this order, the first three components are the moment of a line vector with respect to the origin and the last three components are the direction of the line vector. In the six coordinates, only four are independent.

Discovery of line coordinates presented a foundation [5] for screw theory. Plücker extended it to ray coordinates, namely a line as a ray joined by two points that were named by Plücker [3] as ray coordinates or Plücker coordinates in ray order[6,7]. In this presentation, the first three components as the primary part present the direction of a line and the last three components as the secondary part implicitly give the location of the line with the moment of the line with respect to the origin. The ray coordinates were further explicitly presented by Klein[8] based on Grassmann determinant principle[9,10] with six determinants of second order from a matrix constituted by two sets of point coordinates.

By adding the primary part with a scalar to the secondary part of a line vector, a screw can be obtained. The scalar being added is coined the pitch of a screw. As a geometrical entity, a screw in the form of six coordinates with five independent quantities plays a key role in mechanics and mechanisms. Attached with a velocity amplitude as presented by Ball [5], a screw carries a twist. A twist written in ray coordinates has the first three components as the primary part presenting an angular velocity and the last three components as the secondary part presenting a linear velocity. Associated with a force intensity as defined by Ball, a screw carries a wrench. In such a way, a wrench could be written in the same coordinate system as that of a twist.

In general, both twists and wrenches can be considered acting about and on a screw with the sixth independent quantity as an amplitude attached to a screw [11] in the same coordinate system that a wrench could be written [12] in ray coordinates. Therefore, a correlation operator [13] needs to be used to interchange both primary and secondary

parts of a wrench to form a reciprocal product to complete the work done by a wrench on a twist. This is essential in working out the reciprocity or work done in robotics[14-16] and in mechanism analysis and synthesis [18-20].

Expressing a wrench in axis coordinates and a twist in ray coordinates leads to two spaces. In a modern approach, a twist is defined as an element of the Lie algebra of the group of rigid-body displacement and a wrench as an element of the dual Lie algebra that has the primary part presenting a moment and the secondary part presenting a force, presented in a vector space of all those dual elements, as a dual vector space. In other literature[21,22], a wrench in axis coordinates is referred to a co-screw in an isomorphic vector space, as a dual vector space.

Though Plücker coordinates in ray order is well received, its counterpart in axis order is relatively not well known and in particular, the geometrical meaning of ray coordinates particularly axis coordinates has not yet been revealed. Further, though duality of a line on its self-dual [14] was stated, the duality and intrinsic relationship between ray and axis coordinates have not yet been revealed. Hence, the geometrical meaning of the relationship particularly line geometry still needs to be revealed and to give the insight to screw property[23-26] and mechanism development[27-29].

2.3 Methodologies on First-Order Kinematics Analysis

Kinematics analysis is the fundamental topic in robotics and studying the kinematics of a manipulator is a necessary procedure to understand its functionality and performance. Forward kinematics establishes the mathematical relation to map the joint displacements to the position and orientation of the end-effector of a manipulator,

whereas the inverse kinematics relates the end-effector configuration to joint movements. Differentiating the forward kinematics equation gives the Jacobian matrix that formulates the velocity map between joint rates and the velocity state of the end-effector. The Jacobian portrays the velocity map from joint space to task space of a manipulator which can be used to identify the singularly, generate the desired trajectory with an appropriate speed, etc. There are several ways to construct the Jacobian of a serial manipulator in the literature[65], the most popular ones are the derivative methods[103] and the screw theory based method[65].

The conventional way to generate Jacobian of a manipulator with the derivative method is to formulate the forward kinematics analysis by the transformation matrices or the geometrical relation first, and then take the time derivative of position and orientation of the end-effector. The transformation matrices that depict the rotation and translation of coordinate frames attached in contiguous links can be developed with D-H parameters[102]. By multiplying transformation matrices in an order, the gesture of the tool frame fixed on the end-defector is revealed with respect to the global coordinate frame though joint displacements and the geometry of the manipulator. As the position and orientation of the end-effector are functions of joint displacements, taking its time derivative will result in the translational velocity and angular velocity expressed by the joint rates and the geometry of the manipulator, in which way the conventional Jacobian is developed.

Screw theory is another way to carry out forward velocity analysis of a serial manipulator. By investigating the line geometry, Plücker [2] and Cayley [1] used the homogenous coordinates to represent a straight line in space, of which the first three

coordinates indicate the direction of the line and the last three tell the moment of the line about the origin. Associating a line vector with a pitch generates a screw which is a geometry entity that can be utilized in mechanism analysis. A twist is defined through attaching a velocity magnitude to a screw, while a wrench is defined through associating a force intensity [5]. A twist with its first three components presenting the angular velocity and last three components presenting the linear velocity is an ideal representation to describe the differential kinematics of a manipulator. The Jacobian is established by relating the joints rate to the twist of the end-effector in the wake of identifying all the joint screws in a serial manipulator.

Though the development of Jacobian of a serial manipulator is well received with both derivative method and screw theory, the relation between the two techniques is not well presented, particularly their transformation and corresponding geometrical interpretation. The derivative method-based Jacobian derives from the time derivation of the position and orientation of the tool frame attached on the end-effector, while the screw theory-based Jacobian depends on the instantaneous geometry of the manipulator. In general, the two Jacobians are not identical, and the interrelation still needs to be revealed to give the insight of the methods geometrically and physically.

2.4 Reconfigurable Base-Integrated Parallel Robots

A typical parallel mechanism consists of a moving platform that is connected to a fixed base by several (at least two) limbs or legs. In general, the moving platform of parallel mechanisms has both rotational and translational motion[32,33]. However, in order to reduce the complexity and cater some specific applications, the low-mobility parallel mechanisms[34,37] have drawn numerous interests from researchers in mechanism and

machine design. In particular, Chablat and Wenger [38] proposed a 3-DOF parallel mechanism to realize three axes rapid machining applications. Zhao et al. [39,40] investigated three and four DOFs parallel mechanisms relying on equivalent screw groups. Kong and Gosselin [41] presented several parallel mechanisms relying on screw theory based type synthesis method. Similarly, Xu and Li [42] applied screw theory to analyze the mobility and stiffness of an over-constrained 3-PRC parallel mechanism and converted it into a non-over-constrained 3-CTC parallel mechanism of the same mobility and kinematic properties. Huda and Yukio [43] invented a 3-URU parallel mechanism with three-dimensional rotation. Such parallel mechanisms were widely adopted to achieve wrist-like motion, such as Argos, proposed by Vischer and Reymond [44] and the 3-RUU mechanism, proposed by Gregorio [45]. Gan et al. [46] studied constraint screw systems of a 3-PUP parallel mechanism and revealed the influence between them and limb arrangements. Zhang et al. [47] discussed the constraint singularity and analyzed the bifurcated motion of a 3-PUP parallel mechanism and the conversion between two bifurcated motion branches. In addition, some redundant parallel mechanisms[48,49] were put forward to avoid singularities and obtain better kinematic properties.

The parallel mechanism mentioned above are all composed of a rigid base and non-configurable moving platform. In other words, their base or moving platform is a component with zero DOF rather than a mechanism with additional moving capability. Recently, the parallel mechanisms with reconfigurable features have been capturing attentions from the researchers in the fields of mechanisms and robotics. Based on the concept reconfigurability and principle of metamorphosis [50], Gan et al. [51] proposed a reconfigurable Hooke (rT) joint and presented a new metamorphic parallel

mechanism that was capable of changing mobility and topological configurations. Zhang et al. [52] identified an axis-variable (vA) joint based on origami fold [53] leading to the development of a metamorphic parallel mechanism that had the capability of changing its mobility from 3 DOFs to 6 DOFs.

In addition, there is another kind of metamorphic parallel mechanisms that can reconfigure themselves through changing the configurations of their moving platform. Yi et al. [54] presented a flexible folded parallel gripper to meet the requests of both grasping and positioning objects with irregular shape and size. Mohamed and Gosselin [55] presented a kind of parallel mechanisms with reconfigurable platforms and analyzed redundancy of proposed parallel mechanisms. Lambert[56] presented and analyzed mobility and kinematics of a PentaG robot, which is a parallel mechanism with a flexible planar platform providing five DOFs in total.

In contrast to the above flexible-platform parallel mechanisms, the concept of parallel mechanisms with a foldable/reconfigurable base can be brought up but no literature shows the relevant investigation. Inspired by the grasp and manipulation of an object with a metamorphic hand containing a reconfigurable palm[57-61].

2.5 Metamorphic Hand with a Reconfigurable Palm

A mobile manipulator consists of a manipulator and a mobile platform such that it has a larger workspace and better flexibility comparing to a fixed-base manipulator benefiting from the mobility provided by the mobile platform. Due to their flexibility, mobile manipulators have a wide range of applications in the different fields such as

rescue[70], elderly assistance[71] and space[72]. In the past two decades, a number of mobile manipulators had been developed and tested such as the NEOBOTIX[104], the KUKA youBot[105] and the Segway HERB[106]. Most of them were designed and developed for some special application purposes and were expensive. The following three sections are to briefly review the historical development of robotic hands and introduce a specific dexterous hand, the Metamorphic hand with a reconfigurable palm.

2.5.1 The Dexterous Hands

Since the introduction of the first industrial robot in the early 1960s, there was a growing interest in the end-effector or grippers research. In industrial applications, most of the grippers are attached to a robot arm to perform some pre-programmed tasks with the one or two-degree-of-freedom as the end-effector only to execute some pick-and-place operations. It's unlikely to use this type of grippers to perform some sophisticated works or in-hand manipulation, namely, hardly these grippers are capable of working in the unstructured environments due to its oversimplified kinematics.

While grippers are mainly designed for simple tasks and dedicated to one task rather than having flexibility for multi-tasks, robot hands are more attractive due to their flexibility and a wide range of applications. Anthropomorphic robot hands as effective extensions of human limbs have become a popular research direction in robotics due to their ability to complete sophisticated actions[73,74]. As an integrative application of mechatronic, electronic and automotive technology, it is dedicated to achieving the active functions of human hands, and thus has a higher integration, stronger perception and more smooth and intricate operability.

Several robotic hands, more or less anthropomorphic, had been developed in the past three decades. These hands contained one to six independent actuators and eight to sixteen joints distributed in various ways in fingers.

The Okada Hand [75] invented in Japan in 1974 was the first genuine multi-fingered robot hand. It consisted of three fingers of which the thumb was with 3 DOFs and the other fingers were with 4. After this, the research on robotic hand attracted much attention that various distinctive dexterous hands were invented. The position, torque, and force transducers were introduced in robotic hands and greatly improved the tactile sensitivity of the fingertips, such as UB-II Hand [76], the Stanford/JPL Hand [77] and the Barrett Hand [78].

To achieve reliability with the less dexterous design, the UBH3 Hand [79] with three fingers attached to a fixed base, applied the under-actuation design driven by tendons. On the contrast, some robotic hands were designed the same size and appearance as human hands, which were more anthropomorphic and dexterous, such as the Utah/MIT Hand[80], the NASA Hand[81], Tokyo Hand[82] and etc. Since the early 21st century, more dexterous hands were developed, such as the Shadow Hand [83], Gifu II [84], the HIT/DLR Hand[85], the BH-4 Hand[86] and the NASA Robonaut Hand[87]. Their integration and controllability had been further improved. These robotic hands are of great dexterity and can generate delicate motion similar to human hands, however, at the expense of high-cost barrier, complicated control process, and costly maintaining spending.

2.5.2 Dexterous Hands with a Reconfigurable Palm

In the development of dexterous hands, most researchers emphasized improving their manipulability and dexterity by increasing finger numbers and finger joints or by changing the structure of the thumb. Apart from flection in a plane, human fingers are able to move in space as a result of the adduction/abduction motion achieved by the Metacarpophalangeal (MCP) joint, which is analogous to the revolute-hook joint in its kinematics equivalent. The finger adduction/abduction motion lays the foundation for dextrous manipulation or in-hand manipulation with the capability of repositioning and reorienting objects, which is the main gap of the robotic hands in contrast to human hands. The adduction/abduction is a critical criterion to distinguish the dexterous robotic hands and the lower-mobility robotic hands. In comparison to human hands with a foldable and flexible palm, the most common robotic anthropomorphic hands are less dexterous.

In particular, with the conventional design of mounting fingers to a rigid palm, a conventional robotic hand cannot adapt to differences in the geometric shapes, which limits the fine-tuning ability [88] and consequently the use of the robotic hand in object grasping and handling. Since a typical robotic hand comprises of a palm and several digits, it is worth noting that, rather than as a rigid holder to contain motors or electronics, the palm with variable geometry can significantly enhance the dexterity of the fingers mounted on it, resulting in augmenting the grasping and manipulation capabilities of the robotic hand. The topology of the hand revamps comparing to conventional robotic hands with an inflexible palm. For instance, Barrett^{TM} [89] presented a hand with three fingers rotating about the rigid palm driven by geared system. Shadow [90] produced an anthropomorphic hand that splits the palm into two

halves with a larger thumb portion. As the palm parameters have a significant impact on the finger workspace, making the palm reconfigurable establishes a new way to design a robotic hand with relative low control complexity and acceptable dexterity.

2.5.3 The Metamorphic Hands

In most unconstructed environments the versatility of the palm is essential for successful grasping and handling. This led to the introduction of the metamorphic robotic hand [91,92], marking a turning point in improving dexterity and manipulability of robotic hands. Metamorphosis is a term from biology meaning the evolution and change of shapes and structure. Under the principle of Metamorphosis, the palm design was inspired by origami with a mechanism equivalent method to relate the panels and crisis to links and joints, respectively. An origami, in generous, has considerable foldability that its geometry varies in a large ratio before and after folding. This characteristic as the main advantage can be migrated to the robotic palm design in a way to alter the workspace of the fingers to adjust the contact points with an object or reposition or reorient an object during a manipulation. The foldable palm that extends the kinematics chain of the fingers can liberate the latter from its motion plane to generate spatial motion analogous to the adduction/abduction motion of the MCP joint of human hands.

The Metamorphic hand broke the barrier by adopting a spherical metamorphic mechanism, leading to a three-fingered robotic hand called Metahand with a reconfigurable palm [93]. The metamorphic palm contributed to mimicking motions of human hands, whose motion depended on both fingers and palm movements. A significant amount of work had been carried out on the analysis of the palm's motion

characteristics, geometric constraint, and palm workspace[60,61]. Dai et al. studied the whole hand and demonstrated how the metamorphic palm affected the posture, dexterity and workspace of the fingers[92,94,95] The metamorphic hand was programmed to accomplish several grasps for objects widely used in our daily life with different geometric features such as balls, bottles, and scissors, etc. [96]. A four-fingered metamorphic hand was developed in light of the optimization of the five-fingered Metamorphic hand applied to deboning operations [98].

2.5.4 Grasping Affordance

Grasping is one of the fundamental issues in robotic manipulation and different concepts and principles have been introduced for grasp investigation. In cognitive robotics, the concept of affordances [98] characterizes the relations between an agent and its environment through the effects of the agent's actions on the environment. Affordances have become a popular formalization for autonomous manipulation processes, bringing valuable insight into how manipulation can be done. Using the concept of affordance, Detry et al. [99] modelled grasp affordances with continuous probability density functions linking object-relative grasp poses to their success grasp probability. Song et al. [100] developed a general framework for estimating grasp affordances from 2-D sources combining texture-based and object level monocular appearance cues for grasp affordance estimation.

Considering the flexible manipulator proposed in this work, by integrating the 3D model of the three-fingered metamorphic robotic hand into the object-based grasp affordance model [101] poses of the reference frame of the robotic hand can be predicted providing a configuration for possible successful grasp. And with the poses

of the reference frame of the robotic hand given, locating the proposed mobile manipulator becomes a problem of solving the inverse kinematics of the arm-wrist set of the manipulator with the mobile platform at the range of the desired task position.

2.6 Conclusions

This chapter introduced the discovery of line geometry and line coordinates, and then led to the introduction to screw algebra and screw coordinates, as well as the construction of the ray coordinates and axis coordinates by Grassmann determinant principle. Following this prior knowledge, twist and wrench were introduced by extending screw theory to the mechanics and mechanisms with given physical meaning.

This chapter also presented the methodologies on the analysis of first-order kinematics of a robot, particularly the screw-based method and derivative method. The development of typical parallel mechanism and low-mobility parallel mechanisms was also presented. Construction of a parallel mechanism was emphasized, with inspiration from the multifingered hand grasping an object, a novel parallel mechanism was proposed.

Moreover, state-of-the-art in the development of multifingered hands was introduced with several well-known dexterous hands, followed by the latest improvement on hand design by introducing a flexible palm to construct a Metamorphic hand. Hence the motion of fingers in the Metamorphic hand depends on the palm geometry variation that awards fingers the additional capability to move in space in such a way to enhance the performance in comparison to the conventional three-fingered, rigid-palm hand.

State-of-the-art in the research of grasping affordance was also presented with the application of the Metamorphic Hand.

Chapter 3 Geometry of Screw Coordinates

3.1 Introduction

Line geometry is a foundation for screw theory. A line in space can be presented with homogeneous coordinates, which are extended by Plücker to ray coordinates and axis coordinates, namely a line as a ray between two points and a line as the intersection of two planes. Ray coordinates, or Plücker coordinates in ray order, are made up of the first three components as the primary part that presents the direction of a line and the last three components as the secondary part implicitly gives the location of the line with the moment of the line with respect to the origin. Axis coordinates, or Plücker coordinates in axis order have the first three components as the moment of the line and the last three components indicating the direction of the line.

In this chapter, in order to make a geometrical presentation to reveal the insight in Euclidean 3-space, that is a three-dimensional real vector space that preserves the Euclidean metric, homogeneous coordinates of a point and a plane are converting to a set of homogeneous coordinates with the last component as 1, using ratios of homogeneous coordinates. Accordingly, we shall use this set of homogeneous coordinates and non-homogeneous coordinates side by side, passing from one to the other when it is in line with the derivation with ratio sign/colon to separate components while in homogeneous coordinates.

3.2 Position Vectors and Their Triangular Resultant for Ray Coordinates

Homogeneous coordinates of points P_1 and P_2 might be presented as $\boldsymbol{r}'_1=(x'_1: y'_1: z'_1: w_1)^T$ and $\boldsymbol{r}'_2=(x'_2: y'_2: z'_2: w_2)^T$ which could be represented with ratios of these four components, namely dividing each by the last component w. Without loss of generality, placing $w_1=w_2=1$, the homogeneous coordinates can be converted to a set of homogeneous coordinates as $\boldsymbol{r}'_1=(x_1: y_1: z_1: 1)^T$ and $\boldsymbol{r}'_2=(x_2: y_2: z_2: 1)^T$ as the homogeneous representation for points P_1 and P_2 in the form of position vectors $\boldsymbol{r}_1=(x_1, y_1, z_1)^T$ and $\boldsymbol{r}_2=(x_2, y_2, z_2)^T$ in their non-homogeneous coordinates. In Euclidean 3-space, we may think of its elements as vectors [30] in a three-dimensional real vector space that preserves the Euclidean metric. These two points that define a straight line in Fig. 3.1 as joint of points can be expressed as position vectors $\boldsymbol{r}_1$ and $\boldsymbol{r}_2$. This gives the direction vector of a line as the primary part of line vector $\boldsymbol{L}=(\boldsymbol{l}^T; \boldsymbol{l}_0^T)$ in the form of

$$\boldsymbol{l} = \boldsymbol{r}_2 - \boldsymbol{r}_1 = \left(l, \quad m, \quad n\right)^T. \tag{3.1}$$

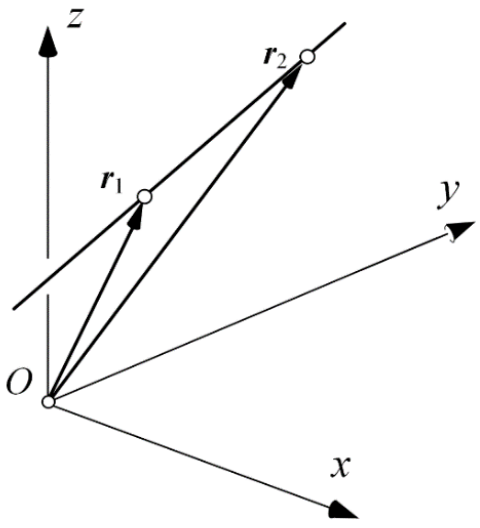

Figure 3.1 A line with two position vectors

Projecting the line onto a plane parallel to x-y plane with its projection angle φ and further projecting its projection to x-axis with projection angle θ, the x-axis component l can be expressed as the function of these two angles and rearranged as a 2×2 minor that is coined as a determinant by Grassmann expansion [31] as follows,

$$l = \|\boldsymbol{l}\| \cos\varphi \, \cos\theta = x_2 - x_1 = \begin{vmatrix} 1 & x_1 \\ 1 & x_2 \end{vmatrix}. \tag{3.2}$$

Similarly, projections of the direction of the line on two remaining coordinate axes can be written as the function of projection angles φ and θ and expressed as 2×2 minors in the form of

$$m = \|\boldsymbol{l}\| \cos\varphi \, \sin\theta = y_2 - y_1 = \begin{vmatrix} 1 & y_1 \\ 1 & y_2 \end{vmatrix}, \tag{3.3}$$

$$n = \|\boldsymbol{l}\| \sin\varphi = z_2 - z_1 = \begin{vmatrix} 1 & z_1 \\ 1 & z_2 \end{vmatrix}. \tag{3.4}$$

This gives three components as the primary part $\boldsymbol{l}$ of line vector $\boldsymbol{L}$ and is represented as three projections l, m and n in Fig. 3.2. The moment of this vector with respect to the origin can be obtained by taking moment of the direction vector $\boldsymbol{l}$ with respect to each of the coordinate axes and gives the secondary part $\boldsymbol{l}_0=(p, q, r)^{\mathrm{T}}$ of line vector $\boldsymbol{L}$.

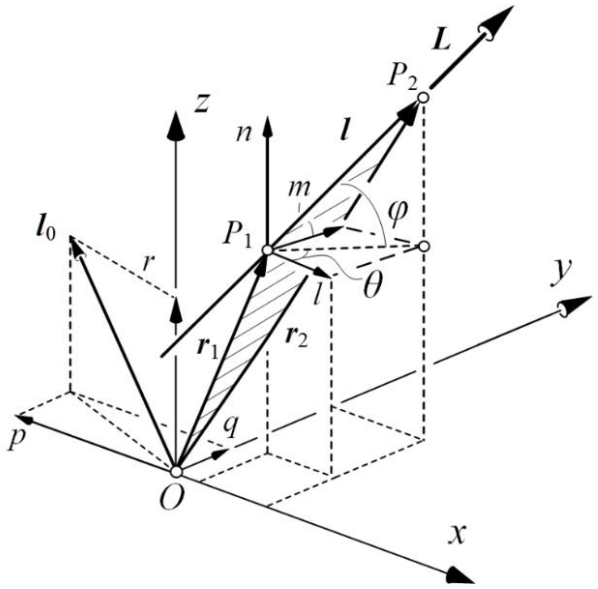

Figure 3.2 Geometrical interpretation of Plücker coordinates in ray order of a line

Moment component p of the direction vector $\boldsymbol{l}$ with respect to coordinate axis x might be obtained as

$$p = \|\boldsymbol{l}\| \sin\varphi y_2 - \|\boldsymbol{l}\| \cos\varphi \sin\theta z_2 .$$

Substituting Eqs. (3.3) and (3.4) in the above gives the following expression that is rearranged as a 2×2 minor in the form of

$$p = (z_2 - z_1) y_2 - (y_2 - y_1) z_2 = y_1 z_2 - y_2 z_1 = \begin{vmatrix} y_1 & z_1 \\ y_2 & z_2 \end{vmatrix} . \tag{3.5}$$

Similarly, moment components q and r can be obtained by taking moment of the direction vector $\boldsymbol{l}$ with respect to coordinate axes y and z, and substituting Eqs. (3.2) to (3.4) for replacing functions of angles φ and θ as follows,

$$\begin{aligned} q &= \|\boldsymbol{l}\|\cos\varphi\cos\theta z_2 - \|\boldsymbol{l}\|\sin\varphi x_2 \\ &= (x_2 - x_1) z_2 - (z_2 - z_1) x_2 = x_2 z_1 - x_1 z_2 = \begin{vmatrix} z_1 & x_1 \\ z_2 & x_2 \end{vmatrix}, \end{aligned} \tag{3.6}$$

$$\begin{aligned} r &= \|\boldsymbol{l}\|\cos\varphi\sin\theta x_2 - \|\boldsymbol{l}\|\cos\varphi\cos\theta y_2 \\ &= (y_2 - y_1) x_2 - (x_2 - x_1) y_2 = x_1 y_2 - x_2 y_1 = \begin{vmatrix} x_1 & y_1 \\ x_2 & y_2 \end{vmatrix}. \end{aligned} \tag{3.7}$$

Following this, it is found that three minors in Eqs. (3.5) to (3.7) present a cross product of position vectors $\boldsymbol{r}_1$ and $\boldsymbol{r}_2$, that gives the moment of the line as the secondary part of the line vector in the following derivation

$$\boldsymbol{l}_0 = \boldsymbol{r} \times \boldsymbol{l} = \boldsymbol{r}_1 \times (\boldsymbol{r}_2 - \boldsymbol{r}_1) = \boldsymbol{r}_1 \times \boldsymbol{r}_2. \tag{3.8}$$

where $\boldsymbol{r}$ is a point on the line defined by Eq (3.1) as in Fig. 3.2. Geometrically, this gives twice the area of the triangle encompassed by $\boldsymbol{r}_1$, $\boldsymbol{r}_2$ and $\boldsymbol{l}$, presenting the geometrical presentation of the secondary part of a line vector. The secondary part could also be presented as vector $\boldsymbol{l}_0$ that is normal to the encompassed triangle in Fig. 3.2 and component p, q, r can be obtained as projections of vector $\boldsymbol{l}_0$.

With the primary part as a subtraction in Eq. (3.1) of two position vectors and the secondary part as a cross product in Eq. (3.8) of them, a line in ray coordinates can be obtained as

$$\boldsymbol{L} = \left((\boldsymbol{r}_2 - \boldsymbol{r}_1)^{\mathrm{T}};\ \ (\boldsymbol{r}_1 \times \boldsymbol{r}_2)^{\mathrm{T}} \right) = \left(\boldsymbol{l}^{\mathrm{T}};\ \ \boldsymbol{l}_0^{\mathrm{T}} \right) = (l,\ \ m,\ \ n;\ \ p,\ \ q,\ \ r)^{\mathrm{T}}. \tag{3.9}$$

The geometrical meaning can be revealed in Fig. 3.2 with the primary part as a side of the triangle constructed by position vectors $\boldsymbol{r}_1$ and $\boldsymbol{r}_2$ and the secondary part as a normal of the triangle. In a special case, if a line is passing the origin, Eq (3.9) becomes $\boldsymbol{L}=(\left(\boldsymbol{r}_2-\boldsymbol{r}_1\right)^{\mathrm{T}};\ \ \mathbf{0}^{\mathrm{T}})$. The six distinct 2×2 minors from Grassmann expansion in Eqs. (3.2) to (3.7) can be summarized as follows by two position vectors in their homogeneous coordinates as

$$\begin{bmatrix} x_1 & y_1 & z_1 & 1 \\ x_2 & y_2 & z_2 & 1 \end{bmatrix}. \tag{3.10}$$

3.3 Projected Triangle for Axis Coordinates with Weighted Plane Normals

3.3.1 Duality in Point-Plane Representations of a Line

Dual to the above of presenting a line as a ray of two points, a line in space can be presented as an intersection of two planes in Fig. 3 to form a system of linear equations. Plane coordinates of these two intersecting planes in homogeneous coordinates can be presented as $\left(A_1^{'}:\ B_1^{'}:\ C_1^{'}:\ D_1^{'}\right)$ and $\left(A_2^{'}:\ B_2^{'}:\ C_2^{'}:\ D_2^{'}\right)$. In this representation, the first three components are the normals of planes π_1 and π_2 and the last component gives the distance from the origin to each of the planes. Taking ratios of four components of the plane coordinates above as coordinates of two vectors, two weighted plane normal can be presented in homogenous coordinates with the last component as 1 as $\boldsymbol{n}_1^{'}=\left(A_1:\ B_1:\ C_1:\ 1\right)^{\mathrm{T}}$ and $\boldsymbol{n}_2^{'}=\left(A_2:\ B_2:\ C_2:\ 1\right)^{\mathrm{T}}$, where A_1, B_1, and C_1 are obtained by dividing the distance $D_1^{'}$ of plane π_1 and A_2, B_2, and C_2

are obtained by dividing the distance D_2' of plane π_2. This representation covers all lines except for lines passing the origin. When lines pass the origin, the case will be discussed in the duality and conformability section.

This gives the following weighted plane normals in the three-dimensional space

$$\begin{cases} \boldsymbol{n}_1 = \left(A_1, \quad B_1, \quad C_1\right)^{\mathrm{T}} \\ \boldsymbol{n}_2 = \left(A_2, \quad B_2, \quad C_2\right)^{\mathrm{T}} \end{cases}. \tag{3.11}$$

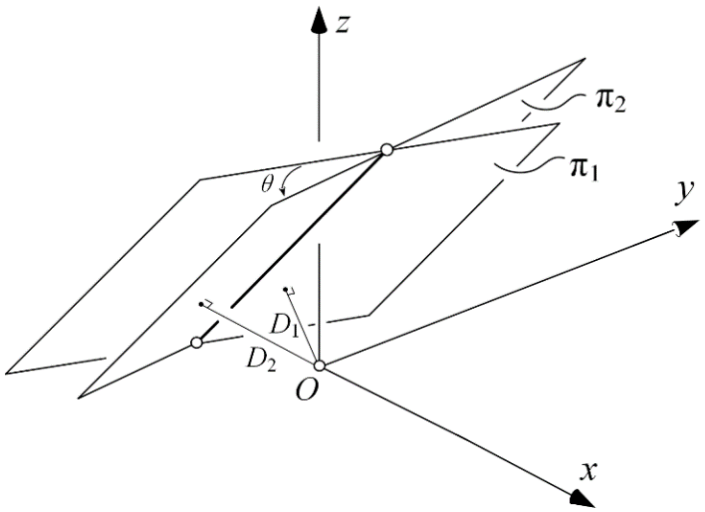

Figure 3.3 A line as the intersection of two planes

Selecting point $\boldsymbol{r}=(x: y: z: 1)^{\mathrm{T}}$ along the intersection of two planes in its homogeneous representation with the last component as 1, the line as the intersection of two planes can be presented as follows

$$\begin{bmatrix} A_1 & B_1 & C_1 & 1 \\ A_2 & B_2 & C_2 & 1 \end{bmatrix} \begin{pmatrix} x \\ y \\ z \\ 1 \end{pmatrix} = \begin{pmatrix} 0 \\ 0 \end{pmatrix}. \tag{3.12}$$

Each of the equations describes a plane sharing common point ***r*** with the other plane, the system of two planes presents the intersection line.

For a line that joins both points P_1 and P_2 and aligns with the intersection of planes π_1 and π_2, four dual equations can be drawn in the context of point connection and that of planes intersection. In the context of taking a line as the intersection of two planes and taking point P_1 as a point in the intersection, the line equation can be presented at point P_1 in the following with respect to planes π_1 and π_2

$$\text{plane } \pi_1 \text{ at } P_1: \quad A_1x_1 + B_1y_1 + C_1z_1 + 1 = 0, \tag{3.13}$$

$$\text{plane } \pi_2 \text{ at } P_1: \quad A_2x_1 + B_2y_1 + C_2z_1 + 1 = 0. \tag{3.14}$$

In the above point-plane equations, replacing point P_1 with point P_2, a new set of plane equations at point P_2 can be given in the following with respect to planes π_1 and π_2

$$\text{plane } \pi_1 \text{ at } P_2: \quad A_1x_2 + B_1y_2 + C_1z_2 + 1 = 0, \tag{3.15}$$

$$\text{plane } \pi_2 \text{ at } P_2: \quad A_2x_2 + B_2y_2 + C_2z_2 + 1 = 0. \tag{3.16}$$

These four equations form a set of point-plane dual equations. In the context of taking a line as an intersection of two planes, Eqs. (3.13) and (3.14) present a line as the intersection of two planes at point P_1 and Eqs. (3.15) and (3.16) at point P_2. Dual to this, in the context of taking a line as a ray of two points, Eqs. (3.13) and (3.15) present a

line as joint of points P_1 and P_2 in plane π_1, and Eqs. (3.14) and (3.16) present the same line as joint of points P_1 and P_2 in plane π_2.

3.3.2 Algebraic Derivation of Axis Coordinates

Thus the above four point-plane dual equations relate two ways of expressing the same line. In the plane intersection at point P_1, subtracting Eq. (3.14) multiplied by B_1 from Eq. (3.13) multiplied by B_2 eliminates y_1 and gives the following

$$\left(A_2B_1 - A_1B_2\right)x_1 + \left(C_2B_1 - C_1B_2\right)z_1 + B_1 - B_2 = 0\,. \tag{3.17}$$

Similarly in the plane intersection at point P_2, operation on Eqs. (3.15) and (3.16) that eliminates y_2 gives the following

$$\left(A_2B_1 - A_1B_2\right)x_2 + \left(C_2B_1 - C_1B_2\right)z_2 + B_1 - B_2 = 0\,. \tag{3.18}$$

These two equations present the same line on its *x*-*z* plane projection related to two sets of plane coordinates and can be rearranged to present the following

$$x_2 - x_1 = \frac{\left(C_1B_2 - C_2B_1\right)\left(z_2 - z_1\right)}{A_1B_2 - A_2B_1} = k\begin{vmatrix} C_1 & B_1 \\ C_2 & B_2 \end{vmatrix} = kL\,. \tag{3.19}$$

A separate derivation on plane intersection at points P_1 and P_2 with its y-z plane projection can be carried out to produce the following

$$y_2 - y_1 = \frac{(C_1A_2 - C_2A_1)(z_2 - z_1)}{A_1B_2 - A_2B_1} = k\begin{vmatrix} C_1 & A_1 \\ C_2 & A_2 \end{vmatrix} = kM \,. \tag{3.20}$$

Further z-axis projection as $z_2 - z_1$ is given as follows

$$z_2 - z_1 = k\begin{vmatrix} A_1 & B_1 \\ A_2 & B_2 \end{vmatrix} = kN \,. \tag{3.21}$$

This gives the secondary part $\boldsymbol{l}'=(L, M, N)^{\mathrm{T}}$ of the intersection line in axis coordinates. Further derivation on the plane intersection at both points P_1 and P_2 gives the following three cross-terms

$$y_1z_2 - y_2z_1 = \frac{(D_1A_2 - D_2A_1)(z_2 - z_1)}{A_1B_2 - A_2B_1} = k\begin{vmatrix} 1 & A_1 \\ 1 & A_2 \end{vmatrix} = kP \,, \tag{3.22}$$

$$x_2z_1 - x_1z_2 = \frac{(D_1B_2 - D_2B_1)(z_2 - z_1)}{A_1B_2 - A_2B_1} = k\begin{vmatrix} 1 & B_1 \\ 1 & B_2 \end{vmatrix} = kQ \,, \tag{3.23}$$

and

$$x_1y_2 - x_2y_1 = \frac{(D_1C_2 - D_2C_1)(z_2 - z_1)}{A_1B_2 - A_2B_1} = k\begin{vmatrix} 1 & C_1 \\ 1 & C_2 \end{vmatrix} = kR \,. \tag{3.24}$$

This gives the primary part $\boldsymbol{l}_0' = (P,\ Q,\ R)^{\mathrm{T}}$ of the intersection line in axis coordinates. Hence, a line in axis coordinates can be expressed in the form of

$$\boldsymbol{L}' = \left(\boldsymbol{l}_0'^{\mathrm{T}};\ \ \boldsymbol{l}'^{\mathrm{T}}\right)^{\mathrm{T}} = (P,\ \ Q,\ \ R;\ \ L,\ \ M,\ \ N)^{\mathrm{T}} \,. \tag{3.25}$$

In the derivation from Eqs. (3.19) to (3.24), it can be seen that axis coordinates can also be obtained by Grassmann expansion of the following array

$$\begin{bmatrix} A_1 & B_1 & C_1 & 1 \\ A_2 & B_2 & C_2 & 1 \end{bmatrix}. \tag{3.26}$$

where (A_1, B_1, C_1) is weighted plane normal $\boldsymbol{n}_1$ and (A_2, B_2, C_2) is weighted plane normal $\boldsymbol{n}_2$ in the three-dimensional space.

3.3.3 Geometrical Presentation of Axis Coordinates

In the six axis coordinates obtained from Eqs. (3.19) to (3.24), it can be seen that components L, M, N in Eqs. (3.19) to (3.21) as the secondary part of the line vector are the result of the cross product of weighted plane normals $\boldsymbol{n}_1$ and $\boldsymbol{n}_2$ of planes π_1 and π_2 in the form of

$$\boldsymbol{l}' = \boldsymbol{n}_1 \times \boldsymbol{n}_2 = \begin{vmatrix} i & j & k \\ A_1 & B_1 & C_1 \\ A_2 & B_2 & C_2 \end{vmatrix} = \begin{vmatrix} B_1 & C_1 \\ B_2 & C_2 \end{vmatrix} i + \begin{vmatrix} C_1 & A_1 \\ C_2 & A_2 \end{vmatrix} j + \begin{vmatrix} A_1 & B_1 \\ A_2 & B_2 \end{vmatrix} k. \tag{3.27}$$

This gives the direction vector of the intersection line $\boldsymbol{L}'$ as in Eq. (3.25) and the triangular presentation in Fig. 3.4 of this secondary part of a line in axis coordinates with twice the area of the triangle encompassed by $\boldsymbol{n}_1$, $\boldsymbol{n}_2$ and as $\boldsymbol{n}_2 - \boldsymbol{n}_1$. Consistent with the secondary part of a line vector in Fig. 3.2 in ray coordinates in Eq. (3.9), it could also be presented by vector $\boldsymbol{l}'$ that is normal to the triangle in Fig. 3.4.

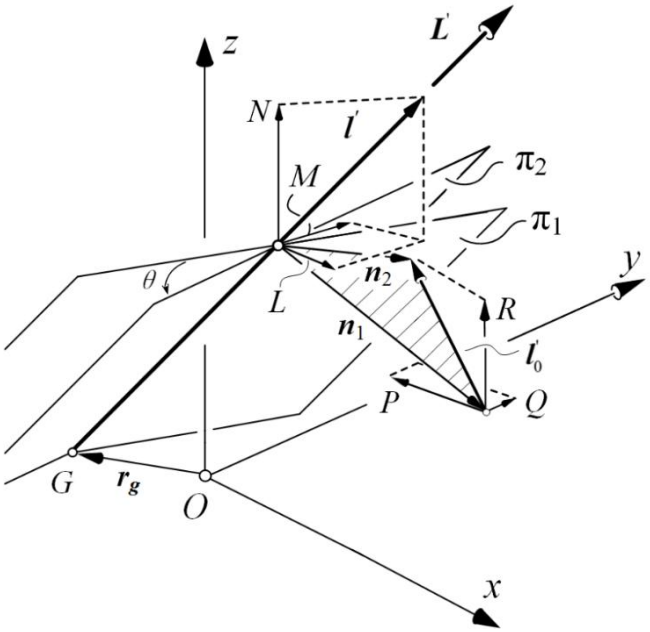

Figure 3.4 Geometrical interpretation of the axis coordinates

To reveal the geometrical meaning of the primary part components P, Q, R of axis coordinates obtained in Eqs. (3.22) to (3.24), assigning z=0 in Eq. (3.12) of the intersection line of two planes, the following can be provided

$$A_1 x + B_1 y + 1 = 0\,, \tag{3.28}$$

$$A_2 x + B_2 y + 1 = 0\,. \tag{3.29}$$

The position vector for the intersection line can be obtained as,

$$\boldsymbol{r}_g = \left(\frac{B_2 - B_1}{A_2 B_1 - A_1 B_2}, \quad \frac{A_1 - A_2}{A_2 B_1 - A_1 B_2}, \quad 0 \right)^{\mathrm{T}}. \tag{3.30}$$

Hence the moment of the intersection line with respect to the origin is given in the form of

$$\boldsymbol{l}_0' = \boldsymbol{r} \times \boldsymbol{l}' = \boldsymbol{r}_g \times \boldsymbol{l}' = \begin{pmatrix} A_2 - A_1, & B_2 - B_1, & C_2 - C_1 \end{pmatrix}^{\mathrm{T}} = \boldsymbol{n}_2 - \boldsymbol{n}_1. \tag{3.31}$$

This gives three components *P*, *Q*, *R* as the primary part of the intersection line in axis coordinates in the form of weighted plane normals. Therefore, this presents vector $\boldsymbol{n}_2 - \boldsymbol{n}_1 = \boldsymbol{l}_0'$ in Fig. 3.4 whose projections give three components *P*, *Q*, *R* as the primary part of the intersection line, in a geometrical presentation consistent with projections of $\boldsymbol{r}_2 - \boldsymbol{r}_1 = \boldsymbol{l}$ in Fig. 3.2 of the primary part of a line vector in ray coordinates.

The geometrical meaning of the primary part in axis coordinates is hence given as a subtraction of two weighted plane normal, consistent with the mathematical structure of the primary part $\boldsymbol{l}$ of the ray coordinates expressed in Eqs. (3.2) to (3.4).

Similarly, the secondary part in axis coordinates is consistent with the mathematical structure in the secondary part of ray coordinates. In these two sets of coordinates, the primary part and secondary part are constructed by position vectors in ray coordinates and by weighted plane normals in axis coordinates.

The geometrical meaning can hence be revealed in Fig. 3.4 with the primary part $\boldsymbol{l}_0'$ as a side of a triangle constructed by two weighted plane normal and the secondary part $\boldsymbol{l}'$ as a normal of the triangle.

3.4 Conclusions

This chapter revealed the geometrical presentation of a line as a ray of two points in the form of position vectors with their triangle presentation and derived the geometrical

presentation of a line as an intersection of two planes in the form of plane normals with another triangle presentation, giving a line in its ray coordinates and axis coordinates. In particular, it was verified for the first time the secondary part (L, M, N) in axis coordinates as the cross product of weighted plane normals of the intersection planes and the primary part (P, Q, R) in axis coordinates as the vector subtraction of the weighted plane normals.

Chapter 4 Geometrically Intrinsic Connections of Screw Coordinates

4.1 Introduction

This chapter reveals the geometrical insight of ray coordinates with twice the area projection in a triangle constructed by two position vectors and presents the geometrical meaning of the axis coordinates with the geometrical presentation for the first time between two normals of the intersecting planes that give a corresponding triangle constructed by these normals. This leads to a natural derivation of the ratio relationship between ray and axis coordinates, and to a duality of these two sets of coordinates. During the derivation, form conformability in the mathematical structures of corresponding parts of two sets of coordinates is revealed, and geometrical conformability is identified in the reciprocal parts of these two sets of coordinates that are presented in two vector spaces that are dual to each other. The study derives naturally the correlation relationship with a correlation coefficient and the correlation operator, leading to a duality and conformability table and a conformability graph.

4.2 Form and Geometry Conformability of Two Sets of Coordinates

In the derivation of ray and axis coordinates, it can be seen that a triangle presentation exists in either set of coordinates. The closing vector of the triangle is a subtraction of

two position vectors in ray coordinates and that of weighted plane normals in axis coordinates and the perpendicular vector of the triangle is a cross product of these two sets of vectors. Integrating the geometrical presentations of these two sets of coordinates, the correspondence between ray coordinates and axis coordinates could be seen in Fig. 4.1 in which a presentation of a line in ray coordinates is given as joint of two position vectors $\boldsymbol{r}_1$ and $\boldsymbol{r}_2$ and a presentation of a line in axis coordinates is given as intersection of two planes with weighted plane normals $\boldsymbol{n}_1$ and $\boldsymbol{n}_2$.

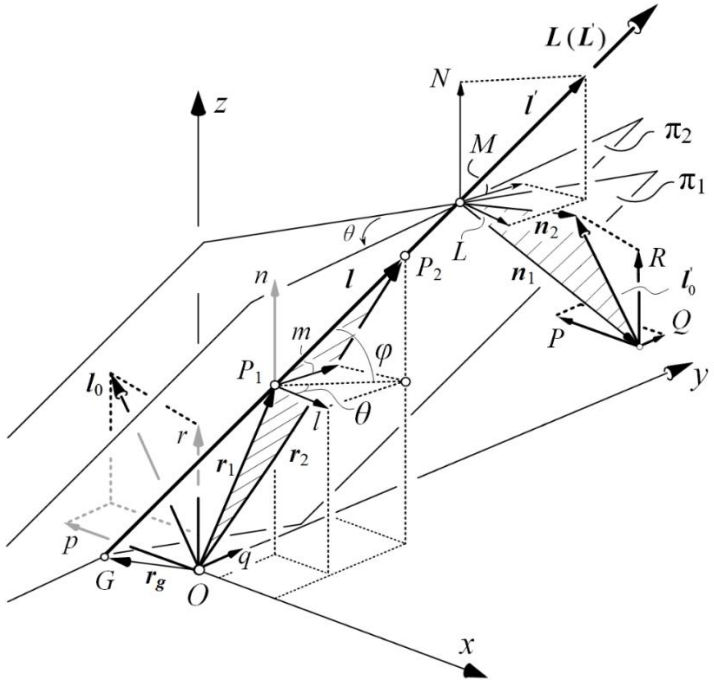

Figure 4.1 Integrated geometrical presentations of ray and axis coordinates

The subtraction vector $\boldsymbol{l}_0'$ in Fig. 4.1 of plane weighted normals $\boldsymbol{n}_1$ and $\boldsymbol{n}_2$ that leads to its projected components P, Q, and R as the primary part in axis coordinates has the same mathematical structure as the subtraction vector $\boldsymbol{l}$ in the same figure of position vectors $\boldsymbol{r}_1$ and $\boldsymbol{r}_2$ that leads to its projected components l, m and n as the primary part in ray coordinates. It could be seen that the primary part presented by $\boldsymbol{l}_0'$ in axis

coordinates is consistent with the primary part presented by $\boldsymbol{l}$ in ray coordinates in the sense of form conformability. Further, the primary part $\boldsymbol{l}_0'$ in axis coordinates has the same geometrical meaning as the secondary part $\boldsymbol{l}_0=\boldsymbol{r}_1\times\boldsymbol{r}_2$ in ray coordinates as the moment of the line in the sense of geometry conformability. In such a case, they have the same direction as in Fig. 4.1 that

$$\boldsymbol{l}_0 = k\boldsymbol{l}_0', \tag{4.1}$$

where k will be discussed in Section 4.4.

The secondary part $\boldsymbol{l}'=\boldsymbol{n}_1\times\boldsymbol{n}_2$ of axis coordinates with its components L, M and N represented by the normal of the triangle constructed by $\boldsymbol{n}_1$ and $\boldsymbol{n}_2$ in Fig. 4.1 has the same mathematical structure as the secondary part $\boldsymbol{l}_0=\boldsymbol{r}_1\times\boldsymbol{r}_2$ of ray coordinates with its components p, q, and r represented by the normal of the triangle constructed by $\boldsymbol{r}_1$ and $\boldsymbol{r}_2$ in the same figure. This gives form conformability. Further, the secondary part $\boldsymbol{l}'$ of axis coordinates has the same geometrical meaning as the primary part $\boldsymbol{l}$ in ray coordinates of the direction of the line in the sense of geometry conformability. In such a case, they are on the same line as in Fig. 4.1 that

$$\boldsymbol{l} = k\boldsymbol{l}', \tag{4.2}$$

where k will be discussed in Section 4.4.

As demonstrated, a line vector as joint of two points in space is dual to a line vector as the intersection of two planes, in the way of ray coordinates dual to axis coordinates.

Placing the former in the vector space and the latter in the dual vector space, their duality is clearly illustrated in the following sections. As such, the coordinates can be mapped onto one another as in the correlation equation in the following section.

4.3 Correlated Ratio Relationships

Duality of a line in its ray and axis coordinates represented by point-plane dual equations (3.13) to (3.16) leads to the correlated ratio relationship between the corresponding primary and secondary parts of ray and axis coordinates that can be derived from the following. Starting from point-plane dual equations Eqs (3.13) and (3.14), it results in

$$\left(A_1 - A_2\right)x_1 + \left(B_1 - B_2\right)y_1 + \left(C_1 - C_2\right)z_1 = 0. \tag{4.3}$$

It can be easily seen that the components in the parentheses are axis coordinates P, Q, R expressed in Eqs. (3.22) to (3.24), the above equation can then be rewritten as

$$Px_1 + Qy_1 + Rz_1 = 0. \tag{4.4}$$

This gives the primary part of axis coordinates in relation to point P_1 given by position vector $\boldsymbol{r}_1$. Similarly, from another set of point-plane dual equations Eqs. (3.15) and (3.16), the following can be derived

$$Px_2 + Qy_2 + Rz_2 = 0. \tag{4.5}$$

This gives the primary part of axis coordinates in relation to point P_2 given by position vector $\boldsymbol{r}_2$. Subtracting Eq. (4.5) that is multiplied by y_1 from Eq. (4.4) that is multiplied by y_2, gives the following

$$P\left(x_1y_2 - x_2y_1\right) + R\left(y_2z_1 - y_1z_2\right) = 0. \tag{4.6}$$

It is clear that the components in the parentheses are secondary part p and r of ray coordinates as in Eqs. (3.5) and (3.7) and this gives a relationship between the secondary part of ray coordinates and the primary part of axis coordinates. Substituting p and r of ray coordinates in Eqs. (3.5) and (3.7) for the components in the parentheses in the above equation and rearranging it, the following is given

$$\frac{P}{R} = \frac{y_1z_2 - y_2z_1}{x_1y_2 - x_2y_1} = \frac{p}{r}. \tag{4.7}$$

In a way similar to the above process that generates Eq. (4.7), subtracting Eq. (4.5) that is multiplied by x_1 from Eq. (4.5) that is multiplied by x_2 and substituting q and r in Eqs. (3.6) and (3.7) of ray coordinates for the components in the parentheses, the following is given

$$\frac{Q}{R} = \frac{x_2z_1 - x_1z_2}{x_1y_2 - x_2y_1} = \frac{q}{r}. \tag{4.8}$$

Thus from Eqs. (4.7) and (4.8), the following part correlated ratio relationship of the primary part of axis coordinates with respect to the secondary part of ray coordinates can be given

$$P:Q:R=p:q:r. \tag{4.9}$$

This gives the P part correlated ratio relationship of ray and axis coordinates.

The relationship of the secondary part of axis coordinates and the primary part of ray coordinates can be given following the similar derivation in point-plane dual equations Eqs. (3.13) and (3.15). Eqs. (3.13) and (3.15) present a line as joint of two points in plane π_1 with components in the parentheses as the secondary part of the line in axis coordinates in Eqs. (3.19) to (3.21), the primary part of ray coordinates of the line can be written in terms of plane coordinates of plane π_1 that form the secondary part of axis coordinates. In a similar way, the primary part of ray coordinates of the line can be written in terms of plane coordinates of plane π_2 that form the secondary part of axis coordinates. These two relations can be rearranged by substituting for the components in the parentheses with the secondary part of axis coordinates from Eqs. (3.19) to (3.21), yielding the following L part relationship

$$L:M:N=l:m:n. \tag{4.10}$$

Hence, both L part and P part ratio relationships are obtained. To associate these two correlated ratio relationships, a L-P cross-part ratio relationship needs to be obtained. In the context of a line as the intersection of planes π_1 and π_2 at point P_1 in Eqs. (3.13) and (3.14) and as the intersection of planes π_1 and π_2 at point P_2 in Eqs. (3.15) and (3.16), manipulation of these equations together with the substitution by axis coordinates between Eqs. (3.19) and (3.22) gives the following cross-part relationship,

$$L:P=l:p. \tag{4.11}$$

Hence, two sets of L part ratio and P part ratio relationships can be associated with the above L-P cross-part ratio between ray and axis coordinates. The part correlated ratio relationship in Eqs. (4.9) and (4.10) and the cross-part correlated ratio relationship in Eq. (4.11) present duality of ray and axis coordinates and can be rearranged to generate the following relationship in the form of

$$L : M : N : P : Q : R = l : m : n : p : q : r . \tag{4.12}$$

The above can be rewritten as

$$l : L = m : M = n : N = p : P = q : Q = r : R = k . \tag{4.13}$$

The above derivation reveals duality between ray and axis coordinates and presents a correlation coefficient *k*.

4.4 Correlation Coefficient and Correlation Operator

Consistent with the above ratio relationship, observing ray coordinates equations from Eqs. (3.2) to (3.7), it can be seen that the left-hand sides of Eqs. (3.19) to (3.21) in Section 3.2 give the direction vector $\boldsymbol{l}=(l, m, n)^{\mathrm{T}}$ in ray coordinates while the right-hand sides give the secondary part $\boldsymbol{l}_0' = \left(L, M, N\right)^{\mathrm{T}}$ in axis coordinates of a line vector, the left-hand sides of Eqs (3.22) to (3.24) in Section 3.3.2 give the moment $\boldsymbol{l}_0=(p, q, r)^{\mathrm{T}}$ in ray coordinates while the right-hand sides give the primary part $\boldsymbol{l}' = \left(P, Q, R\right)^{\mathrm{T}}$ in axis coordinates of the line vector. This leads to the following correlation between two sets of coordinates,

$$\begin{aligned}\boldsymbol{L} &= \left(l,\quad m,\quad n;\quad p,\quad q,\quad r\right)^{\mathrm{T}} \\ &= \left(x_2 - x_1,\quad y_2 - y_1,\quad z_2 - z_1;\quad y_1z_2 - y_2z_1,\quad x_2z_1 - x_1z_2,\quad x_1y_2 - x_2y_1\right)^{\mathrm{T}} \\ &= k\left(C_1B_2 - C_2B_1,\quad C_1A_2 - C_2A_1,\quad A_1B_2 - A_2B_1;\quad A_2 - A_1,\quad B_2 - B_1,\quad C_2 - C_1\right)^{\mathrm{T}} \\ &= k\left(L,\quad M,\quad N;\quad P,\quad Q,\quad R\right)^{\mathrm{T}} = k\Delta\boldsymbol{L}'\end{aligned} \tag{4.14}$$

giving rise naturally to use the following correlation operator,

$$\Delta = \begin{bmatrix} \mathbf{0} & \boldsymbol{I} \\ \boldsymbol{I} & \mathbf{0} \end{bmatrix}, \tag{4.15}$$

and the correlation coefficient as

$$k = \frac{z_2 - z_1}{A_1B_2 - A_2B_1} = \frac{n}{N}. \tag{4.16}$$

It again can be seen that this correlation coefficient k is a ratio between two sets of coordinates that is given in Eq (4.13) and is invariant.

Considering points P_1 and P_2 being distinct with at least one of the three coordinates distinct, Eq. (4.14) gives the correlation between ray coordinates $\boldsymbol{L}$ and axis coordinates $\boldsymbol{L}'$ when presenting the same line.

As six coordinates provide ratios as in Eq (4.12) in homogeneous coordinates, the magnitude change of a line vector does not change itself. Hence, without loss of generality, k can be assigned with 1 and the correlation equation (4.14) can be

developed into the following relationship of ray and axis coordinates relating the vector space and dual vector space as

$$\boldsymbol{L} = \begin{pmatrix} l \\ m \\ n \\ p \\ q \\ r \end{pmatrix} = \begin{bmatrix} 0 & 0 & 0 & 1 & 0 & 0 \\ 0 & 0 & 0 & 0 & 1 & 0 \\ 0 & 0 & 0 & 0 & 0 & 1 \\ 1 & 0 & 0 & 0 & 0 & 0 \\ 0 & 1 & 0 & 0 & 0 & 0 \\ 0 & 0 & 1 & 0 & 0 & 0 \end{bmatrix} \begin{pmatrix} P \\ Q \\ R \\ L \\ M \\ N \end{pmatrix} = \Delta \boldsymbol{L}^{'}. \tag{4.17}$$

The correlation operator Δ is derived from the correlation relationship in Eq (4.14). It could be seen that axis coordinates of a line vector could be obtained by interchanging [12] both primary and secondary parts of a line vector that is in ray coordinates. This gives the duality [10,31] between ray and axis coordinates of a line vector and the duality between two spaces.

The correlation operator changes a vector in a dual vector space to a vector space and gives the relationship between a vector space and a dual vector space that could be distinguished by two sets of coordinates. While a twist could be presented in a vector space with ray coordinates and a wrench in a dual vector space with axis coordinates, the virtual work could be calculated with a scalar product of both. When a wrench is written in the same coordinates as a twist in ray coordinates, the virtual work is to be calculated by resorting to the correlation operator by transforming the wrench to a dual vector to complete the calculation of work done.

4.5 Duality and Conformability

The above revelation of duality between ray and axis coordinates and the derivation of axis coordinates algebraically and geometrically can be summarized in the duality and conformability Table 4.1.

Duality is represented in general in relation to both coordinates by interchanging a ray of two points with an intersection of two planes, and in particular by geometry conformability between two sets of coordinates, following the same arrangement of both position vectors and weighted plane normals, relating the vector space to the dual vector-space. This particular duality is illustrated in the conformability graph in Fig. 4.2 with the correlation map that generates the congruence relationship. In Fig. 4.2, vertical correspondences give form conformability in the sense of the same mathematical structure and the cross correspondences give geometry conformability in the sense of direction and moment of a line vector that is explained in Section 4.2.

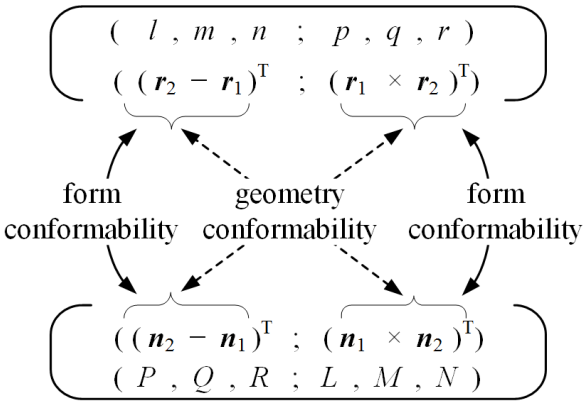

Figure 4.2 Conformability graph

Table 4.1 Duality and conformability

			Primary part	Secondary part
			form conformability column	form conformability column
Vector space	Ray coordinates	$\boldsymbol{L} = \begin{pmatrix} \boldsymbol{l}; & \boldsymbol{l}_0 \end{pmatrix}^{\mathrm{T}}$	$\boldsymbol{l} = (l,m,n)^{\mathrm{T}}$	$\boldsymbol{l}_0 = (p,q,r)^{\mathrm{T}}$
		geometrical representation	$\boldsymbol{l} = \boldsymbol{r}_1 - \boldsymbol{r}_1$ Eq. (3.1)	$\boldsymbol{l}_0 = \boldsymbol{r}_1 \times \boldsymbol{r}_2$ Eq. (3.8)
		position vectors	$\boldsymbol{r}_1 = (x_1, \ y_1, \ z_1)^{\mathrm{T}}$ $\boldsymbol{r}_2 = (x_2, \ y_2, \ z_2)^{\mathrm{T}}$	
Dual Vector space	Axis coordinates	$\boldsymbol{L}' = \begin{pmatrix} \boldsymbol{l}_0'^{\mathrm{T}}; & \boldsymbol{l}'^{\mathrm{T}} \end{pmatrix}$	$\boldsymbol{l}_0' = (P,Q,R)^{\mathrm{T}}$	$\boldsymbol{l}' = (L,M,N)^{\mathrm{T}}$
		geometrical representation	$\boldsymbol{l}_0' = \boldsymbol{n}_2 - \boldsymbol{n}_1$ Eq. (3.31)	$\boldsymbol{l}' = \boldsymbol{n}_1 \times \boldsymbol{n}_2$ Eq. (3.27)
		weighted plane normals	$\boldsymbol{n}_1 = (A_1, \ B_1, \ C_1)^{\mathrm{T}}$ $\boldsymbol{n}_2 = (A_2, \ B_2, \ C_2)^{\mathrm{T}}$	
Correlation		Ratio relationship	$l:m:n:p:q:r$ $= L:M:N:P:Q:R$ Eq. (4.12)	
		Duality	$\boldsymbol{L} = \Delta \boldsymbol{L}'$ Eq. (4.17)	
		Correlation coefficient	$k = l:L = m:M = n:N = p:P = q:Q = r:R$ Eq. (4.13)	

Conformability can also be seen in Table 4.1 on their conformable mathematical structure in corresponding primary and secondary parts with position vectors for ray

coordinates and weighted plane normals for axis coordinates. Parts in each column of Table 4.1 are conformable in their mathematical structures as form conformability.

Duality and geometry conformability always coexist. But duality and form conformability only coexist when there is no point in the infinity in the vector space such as $w_i \neq 0$ and there is no plane passing through the origin in the dual vector space such as $D_i \neq 0$.

While any scaling factor that is the last component in homogeneous coordinates is equal to zero, duality and geometry conformability still coexist, but duality and form conformability are disconnected. This can be seen that when a line is passing the origin in ray coordinates as $((\boldsymbol{r}_2-\boldsymbol{r}_1)^{\mathrm{T}}; \mathbf{0}^{\mathrm{T}})$, its dual in axis coordinates is $(\mathbf{0}^{\mathrm{T}}; (\boldsymbol{n}_1\times\boldsymbol{n}_2)^{\mathrm{T}})$. As a matter of interest, its form-conformable axis coordinates could be $((\boldsymbol{n}_2-\boldsymbol{n}_1)^{\mathrm{T}}; \mathbf{0}^{\mathrm{T}})$ that presents a line in the infinity. Vice versa, when a line is in the infinity in ray coordinates as $(\mathbf{0}^{\mathrm{T}}; (\boldsymbol{r}_1\times\boldsymbol{r}_2)^{\mathrm{T}})$, its dual in axis coordinates is $((\boldsymbol{n}_2-\boldsymbol{n}_1)^{\mathrm{T}}; \mathbf{0}^{\mathrm{T}})$. But as a matter of interest, its form-conformable axis coordinates could be $(\mathbf{0}^{\mathrm{T}}; (\boldsymbol{n}_1\times\boldsymbol{n}_2)^{\mathrm{T}})$ that presents a line passing the origin. In such an occasion, though duality and geometry conformability always coexist, duality and form conformability no longer coexists.

4.6 Conclusions

In the derivation, it was found that the subtraction vector of two position vectors in ray coordinates and that of two weighted plane normals in axis coordinates are a closing vector of the triangle formed by two vectors in each coordinate set and the cross-product vector was perpendicular to the triangle formed by these two vectors in each coordinate set. Two presentations were related geometrically and algebraically and presented

conformability and duality between corresponding and reciprocal parts of ray and axis coordinates, with an illustration presenting an integration of geometrical presentations for both ray and axis coordinates in their form conformability and geometry conformability.

In this chapter, the work was then extended to presenting a correlation between ray and axis coordinates with their correlated part ratios to relate the vector space to the dual vector space, and to deriving a correlation between two sets of coordinates with a correlation coefficient, giving rise to a derivation of the correlation operator. The duality was then recapitulated in a duality and conformability table and in a conformability graph, outlining the relationship between ray and axis coordinates of a line vector.

The study presented a geometrical and algebraic foundation for using line vectors in their two sets of coordinates for mechanism analysis and synthesis.

Chapter 5 Geometrical Meaning of a Twist Based on Screw Algebra

5.1 Introduction

Line geometry and line vectors, particularly the ray coordinates and axis coordinates and their interrelation are well received in Chapters 3 and 4. By associating a line vector with a pitch, a screw is formed. A screw is a geometrical entity, and is an element of the projective Lie algebra *se*(3). The geometrical meaning of the pitch of a screw is the ratio of the magnitude of the second component of the secondary part over that of the primary part.

A twist is formed by attaching a screw with a velocity amplitude, and it is an element of the Lie algebra *se*(3). The primary part of a twist indicates the angular velocity of a rigid body, whereas the secondary part indicates the linear velocity of a point on this rigid body instantaneously coincident with the reference point. The twists that represent the instantaneous velocity of links in a serial manipulator can be assembled to generate a resultant twist of the end-effector. Geometrical meaning of the resultant twist is revealed in this chapter and the Jacobian of a planar serial manipulator is formed through screw algebra.

5.2 Homogenous Coordinates of Screws as 6-Dimensional Vector

5.2.1 Homogenous Screw Coordinates

A screw is essentially the geometrical entity of instantaneous twist and wrench in kinematics and statics, which in general can be regarded as a line vector in 3-dimensional affine space $\mathbb{R}^3$ together with pitch h. The screw can be expressed by dual vector and 6-dimensional vector respectively as follows

$$\boldsymbol{S} = \boldsymbol{s} + \varepsilon \boldsymbol{s}_0 = \begin{pmatrix} \boldsymbol{s} \\ \boldsymbol{s}_0 \end{pmatrix} = \begin{pmatrix} \boldsymbol{s} \\ \boldsymbol{r}_0 \times \boldsymbol{s} + h\boldsymbol{s} \end{pmatrix}. \tag{5.1}$$

where the vector $\boldsymbol{s}$ is the primary part of the screw, representing the direction vector of screw axis, the vector $\boldsymbol{s}_0$ is the secondary part of the screw that consists of the moment with respect to the origin and the scalar product of the primary part by pitch h, the 3-dimensional vector $\boldsymbol{r}_0$ represents the position vector of the screw axis with respect to the origin and ε is dual unit of dual vector satisfying the condition $\varepsilon^2 = 0$. The conception of dual vector originally comes from dual number brought forward by Clifford (1876) in his research on quaternions and extensively developed by Brand (1940) in his exploration on motor algebra in which the screw is seen as dual vector called *motor*.

Obviously, screw as a geometrical entity can be described as a 6-dimensional vector, that is to say, screw and 6-dimensional vector are equivalent so that all the operations of screws can be performed in the form of vector operations and further by matrix

operations. Similar to an arbitrary 6-dimensional vector, screw can be represented by six coordinates as follows

$$\boldsymbol{S} = \left(\xi_0,\ \xi_1,\ \xi_2,\ \xi_3,\ \xi_4,\ \xi_5\right)^{\mathrm{T}}. \tag{5.2}$$

which are analogous to Plücker coordinates of lines in $\mathbb{R}^3$, and are homogeneous coordinates. Two points in $\mathbb{R}^3$ lying on the screw axis, described by homogeneous coordinates $(x_0, x_1, x_2, x_3)^{\mathrm{T}}$, $(y_0, y_1, y_2, y_3)^{\mathrm{T}}$, together with the pitch h can generate the above screw coordinates by the means of six Grassmann determinants and it has

$$\begin{gathered}
\xi_0 = \begin{vmatrix} x_0 & x_1 \\ y_0 & y_1 \end{vmatrix}, \qquad \xi_1 = \begin{vmatrix} x_0 & x_2 \\ y_0 & y_2 \end{vmatrix}, \qquad \xi_2 = \begin{vmatrix} x_0 & x_3 \\ y_0 & y_3 \end{vmatrix} \\
\xi_3 = \begin{vmatrix} x_2 & x_3 \\ y_2 & y_3 \end{vmatrix} - h\begin{vmatrix} x_0 & x_1 \\ y_0 & y_1 \end{vmatrix}, \quad \xi_4 = \begin{vmatrix} x_3 & x_1 \\ y_3 & y_1 \end{vmatrix} - h\begin{vmatrix} x_0 & x_2 \\ y_0 & y_2 \end{vmatrix}, \quad \xi_5 = \begin{vmatrix} x_1 & x_2 \\ y_1 & y_2 \end{vmatrix} - h\begin{vmatrix} x_0 & x_3 \\ y_0 & y_3 \end{vmatrix}
\end{gathered} \tag{5.3}$$

In the above representation of screw, the scalars x_0, y_0 acting as the first coordinates of the points in screw axis are of significance since they determine whether the points stay in 3-dimensional affine space $\mathbb{R}^3$ or not. They are non-zero usually and in this case, the points in the screw axis do not lie at infinity and hence lie in $\mathbb{R}^3$, while if x_0, y_0 are equal to zero, the points are at infinity so that the screw axis lie in 3-dimensional projective space $\mathbb{P}^3$ including $\mathbb{R}^3$ and the infinite area.

5.2.2 Screw System of nth Order

Naturally, there exists a bijective map between n-dimensional vector subspaces $\mathbf{V}^n$ of six-dimensional vector space $\mathbf{V}^6$ spanned by n linearly independent vectors and screw systems of order n donated as $\mathbb{S}_n$ consist precisely of all linear combinations of the screws $\boldsymbol{S}_i$ as a set of basis of $\mathbb{S}_n$. Simultaneously, an arbitrary screw system of n^{th} order, also called n-system can be defined as

$$\mathbb{S}_n = \left\{ \boldsymbol{S} \middle| \boldsymbol{S} = \sum_{i=1}^{n} \lambda_i \boldsymbol{S}_i,\ \lambda_i \in \mathbf{R},\ \boldsymbol{S}_i \in \mathbf{V}^6 \right\}. \tag{5.4}$$

At the moment screw can be seen as an element of 6-dimensional vector space $\mathbf{V}^6$ and expressed by six homogenous coordinates generated by Grassmann determinates together with pitch h as Eq. (5.3). Screw system of n^{th} order n can be viewed as n-dimensional vector subspace of $\mathbf{V}^6$.

5.3 The Helicoidal Velocity Field

Motion of a rigid body in three dimensions can be represented by a rotation about an axis together with a translation parallel to that axis. Such motion is similar to that which would occur if the body is connected to its surroundings by a screw thread. This general motion is referred to as a twist on a screw axis or simply *twist*. *A twist is a screw with the rate amplitude and an element of the Lie algebra se*(3) that can be expressed in Eq. (5.6),

$$\boldsymbol{T} = \omega \boldsymbol{S} = \omega \begin{bmatrix} \boldsymbol{s} \\ \boldsymbol{r}_0 \times \boldsymbol{s} + h\boldsymbol{s} \end{bmatrix} = \begin{bmatrix} \boldsymbol{\omega} \\ \boldsymbol{r}_0 \times \boldsymbol{\omega} + h\boldsymbol{\omega} \end{bmatrix} = \begin{bmatrix} \boldsymbol{\omega} \\ \boldsymbol{v}_0 \end{bmatrix}. \tag{5.5}$$

where $\boldsymbol{S}$ is the screw associated with the twist $\boldsymbol{T}$, $\boldsymbol{s}$ is the direction vector of this screw, $\boldsymbol{r}_0$ is the position vector that locates the axis of this screw, and h is the pitch gives the ratio of the magnitude of the second component of the secondary part over that of the primary part. The axis of rotation is the *screw axis* and the pitch of the screw is equal to the ratio of the translational velocity to the rotational velocity while translation is parallel to the axis of rotation.

With the screw axis, the body has an angular velocity $\boldsymbol{\omega}$. Point P on the body has velocity $\boldsymbol{v}_p$. The velocity of any point on the body consists of a component $h\boldsymbol{\omega}$ parallel to the screw axis and another component normal to it expressed as $\boldsymbol{\omega}\times(\boldsymbol{r}_p-\boldsymbol{r}_o)$ in Fig. 5.1.

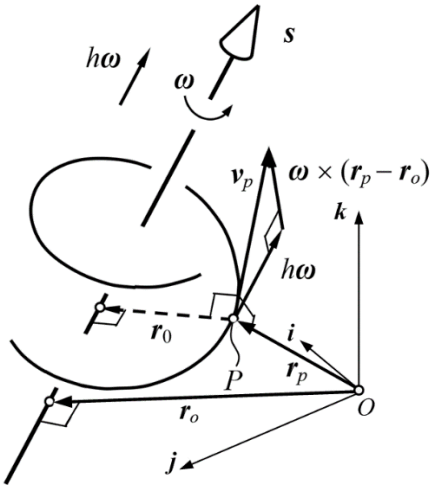

Figure 5.1 Instantaneous screw axis and the helicoidal velocity field

Figure 5.1 shows a body with an instantaneous angular velocity $\boldsymbol{\omega}$ about an axis located at $\boldsymbol{r}_O$ such that every point on the body has the same angular velocity $\boldsymbol{\omega}$. On the axis, there is only translational velocity $h\boldsymbol{\omega}$ along the axis. This axis is known as the *instantaneous screw axis* (ISA) which was first put forward by Mozzi (1763). The velocity $\boldsymbol{v}$ at point P of the body is resolved into two parts including the parallel component and the perpendicular component as follows,

$$\boldsymbol{v} = \boldsymbol{v}_s + \boldsymbol{v}_n = h\boldsymbol{\omega} + \boldsymbol{\omega} \times \left(\boldsymbol{r}_p - \boldsymbol{r}_o \right). \tag{5.6}$$

The set of all velocity vectors with respect to this instantaneous screw axis forms a helicoidal velocity field. When $\boldsymbol{r}_p = \boldsymbol{r}_o$ occurs, point P is on the screw axis, and the velocity $\boldsymbol{v}$ is equal to the pitch component $h\boldsymbol{\omega} = \boldsymbol{vs}$. When $\boldsymbol{r}_p = \boldsymbol{0}$, the origin is at point P and $\boldsymbol{v}_n$ is equal to the secondary part of the twist. Thus the secondary part of twist $\boldsymbol{T}$ is the instantaneous linear velocity of a point on the body instantaneously coincident with the origin O.

5.4 Linear Velocity from a Twist

5.4.1 Point on a Rigid Body Coincident with the Reference Point

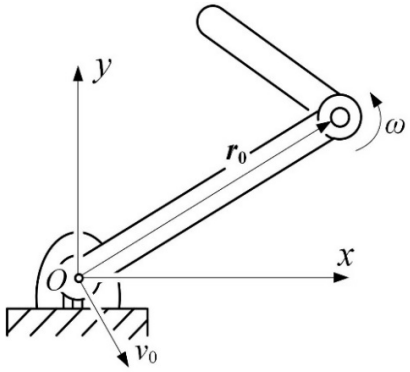

Figure 5.2 A Twist modeled by a revolute joint of a rigid body

Figure 5.2 depicts a rigid body rotates about a revolute joint with an instantaneous angular velocity $\boldsymbol{\omega}$, which is perpendicular to the *xy*-plane. Without loss of generality, we establish the reference coordinate frame in an arbitrary point O with the x-axis and y-axis locating in the plane and z-axis directing outward the plane. The corresponding twist of this rigid body can be expressed as,

$$\boldsymbol{T} = \|\boldsymbol{\omega}\|\boldsymbol{S} = \|\boldsymbol{\omega}\|\begin{bmatrix} \boldsymbol{s} \\ \boldsymbol{r}_0 \times \boldsymbol{s} \end{bmatrix} = \begin{bmatrix} \boldsymbol{\omega} \\ \boldsymbol{r}_0 \times \boldsymbol{\omega} \end{bmatrix} = \begin{bmatrix} \boldsymbol{\omega} \\ \boldsymbol{v}_0 \end{bmatrix}. \tag{5.7}$$

where $\|\boldsymbol{\omega}\|$ is the magnitude of the angular velocity of the rigid body, $\boldsymbol{S}$ is the joint screw associated with the revolute joint and $\boldsymbol{r}_0$ is the position vector that directs from the origin to the rotational axis to locate the screw axis $\boldsymbol{s}$, $\boldsymbol{v}_0 = \boldsymbol{r}_0 \times \boldsymbol{\omega}$ represents the instantaneous velocity of a point on this rigid body coincident with the origin *O* in the *xy* plane. The primary part $\boldsymbol{\omega}$, standing for the angular velocity, and the second part $\boldsymbol{v}_0$, standing for the linear velocity constitute the twist $\boldsymbol{T}$ to describe the instantaneous motion of a rigid body. It's not hard to recognize that the twist of a rigid body depends on the selection of the reference frame. If the origin of the reference frame concurs with the revolute

joint; that is $\boldsymbol{r}_0 = \mathbf{0}$, the linear velocity vanishes and the twist represents a pure differential rotation.

5.4.2 Geometrical Meaning of Secondary Part of a Screw

A serial manipulator is comprised of sequential rigid bodies connected with mechanical pairs. The twists that depict the instantaneous motion of components in this manipulator can be assembled to generate a resultant twist in such a way to describe the instantaneous motion of the end-effector with respect to the global reference frame.

The geometrical interpretation of the resultant twist is exemplified with a planar 3R serial mechanism, exhibited in Fig. 5.3.

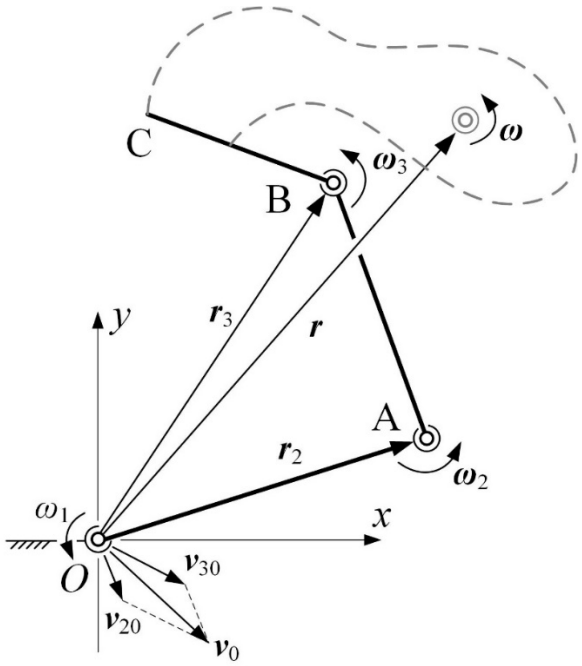

Figure 5.3 Geometry representation of a resultant twist in a serial manipulator

Links OA, AB and BC are serially connected by revolute joints O, A and B that constructs this 3R serial mechanism. The reference coordinate system is attached to ground with its origin O matching with the first revolute joint O and z-axis directing outward the plane. The time derivative of the rotation of link OA, which is noted as the twist of link OA with respect to the ground, can be expressed as

$$\boldsymbol{T}_1 = \begin{bmatrix} \boldsymbol{\omega}_1 \\ \boldsymbol{v}_{10} \end{bmatrix} = \|\boldsymbol{\omega}_1\| \begin{bmatrix} \boldsymbol{s}_1 \\ \boldsymbol{r}_1 \times \boldsymbol{s}_1 \end{bmatrix} = \|\boldsymbol{\omega}_1\| \boldsymbol{S}_1 . \tag{5.8}$$

where $\boldsymbol{\omega}_1$ is the angular velocity of joint O, $\boldsymbol{v}_{10}$ is the linear velocity of link OA, which indicates the velocity of the point on OA coincident with the origin, $\boldsymbol{S}_1$ is the joint screw of joint O with $\boldsymbol{s}_1$ representing the direction vector of this joint screw. Similarly, the twist of link AB with respect to the link OA in the coordinate frame is described as

$$\boldsymbol{T}_2 = \begin{bmatrix} \boldsymbol{\omega}_2 \\ \boldsymbol{v}_{20} \end{bmatrix} = \|\boldsymbol{\omega}_2\| \begin{bmatrix} \boldsymbol{s}_2 \\ \boldsymbol{r}_2 \times \boldsymbol{s}_2 \end{bmatrix} = \|\boldsymbol{\omega}_2\| \boldsymbol{S}_2 . \tag{5.9}$$

where $\boldsymbol{\omega}_2$ is the angular velocity of joint A, $\boldsymbol{r}_2$ is the position vector that determines the position of screw axis $\boldsymbol{s}_2$ of the joint screw $\boldsymbol{S}_2$, $\boldsymbol{v}_{20}$ is the linear velocity of the point on link AB coincident with the origin O instantaneously.The twist of link BC with respect to link AB is described as

$$\boldsymbol{T}_3 = \begin{bmatrix} \boldsymbol{\omega}_3 \\ \boldsymbol{v}_{30} \end{bmatrix} = \|\boldsymbol{\omega}_3\| \begin{bmatrix} \boldsymbol{s}_3 \\ \boldsymbol{r}_3 \times \boldsymbol{s}_3 \end{bmatrix} = \|\boldsymbol{\omega}_3\| \boldsymbol{S}_3 . \tag{5.10}$$

where $\boldsymbol{\omega}_3$ is the angular velocity of joint A, $\boldsymbol{r}_3$ is the position vector that positions the screw axis $\boldsymbol{s}_3$ of the joint screw $\boldsymbol{S}_3$, $\boldsymbol{v}_{30}$ is the instantaneous linear velocity of the point on link AB coincident with the origin O.

This 3R serial mechanism is a typical planar manipulator with its distal link commonly selected as the end-effector; that is link BC in Fig. 5.3. The twist of the end-effector, which indicates the instantaneous velocity of link BC with respect to the ground, is a combination of twists of the previous links in this serial chain, which is given by

$$\boldsymbol{T} = \boldsymbol{T}_1 + \boldsymbol{T}_2 + \boldsymbol{T}_3 . \tag{5.11}$$

The above equation can be rearranged in another form as

$$\boldsymbol{T} = \begin{bmatrix} \boldsymbol{\omega}_1 \\ \boldsymbol{v}_{10} \end{bmatrix} + \begin{bmatrix} \boldsymbol{\omega}_2 \\ \boldsymbol{v}_{20} \end{bmatrix} + \begin{bmatrix} \boldsymbol{\omega}_3 \\ \boldsymbol{v}_{30} \end{bmatrix} = \begin{bmatrix} \boldsymbol{\omega}_1 + \boldsymbol{\omega}_2 + \boldsymbol{\omega}_3 \\ \boldsymbol{v}_{10} + \boldsymbol{v}_{20} + \boldsymbol{v}_{30} \end{bmatrix}. \tag{5.12}$$

It can be seen from Eq. (5.12) that the sum of twists of previous links composes the resultant twist, of which the resultant angular velocity is perpendicular the xy-plane, and resultant linear velocity, shown in Fig.5.3, represents the instantaneous motion of a point on link BC matching the origin. Generally, the twist of the output link BC about the ground can be expressed in a general representation as,

$$\boldsymbol{T} = \begin{bmatrix} \boldsymbol{\omega} \\ \boldsymbol{v} \end{bmatrix} = \|\boldsymbol{\omega}\| \begin{bmatrix} \boldsymbol{s} \\ \boldsymbol{r} \times \boldsymbol{s} \end{bmatrix} \tag{5.13}$$

where $\boldsymbol{s}$ indicates the instantaneous screw axis (ISA) of the twist $\boldsymbol{T}$, and $\boldsymbol{r}$ is the position vector from the origin pointing to the screw axis. Combining the Eqs. (5.12) and (5.13) yields the resultant angular velocity and resultant linear velocity of the end-effector BC as follows

$$\boldsymbol{\omega} = \boldsymbol{\omega}_1 + \boldsymbol{\omega}_2 + \boldsymbol{\omega}_3 , \tag{5.14}$$

$$\boldsymbol{v} = \boldsymbol{v}_{10} + \boldsymbol{v}_{20} + \boldsymbol{v}_{30} . \tag{5.15}$$

It can be seen from Eqs. (5.14), the resultant angular velocity which composes the twist of the effector in a serial robot is the sum of the angular velocities of previous links. The direction of the angular velocity follows the ISA of the resultant twist. In addition, the linear velocity which composes the secondary part of the resultant twist is the sum of the linear velocities of previous links, and its direction is compounded by the each individual elements.

5.4.3 Position Vector of the Resultant Twist

It is illustrated that the angular velocity $\boldsymbol{\omega}_1$, $\boldsymbol{\omega}_2$ and $\boldsymbol{\omega}_3$ have the same direction in Fig. 5.3 that points outward the plane, so the magnitude of resultant angular velocity $\boldsymbol{\omega}$ is

$$\|\boldsymbol{\omega}\| = \|\boldsymbol{\omega}_1 + \boldsymbol{\omega}_2 + \boldsymbol{\omega}_3\| . \tag{5.16}$$

Substituting linear velocities of the Eqs. (5.8) to (5.10) into Eq. (5.16) yields

$$\|\boldsymbol{\omega}\|(\boldsymbol{r} \times \boldsymbol{s}) = \|\boldsymbol{\omega}_1\|(\boldsymbol{r}_1 \times \boldsymbol{s}_1) + \|\boldsymbol{\omega}_2\|(\boldsymbol{r}_2 \times \boldsymbol{s}_2) + \|\boldsymbol{\omega}_3\|(\boldsymbol{r}_3 \times \boldsymbol{s}_3) . \tag{5.17}$$

Since $\boldsymbol{s}_1$, $\boldsymbol{s}_2$ and $\boldsymbol{s}_3$ have the same direction with s, the above equation can be written in a compact form as

$$\|\boldsymbol{\omega}\|(\boldsymbol{r}\times\boldsymbol{s}) = \left(\|\boldsymbol{\omega}_1\|\boldsymbol{r}_1 + \|\boldsymbol{\omega}_2\|\boldsymbol{r}_2 + \|\boldsymbol{\omega}_3\|\boldsymbol{r}_3\right)\times\boldsymbol{s}\,. \tag{5.18}$$

The direction vector $\boldsymbol{s}_i$ of the joint screw $\boldsymbol{S}_i$ (i=1,2,3) align with the z-axis, which has the relation $\boldsymbol{s}_1$=$\boldsymbol{s}_2$=$\boldsymbol{s}_3$=$\boldsymbol{s}$, the position vector of the resultant twist that situates the ISA is the linear combination of weighted position vectors of all the joints, which is expressed as

$$\boldsymbol{r} = \frac{\|\boldsymbol{\omega}_1\|}{\|\boldsymbol{\omega}\|}\boldsymbol{r}_1 + \frac{\|\boldsymbol{\omega}_2\|}{\|\boldsymbol{\omega}\|}\boldsymbol{r}_2 + \frac{\|\boldsymbol{\omega}_3\|}{\|\boldsymbol{\omega}\|}\boldsymbol{r}_3\,. \tag{5.19}$$

The position vectors of all the joint screws and corresponding joint rates comprise the position vector that determines the location of the ISA associated with the resultant twist of the end-effector.

5.4.4 Coordinated ISA of the End-Effector of a Serial Manipulator

As mentioned, the instantaneous motion of a rigid body composes of a differential rotation about a unique axis and the differential translation along this axis. This axis is named as the instantaneous screw axis of this differential motion. Suppose an arbitrary point Q is located at the ISA, it can thus be seen that the linear velocity of point Q is equal to translational velocity along this ISA. The twist of Q is given by

$$\boldsymbol{T} = \begin{bmatrix} \boldsymbol{\omega}_q \\ \boldsymbol{v}_{q0} \end{bmatrix} = \begin{bmatrix} \boldsymbol{\omega}_q \\ \boldsymbol{r}_{q0} \times \boldsymbol{\omega}_q + h\boldsymbol{\omega}_q \end{bmatrix}. \tag{5.20}$$

where $\boldsymbol{\omega}_q$, $\boldsymbol{v}_{q0}$, and h represent the angular velocity, linear velocity and pitch of this instantaneous motion on point Q, respectively, and $\boldsymbol{r}_{q0}$ is perpendicular to the angular velocity vector $\boldsymbol{\omega}_q$. To obtain the position vector $\boldsymbol{r}_{q0}$, we take the cross product of $\boldsymbol{\omega}_q$ and $\boldsymbol{v}_{q0}$, that yields

$$\boldsymbol{\omega}_q \times \boldsymbol{v}_{q0} = \boldsymbol{\omega}_q \times \left(\boldsymbol{r}_{q0} \times \boldsymbol{\omega}_q\right) = \boldsymbol{r}_{q0}\left(\boldsymbol{\omega}_q \cdot \boldsymbol{\omega}_q\right) - \boldsymbol{\omega}_q\left(\boldsymbol{\omega}_q \cdot \boldsymbol{r}_{q0}\right) = \boldsymbol{\omega}_q^2 \boldsymbol{r}_{q0}. \tag{5.21}$$

Dividing both sides of the Eq. (5.21) by $\boldsymbol{\omega}_q^2$ yields,

$$\boldsymbol{r}_{q0} = \frac{\boldsymbol{\omega}_q \times \boldsymbol{v}_{q0}}{\boldsymbol{\omega}_q^2}. \tag{5.22}$$

Equation (5.22) shows that the position vector of point Q is calculated by the inverse square of the angular velocity times cross product of the angular velocity and instantaneous linear velocity of point Q. As Q is an arbitrary point on the ISA, its position can be expressed as,

$$\boldsymbol{r}_q = \boldsymbol{r}_{q0} + \lambda\boldsymbol{\omega}_q = \frac{\boldsymbol{\omega}_q \times \boldsymbol{v}_{q0}}{\boldsymbol{\omega}_q^2} + \lambda\boldsymbol{\omega}_q \tag{5.23}$$

where λ is an arbitrary scalar.

The ISA of the end-effector in a serial manipulator can be obtained from Eq. (5.23) by replacing the angular velocity and linear velocity with the resultant angular velocity and

velocity of the end-effector, whose points on the axis only have the angular velocity and the linear velocity vanishes.

5.5 Screw based Jacobian Derivation of Serial Robots

5.5.1 Jacobian Matrix of a Planar Serial Manipulator

As a fundamental topic in robotics, kinematics play a crucial role in identifying the functionality and performance of a robot. The mathematical relation that maps the joint displacements to the position and orientation of the end-effector of a manipulator forms the forward kinematics analysis, whereas the inverse kinematics relates the end-effector configuration to joint movements. The first-order kinematics analysis gives the velocity map that establishes the relationship between joint rates and velocity state of the end-effector, which is also known as Jacobian matrix or Jacobian. Screw algebra has the capability to formulate the Jacobian to bridge the velocity map from joint space to task space of a manipulator.

Figure 5.4 displays a planar 3R serial robot with the distal link as the end-effector. The reference coordinate {O-*xyz*} is established at the origin O with the *x*-axis aligns the horizontal line and *z*-axis directs outward the plane. The three links OA, AB, and BC are serially connected through revolute pair with the joint axis perpendicular to the plane. The displacement of joint O, which represents the relative rotation of link OA with respect to the x-axis of the coordinate systems, is denoted as θ_1. Similar to this definition, the displacements of joint B and joint C are described as θ_2 and θ_3, respectively.

We derive the screw algebra based Jacobian of the 3R planar serial manipulator. In the reference coordinate frame {O-*xyz*}, the axes of the revolute joints O, A, B have the same direction with *z*-axis as $\boldsymbol{s}_1 = \boldsymbol{s}_2 = \boldsymbol{s}_3 = [0, 0, 1]^T$. The position vectors that locate the joint A and B can be derived from the geometry of the manipulator as $\boldsymbol{r}_A = [\boldsymbol{l}_1 c\theta_1, \boldsymbol{l}_1 s\theta_1, 0]^T$, and $\boldsymbol{r}_B = [\boldsymbol{l}_1 c\theta_1 + \boldsymbol{l}_2 c\theta_{12}, \boldsymbol{l}_1 c\theta_1 + \boldsymbol{l}_2 c\theta_{12}, 0]^T$, where *s* and *c* stand for the sine and cosine functions, and θ_{12} stands $\theta_1+\theta_2$.

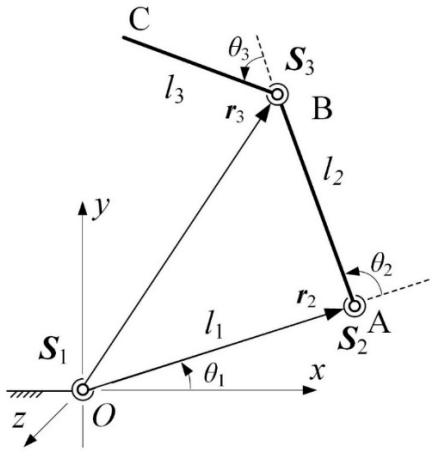

Figure 5.4 A 3R planar serial manipulator

The normalized motion screws of the revolute joints O, A, and B are given by in the reference frame as,

$$\boldsymbol{S}_1 = \begin{bmatrix} \boldsymbol{z} \\ \boldsymbol{0} \end{bmatrix} = [0, 0, 1, 0, 0, 0]^T \tag{5.24}$$

$$\boldsymbol{S}_2 = \begin{bmatrix} \boldsymbol{z} \\ \boldsymbol{r}_2 \times \boldsymbol{z} \end{bmatrix} = [0 \quad 0 \quad 1 \quad l_1 \mathrm{s}\theta_1 \quad -l_1 \mathrm{c}\theta_1 \quad 0]^T \tag{5.25}$$

$$\boldsymbol{S}_3 = \begin{bmatrix} \boldsymbol{z} \\ \boldsymbol{r}_3 \times \boldsymbol{z} \end{bmatrix} = [0 \quad 0 \quad 1 \quad l_1 \mathrm{s}\theta_1 + l_2 s\theta_{12} \quad -l_1 \mathrm{c}\theta_1 - l_2 c\theta_{12} \quad 0]^T \tag{5.26}$$

The twist of the link BC with respect to the ground is expressed by substituting Eqs. (5.24) to (5.26) into Eq. (5.11) as follows,

$$\boldsymbol{T} = \begin{bmatrix} \boldsymbol{\omega}_{BC} \\ \boldsymbol{v}_{BC} \end{bmatrix} = \dot{\theta}_1 \boldsymbol{S}_1 + \dot{\theta}_2 \boldsymbol{S}_2 + \dot{\theta}_3 \boldsymbol{S}_3 = \begin{bmatrix} \boldsymbol{S}_1 & \boldsymbol{S}_2 & \boldsymbol{S}_3 \end{bmatrix} \begin{bmatrix} \dot{\theta}_1 \\ \dot{\theta}_2 \\ \dot{\theta}_3 \end{bmatrix} = \boldsymbol{J}\dot{\boldsymbol{\theta}} \tag{5.27}$$

where the joint velocity vector $\dot{\boldsymbol{\theta}} = \begin{bmatrix} \dot{\theta}_1 & \dot{\theta}_2 & \dot{\theta}_3 \end{bmatrix}^{\mathrm{T}}$ and Jacobin is

$$\boldsymbol{J} = \begin{bmatrix} 0 & 0 & 0 \\ 0 & 0 & 0 \\ 1 & 1 & 1 \\ 0 & l_1 s\theta_1 & l_1 \mathrm{s}\,\theta_1 + l_2 s\theta_{12} \\ 0 & -l_1 c\theta_1 & -l_1 c\theta_1 - l_2 cs\theta_{12} \\ 0 & 0 & 0 \end{bmatrix} \tag{5.28}$$

The columns of the Jacobian are the unit joint screws of this manipulator, while their corresponding magnitudes comprise the joint velocity vector. It can be seen from the Eq. (5.27) that the screw theory based Jacobian is irrelevant with the distal joint variable.

5.5.2 Resultant Twist of a Spatial Serial Manipulator

It can be seen from the Eq. (5.11) the twist of the end-effector in a 3R serial manipulator is the sum of the twists of previous links. To be more general, the twist of a serial robot is the assemblage of twists of previous links as,

$$\boldsymbol{T} = \begin{bmatrix} \boldsymbol{\omega} \\ \boldsymbol{v} \end{bmatrix} = \sum_{i=1}^{n} \boldsymbol{T}_i = \sum_{i=1}^{n} \dot{q}_i \boldsymbol{S}_i \tag{5.29}$$

where $\boldsymbol{\omega}$ is the angular velocity of the end-effector, while $\boldsymbol{v}$ is the linear velocity coincident with the origin of the reference coordinate frame, $\dot{q}_i$ is the rate of change of each joint, and $\boldsymbol{S}_i$ is the unit screw associated with the joint axis in this manipulator. The Jacobian can be obtained if all the joint screws of a serial manipulator are identified in one coordinate frame. It turns out that the coordinates of the joint screws can be written in any reference frames by investigating the geometry of the manipulator. As the joint axis and its position determine the corresponding joint screw for typical serial manipulators composed of prismatic joints or revolute joints, the Jacobian is accomplished through the geometry of the manipulator.

5.6 Conclusions

This chapter investigated the motion of a rigid body in three dimensions that could be decomposed into a rotation about an axis and a translation parallel to that axis. The motion could be represented by a twist with its primary part indicating the angular velocity of the rigid body, and secondary part indicating the instantaneous linear velocity.

The resultant twist of a serial manipulator could be presented by the assembly of unit joint screws with their corresponding velocity amplitudes. The ISA of the resultant twist was coordinated through the condition of zero linear velocity on this axis, and its position vector was formulated by the combination of weighted position vectors of joint screws. The screw-based Jacobian of a planar serial manipulator was established after identifying all the joint screws, followed by the expansion to general serial manipulators.

Chapter 6 Geometrical Interpretation of the Transformation between Robot Jacobian and Screw Jacobian

6.1 Introduction

This chapter investigates the relationship of the Jacobians of a serial manipulator with the derivative method and screw theory. Forward kinematics analysis of a typical 3R planner manipulator is formulated, followed by its time derivative to generate the conventional Jacobian. Its counterpart, the screw-based Jacobian is developed with the assemblage of all the unit joint screws. The comparison from both geometrical meaning and physical meaning is conducted in an attempt to accomplish the reconciliation of the two methods. Further, a more complicated spatial kinematic chain is investigated to verify the derivation.

The transformation between conventional Jacobian and screw Jacobian is revealed through investigating the geometry meaning of the resultant twist of the end-effector and the velocity of a reference point. The Jacobian matrices are formulated by the derivative method and screw algebra and their relation is interpreted.

6.2 Derivative Method based Jacobian of a 3R Planar Serial Manipulator

6.2.1 Linear Velocity of a 3R Planar Serial Manipulator

The position and orientation of a serial manipulator can be obtained in the wake of forward kinematics analysis. The Jacobian matrix that describes the motion of a rigid body in the velocity field is conventionally derived through the differential kinematics. The forward kinematics of a serial manipulator can be developed in various methods such as Denavit-Hartenberg matrices [102], screw algebra, etc. A typical planar manipulator is shown in Fig. 5.4. To acquire the translational velocity of point C, a geometric method is to find its position and then take its time derivative. The position of point C in the reference coordinate frame {O-*xyz*} can be derived from the geometry of the 3R manipulator as,

$$P_C = \begin{bmatrix} x_{\mathrm{C}} \\ y_{\mathrm{C}} \\ z_{\mathrm{C}} \end{bmatrix} = \begin{bmatrix} l_1 \mathrm{c}\,\theta_1 + l_2 \mathrm{c}\,\theta_{12} + l_3 \mathrm{c}\,\theta_{123} \\ l_1 \mathrm{s}\,\theta_1 + l_2 \mathrm{s}\,\theta_{12} + l_3 \mathrm{s}\,\theta_{123} \\ 0 \end{bmatrix} \tag{6.1}$$

where θ_{ijk} is the simplified representation of $\theta_i + \theta_j + \theta_k$. Taking the time derivation of the position of point C with respect to the global frame gives its linear velocity $\boldsymbol{v}_{\mathrm{C}}$, which can be expressed as,

$$\boldsymbol{v}_C = \begin{bmatrix} \dot{x}_C \\ \dot{y}_C \\ \dot{z}_C \end{bmatrix} = \begin{bmatrix} -\dot{\theta}_1 l_1 s\theta_1 - \dot{\theta}_{12} l_2 s\theta_{12} - \dot{\theta}_{123} l_3 s\theta_{123} \\ \dot{\theta}_1 l_1 c\theta_1 + \dot{\theta}_{12} l_2 c\theta_{12} + \dot{\theta}_{123} l_3 c\theta_{123} \\ 0 \end{bmatrix} \tag{6.2}$$

where $\dot{\theta}_{123}$ stands for $\dot{\theta}_1 + \dot{\theta}_2 + \dot{\theta}_3$. Different from the linear velocity derived from screw algebra which indicates the instantaneous velocity of the point on a rigid body coincident with the origin, the linear velocity $\boldsymbol{v}_C$ represents the velocity of point C with respect to the origin. The two types of velocities can both describe the instantaneous state of the end-effector of a serial manipulator, and are usually not identical. The relation of these velocities will be discussed in the following sections.

6.2.2 Jacobian Generation based on the Derivative Method

Shown in Eq. (6.2), the linear velocity of point C is determined by the angular velocity of all the joints connected from the ground and current configuration of the manipulator. From the geometry of the manipulator, the orientation of link BC is the sum of joint displacement of joint O, A and B, which is expressed as,

$$\theta_C = \theta_1 + \theta_2 + \theta_3 \tag{6.3}$$

Taking the time derivative of Eq. (6.3) yields the angular velocity of point C, which is written in a vector form as,

$$\boldsymbol{\omega}_C = \begin{bmatrix} 0 \\ 0 \\ \dot{\theta}_1 + \dot{\theta}_2 + \dot{\theta}_3 \end{bmatrix} \tag{6.4}$$

Combining the Eqs. (6.2) and (6.4) and rearranging the vectors yields the velocity of point C expressed in the reference frame as,

$$\boldsymbol{V}_C = \begin{bmatrix} \boldsymbol{\omega}_C \\ \boldsymbol{v}_C \end{bmatrix} = \begin{bmatrix} 0 \\ 0 \\ 1 \\ -\dot{\theta}_1 l_1 s\theta_1 - \dot{\theta}_{12} l_2 s\theta_{12} - \dot{\theta}_{123} l_3 s\theta_{123} \\ \dot{\theta}_1 l_1 c\theta_1 + \dot{\theta}_{12} l_2 c\theta_{12} + \dot{\theta}_{123} l_3 c\theta_{123} \\ 0 \end{bmatrix} = \mathbf{J}_C \dot{\boldsymbol{\theta}} \tag{6.5}$$

where the joint velocity vector $\dot{\boldsymbol{\theta}} = \begin{bmatrix} \dot{\theta}_1 & \dot{\theta}_2 & \dot{\theta}_3 \end{bmatrix}^{\mathrm{T}}$,and the screw algebra based Jacobian

$$\mathbf{J}_C = \begin{bmatrix} 0 & 0 & 0 \\ 0 & 0 & 0 \\ 1 & 1 & 1 \\ -l_1 s\theta_1 - l_2 s\theta_{12} - l_3 s\theta_{123} & -l_2 s\theta_{12} - l_3 s\theta_{123} & -l_3 s\theta_{123} \\ l_1 c\theta_1 + l_2 c\theta_{12} + l_3 c\theta_{123} & l_2 c\theta_{12} + l_3 c\theta_{123} & l_3 c\theta_{123} \\ 0 & 0 & 0 \end{bmatrix} \tag{6.6}$$

The Jacobian matrix derived in Eq. (6.5) depends on the instantaneous geometry of the manipulator and is relevant with all joint displacements, which is different from the Jacobian acquired in Eq. (5.28) by screw algebra irrelevant with the last joint displacement.

6.3 Reconciliation of the Jacobian based on Screw Algebra and Derivative Method

6.3.1 Transformation Using a Skew-Symmetric Matrix

The displacement of a line vector can be performed by a *screw displacement operator,* which is expressed as a 3×3 dual-number orthogonal matrix or a 6×6 matrix. In the form

of the 3×3 dual-number matrix, a displacement acting on a line vector is given by the following operator

$$\mathbf{R}+\varepsilon\,\mathbf{AR}\,, \tag{6.7}$$

where matrix **R** is a 3×3 rotation matrix that belongs to the *special orthogonal group SO*(3) as the primary part of the dual-number matrix, matrix **A** is a skew-symmetric matrix representing the translation in the form of,

$$\mathbf{A}=\begin{bmatrix} 0 & -d_z & d_y \\ d_z & 0 & -d_x \\ -d_y & d_x & 0 \end{bmatrix}=\left[\boldsymbol{d}\times\right] \tag{6.8}$$

This matrix leads to a translation of the rotated line vector with a distance ***d***. Besides this representation, the dual-number matrix can be expressed in the form of a 6×6 finite displacement-screw matrix as

$$\mathbf{T}=\begin{bmatrix} \mathbf{R} & \mathbf{0} \\ \mathbf{A}\,\mathbf{R} & \mathbf{R} \end{bmatrix}, \tag{6.9}$$

Where matrices **R** and **AR** are the primary part and second part, respectively. Acting the 6×6 displacement matrix in Eq. (6.9) on a line vector results in the corresponding displacement of this line vector. Further, exerting this 6×6 finite displacement-screw matrix on a screw, the new screw after the displacement is given by,

$$\boldsymbol{S}'=\mathbf{T}\boldsymbol{S}=\begin{bmatrix} \mathbf{R} & \mathbf{0} \\ \mathbf{AR} & \mathbf{R} \end{bmatrix}\begin{bmatrix} \boldsymbol{s} \\ \boldsymbol{s}_0 \end{bmatrix}=\begin{bmatrix} \mathbf{R}\boldsymbol{s} \\ \mathbf{AR}\boldsymbol{s}+\mathbf{R}\boldsymbol{s}_0 \end{bmatrix}=\begin{bmatrix} \mathbf{R}\boldsymbol{s} \\ \left[\boldsymbol{d}\times\right]\mathbf{R}\boldsymbol{s}+\mathbf{R}\boldsymbol{s}_0 \end{bmatrix} \tag{6.10}$$

6.3.2 Reconciliation of the Jacobian of a 3R Serial Manipulator

The physical meaning of the linear velocity $\boldsymbol{v}_{\mathrm{C}}$ exhibited in Eq. (6.2) is the linear velocity of point C with respect to the origin expressed in the reference coordinate frame. Dissimilarly, the physical meaning of the twist of link BC exhibited in Eq. (5.27) comprise the angular velocity and linear velocity of link BC, of which the linear velocity $\boldsymbol{v}_{C0}$ represents the instantaneous linear velocity of a point on the link BC instantaneously coincident with the origin O. Based on this definition, we can draw the conclusion that $\boldsymbol{v}_{\mathrm{C0}}$ and $\boldsymbol{v}_{C}$ are the linear velocities of link BC expressed in different reference points, namely point C and the point instantaneously coincident with the origin O, respectively. As the one rigid body has the same angular velocity everywhere, we adopt $\boldsymbol{\omega} = \boldsymbol{\omega}_{\mathrm{C}} = \boldsymbol{\omega}_{\mathrm{BC}}$ for simplified notation. This mentioned interrelation leads to translating $\boldsymbol{v}_{\mathrm{C0}}$ from the origin to point C to acquire $\boldsymbol{v}_{\mathrm{C}}$, which is given by,

$$\boldsymbol{v}_{\mathrm{C}} = \boldsymbol{\omega} \times \boldsymbol{r}_{\mathrm{OB}} + \boldsymbol{v}_{\mathrm{BC}} \tag{6.11}$$

The Eq. (6.11) is demonstrated in **Appendix A**. Rewriting the Eq. (6.11) with angular velocities in a matrix form as,

$$\begin{bmatrix} \boldsymbol{\omega}_{\mathrm{C}} \\ \boldsymbol{v}_{\mathrm{C}} \end{bmatrix} = \begin{bmatrix} \boldsymbol{\omega} \\ \boldsymbol{\omega} \times \boldsymbol{r}_{\mathrm{OB}} + \boldsymbol{v}_{\mathrm{BC}} \end{bmatrix} = \begin{bmatrix} \mathbf{I} & \boldsymbol{0} \\ -[\mathbf{r}_{OB} \times] & \mathbf{I} \end{bmatrix} \begin{bmatrix} \boldsymbol{\omega}_{\mathrm{BC}} \\ \boldsymbol{v}_{\mathrm{BC}} \end{bmatrix} \tag{6.12}$$

Substituting Eqs. (5.27) and (6.5) into Eq.(6.12) to obtain the relationship of Jacobian matrices derived by the derivative method and screw algebra which is given by,

$$\boldsymbol{V}_{\mathrm{C}} = \boldsymbol{J}_{\mathrm{C}}\dot{\boldsymbol{\theta}} = \begin{bmatrix} \mathbf{I} & \boldsymbol{0} \\ -[\mathbf{r}_{OB}\times] & \mathbf{I} \end{bmatrix} \boldsymbol{J}\dot{\boldsymbol{\theta}} \tag{6.13}$$

The Jacobian acquired from derivative method and the Jacobian acquired from screw algebra have the following relation as,

$$\mathbf{J}_D = \begin{bmatrix} \boldsymbol{I} & \boldsymbol{0} \\ -[\mathbf{r}_{OB}\times] & \boldsymbol{I} \end{bmatrix} \boldsymbol{J}_S = \begin{bmatrix} \boldsymbol{I} & \boldsymbol{0} \\ [\mathbf{r}_{BO}\times] & \boldsymbol{I} \end{bmatrix} \boldsymbol{J}_S = \mathrm{Ad}(g)\mathbf{J}_S \tag{6.14}$$

where g has the effect of translation from point B to origin O.

More generally, the relationship between the twist of a rigid body and the velocity of point P on this rigid body can be established by substituting the secondary part of Eq.(5.5) into Eq. (5.6), which yields,

$$\boldsymbol{v} = h\boldsymbol{\omega} - \boldsymbol{\omega}\times\boldsymbol{r}_o + \boldsymbol{\omega}\times\boldsymbol{r}_p = \boldsymbol{v}_o + \boldsymbol{\omega}\times\boldsymbol{r}_p \tag{6.15}$$

Equation (6.15) can be written in a similar matrix form with Eq. (5.15) as,

$$\begin{bmatrix} \boldsymbol{\omega} \\ \boldsymbol{v} \end{bmatrix} = \begin{bmatrix} \boldsymbol{\omega} \\ \boldsymbol{v}_o + \boldsymbol{\omega}\times\boldsymbol{r}_p \end{bmatrix} = \begin{bmatrix} \mathbf{I} & \mathbf{0} \\ -[\boldsymbol{r}_p\times] & \mathbf{I} \end{bmatrix} \begin{bmatrix} \boldsymbol{\omega} \\ \boldsymbol{v}_o \end{bmatrix} = \begin{bmatrix} \mathbf{I} & \mathbf{0} \\ -[\boldsymbol{r}_p\times] & \mathbf{I} \end{bmatrix} \boldsymbol{T} \tag{6.16}$$

Equations (6.13) and (6.16) illustrates the interrelation of velocities of a rigid body with different reference points, typically a point attached to the end-effector and the point instantaneous coincident with the origin. The velocity of a point in the end-effector, or the origin of the tool frame of the serial manipulator, can be generated by the differentiation of its position and orientation calculated by transformation matrices with

DH parameters. The screw algebra is another method to acquire velocity of the point on the output link instantaneous matching the origin of the reference frame. Reconciliation of the two velocities is built by the velocity translation formulated in Eq. (6.12), followed by the reconciliation of Jacobian matrices obtained from the derivative method and screw algebra formulated in Eq. (6.13)

6.4 Reconciliation of Jacobian Matrices a Spatial Serial Manipulator

6.4.1 Screw Algebra based Jacobian for a Spatial Serial Manipulator

The transformation between screw based Jacobian and derivative method based Jacobian was proposed, followed by the verification of a planar serial Manipulator. In this section, a more complicated example was used to formulate the Jacobian matrices.

Figure 6.1 shows a RRPRR spatial serial manipulator. The global coordinate frame $\{O_0\text{-}x_0y_0z_0\}$ is fixed at point O_0, its z_0-axis aligns along the axis of the first revolute joint, and ix_0-axis lies along the axis of the second revolute joint in its initial configuration. The motion screw $\boldsymbol{S}_i$ (i = 1 to 5) are attached to each joint shown in Fig. 6.1.

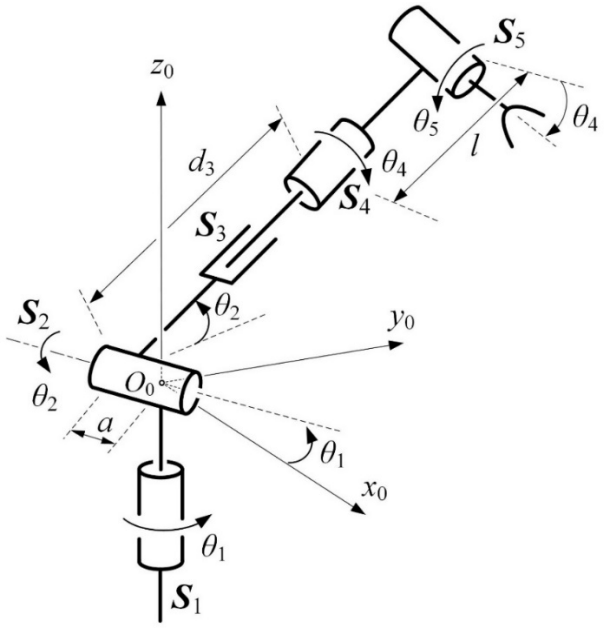

Figure 6.1 Screw coordinates with respect to the global reference frame of A RRPRR spatial serial manipulator

Through the geometrical relation of joint axes of this manipulator, the unit motion screws of each joint can be express in the global coordinate frame as,

$$\boldsymbol{S}_1 = \left(0\,,0\,,1\,,0\,,0\,,0\right)^{\mathrm{T}} \tag{6.17}$$

$$\boldsymbol{S}_2 = \left(\mathrm{c}\,\theta_1\,,\mathrm{s}\,\theta_1\,,0\,,0\,,0\,,0\right)^{\mathrm{T}} \tag{6.18}$$

$$\boldsymbol{S}_3 = \left(0\,,0\,,0\,,-\mathrm{c}\,\theta_2\mathrm{s}\theta_1\,,\mathrm{c}\,\theta_2\mathrm{c}\theta_1\,,\mathrm{s}\theta_2\right)^{\mathrm{T}} \tag{6.19}$$

$$\boldsymbol{S}_4 = \left(-\mathrm{c}\,\theta_2\mathrm{s}\theta_1\,,\mathrm{c}\,\theta_2\mathrm{c}\theta_1\,,\mathrm{s}\theta_2\,,-a\mathrm{s}\theta_1\mathrm{s}\theta_2\,,a\mathrm{c}\theta_1\mathrm{s}\theta_2\,,-a\mathrm{c}\,\theta_2\right)^{\mathrm{T}} \tag{6.20}$$

$$\boldsymbol{S}_5 = \left(\mathrm{c}\,\theta_1\mathrm{c}\,\theta_4 - \mathrm{s}\theta_1\mathrm{s}\,\theta_2\mathrm{s}\theta_4\,,\mathrm{c}\,\theta_4\mathrm{s}\theta_1 + \mathrm{c}\,\theta_1\mathrm{s}\,\theta_2\mathrm{s}\theta_4\,,-\mathrm{c}\,\theta_2\mathrm{s}\theta_4\,,p_5\,,q_5\,,r_5\right)^{\mathrm{T}} \tag{6.21}$$

where

$$\begin{cases} p_5 = \left(l+d_3\right)\left(-\mathrm{c}\,\theta_1 s\theta_4 - \mathrm{s}\theta_1\mathrm{s}\,\theta_2\mathrm{c}\,\theta_4\right) + a\mathrm{s}\theta_1\mathrm{c}\,\theta_2 s\theta_4 \\ q_5 = \left(l+d_3\right)\left(-\mathrm{s}\theta_1 s\theta_4 + \mathrm{c}\,\theta_1\mathrm{s}\,\theta_2\mathrm{c}\,\theta_4\right) - a\mathrm{c}\,\theta_1\mathrm{c}\,\theta_2 s\theta_4 \\ r_5 = -\left(l+d_3\right)\mathrm{c}\,\theta_2\mathrm{c}\,\theta_4 - a\mathrm{s}\theta_2 s\theta_4 \end{cases} \tag{6.22}$$

The resultant twist of the end-effector is the assembly of unit joint screws derived in Eqs. (6.17) to (6.21) with their corresponding change rates according to Eq. (5.29), which is given by,

$$\boldsymbol{T} = \dot{\theta}_1\boldsymbol{S}_1 + \dot{\theta}_2\boldsymbol{S}_2 + \dot{d}_3\boldsymbol{S}_3 + \dot{\theta}_4\boldsymbol{S}_4 + \dot{\theta}_5\boldsymbol{S}_5 \tag{6.23}$$

The above equation can be written in the matrix form as,

$$\boldsymbol{T} = \mathbf{J}_s\dot{\boldsymbol{\theta}}, \tag{6.24}$$

where $\mathbf{J}_s$ is the Jacobian comprises of the joint screws $\mathbf{J}_s = \begin{bmatrix}\boldsymbol{S}_1 & \boldsymbol{S}_2 & \boldsymbol{S}_3 & \boldsymbol{S}_4 & \boldsymbol{S}_5\end{bmatrix}$, and $\dot{\boldsymbol{\theta}}$ is the joint velocity vector as $\dot{\boldsymbol{\theta}} = \begin{bmatrix}\dot{\theta}_1 & \dot{\theta}_2 & \dot{d}_3 & \dot{\theta}_4 & \dot{\theta}_5\end{bmatrix}^{\mathrm{T}}$. More specifically, each column of the screw based Jacobian the unit joint screws of this manipulator, which is expressed as,

$$\mathbf{J}_s = \begin{bmatrix} 0 & \mathrm{c}\theta_1 & 0 & -\mathrm{c}\theta_2\mathrm{s}\theta_1 & \mathrm{c}\theta_1\mathrm{c}\theta_4 - \mathrm{s}\theta_1\mathrm{s}\theta_2\mathrm{s}\theta_4 \\ 0 & \mathrm{s}\theta_1 & 0 & \mathrm{c}\theta_2\mathrm{c}\theta_1 & \mathrm{c}\theta_4\mathrm{s}\theta_1 + \mathrm{c}\theta_1\mathrm{s}\theta_2\mathrm{s}\theta_4 \\ 1 & 0 & 0 & \mathrm{s}\theta_2 & -\mathrm{c}\theta_2\mathrm{s}\theta_4 \\ 0 & 0 & -\mathrm{c}\theta_2\mathrm{s}\theta & -a\mathrm{s}\theta_1\mathrm{s}\theta_2 & p_5 \\ 0 & 0 & \mathrm{c}\theta_2\mathrm{c}\theta_1 & a\mathrm{c}\theta_1\mathrm{s}\theta_2 & q_5 \\ 0 & 0 & \mathrm{s}\theta_2 & -a\mathrm{c}\theta_2 & r_5 \end{bmatrix} \tag{6.25}$$

It can be seen from Eq. (6.25), the screw based Jacobian only depends on the current instantaneous geometry of the manipulator and is irrelevant with the last joint displacement.

6.4.2 Transformation Matrices of a Spatial Serial Manipulator

Establishing transformation matrices is another widely used method in robotics to conduct the kinematics analysis and, in particular, derive the position and orientation of the tool frame attached on the end-effector. A coordinate system is attached to each link illustrated in Fig. 6.2. A global coordinate frame is established the same as the global coordinate frame shown in Fig. 6.1.

In order to derive the overall transformation matrices of the manipulator, each individual transformation matrix has been derived based on the local coordinate system in Fig. 6.2.

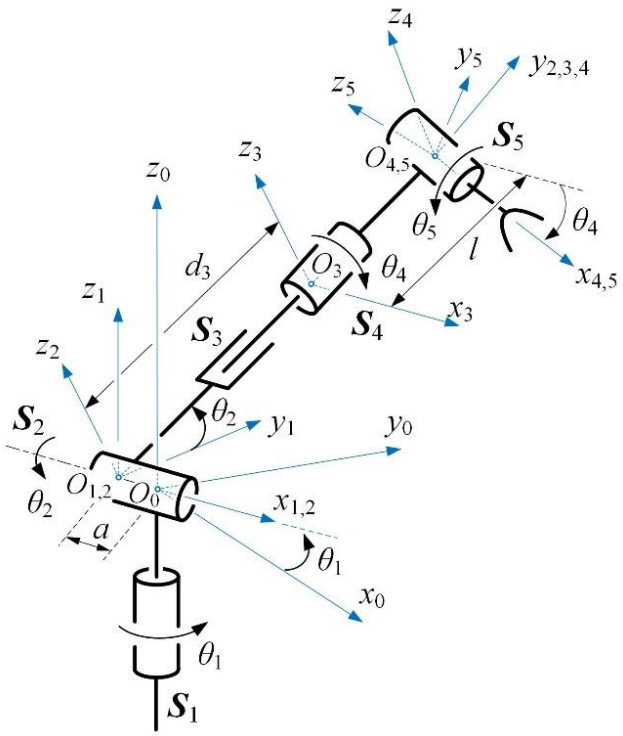

Figure 6.2 A spatial 5-DOF RRPRR serial manipulator

The transformation matrices between adjacent coordinate frames are calculated below as,

$$ {}^{0}\mathbf{T}_{1} = \begin{bmatrix} \mathrm{c}\theta_1 & -\mathrm{s}\theta_1 & 0 & -a\,\mathrm{c}\theta_1 \\ \mathrm{s}\theta_1 & \mathrm{c}\theta_1 & 0 & -a\,\mathrm{s}\theta_1 \\ 0 & 0 & 1 & 0 \\ 0 & 0 & 0 & 1 \end{bmatrix} \tag{6.26} $$

$$ {}^{1}\mathbf{T}_{2} = \begin{bmatrix} 1 & 0 & 0 & 0 \\ 0 & \mathrm{c}\theta_2 & -\mathrm{s}\theta_2 & 0 \\ 0 & \mathrm{s}\theta_2 & \mathrm{c}\theta_2 & 0 \\ 0 & 0 & 0 & 1 \end{bmatrix} \tag{6.27} $$

$$ {}^{2}\mathbf{T}_{3} = \begin{bmatrix} 1 & 0 & 0 & 0 \\ 0 & 1 & 0 & d_3 \\ 0 & 0 & 1 & 0 \\ 0 & 0 & 0 & 1 \end{bmatrix} \tag{6.28} $$

$$ {}^{3}\mathbf{T}_{4} = \begin{bmatrix} \mathrm{c}\theta_4 & 0 & \mathrm{s}\theta_4 & 0 \\ 0 & 1 & 0 & l \\ -\mathrm{s}\theta_4 & 0 & \mathrm{c}\theta_4 & 0 \\ 0 & 0 & 0 & 1 \end{bmatrix} \tag{6.29} $$

$$ {}^{4}\mathbf{T}_{5} = \begin{bmatrix} 1 & 0 & 0 & 0 \\ 0 & \mathrm{c}\theta_5 & -\mathrm{s}\theta_5 & 0 \\ 0 & \mathrm{s}\theta_5 & \mathrm{c}\theta_5 & 0 \\ 0 & 0 & 0 & 1 \end{bmatrix} \tag{6.30} $$

Multiplying Eqs.(6.26) to (6.30) yields,

$$ {}^{0}\mathbf{T}_{5} = {}^{0}\mathbf{T}_{1}\,{}^{1}\mathbf{T}_{2}\,{}^{2}\mathbf{T}_{3}\,{}^{3}\mathbf{T}_{4}\,{}^{4}\mathbf{T}_{5} = \begin{bmatrix} * & * & * & -a\mathrm{c}\theta_1 - \left(l + d_3\right)c\theta_2\mathrm{s}\theta_1 \\ * & * & * & -a\mathrm{s}\theta_1 + \left(l + d_3\right)c\theta_2\mathrm{c}\theta_1 \\ * & * & * & \left(l + d_3\right)\mathrm{s}\theta_2 \\ 0 & 0 & 0 & 1 \end{bmatrix} \tag{6.31} $$

The position of the origin of the tool frame $\{O_5\text{-}x_5y_5z_5\}$ is acquired as,

$$ {}^{0}\boldsymbol{P}_{O_5} = \left[-a\mathrm{c}\theta_1 - \left(l + d_3\right) c\theta_2 \mathrm{s}\theta_1,\ -a\mathrm{s}\theta_1 + \left(l + d_3\right) c\theta_2 \mathrm{c}\theta_1,\ \left(l + d_3\right) \mathrm{s}\theta_2 \right]^{\mathrm{T}}. \qquad (6.32) $$

6.4.3 Derivative Method based Jacobian for a Spatial Serial Manipulator

To derive the Jacobian matrix of the manipulator, we take the time derivative of the position of the tool frame origin in Eq.(6.32) with respect to the global frame, then its linear velocity and the corresponding Jacobian matrix are expressed in the global frame as,

$$ \begin{bmatrix} v_x \\ v_y \\ v_z \end{bmatrix} = \begin{bmatrix} \frac{\delta x}{\delta\theta_1} & \frac{\delta x}{\delta\theta_2} & \frac{\delta x}{\delta d_3} & \frac{\delta x}{\delta\theta_4} & \frac{\delta x}{\delta\theta_5} \\ \frac{\delta y}{\delta\theta_1} & \frac{\delta y}{\delta\theta_2} & \frac{\delta y}{\delta d_3} & \frac{\delta y}{\delta\theta_4} & \frac{\delta y}{\delta\theta_5} \\ \frac{\delta z}{\delta\theta_1} & \frac{\delta z}{\delta\theta_2} & \frac{\delta z}{\delta d_3} & \frac{\delta z}{\delta\theta_4} & \frac{\delta z}{\delta\theta_5} \end{bmatrix} \begin{bmatrix} \dot{\theta}_1 \\ \dot{\theta}_2 \\ \dot{d}_3 \\ \dot{\theta}_4 \\ \dot{\theta}_5 \end{bmatrix} = \mathbf{J}_v \begin{bmatrix} \dot{\theta}_1 \\ \dot{\theta}_2 \\ \dot{d}_3 \\ \dot{\theta}_4 \\ \dot{\theta}_5 \end{bmatrix} \qquad (6.33) $$

where the Jacobian matrix that maps the joint rates to the linear velocity of the end-effector is expressed as,

$$ \mathbf{J}_v = \begin{bmatrix} as\theta_1 - \left(l + d_3\right) c\theta_2 c\theta_1 & \left(l + d_3\right) s\theta_2 \mathrm{s}\theta_1 & -c\theta_2 \mathrm{s}\theta_1 & 0 & 0 \\ -ac\theta_1 - \left(l + d_3\right) c\theta_2 s\theta_1 & -\left(l + d_3\right) s\theta_2 \mathrm{c}\theta_1 & c\theta_2 \mathrm{c}\theta_1 & 0 & 0 \\ 0 & \left(l + d_3\right) c\theta_2 & \mathrm{s}\theta_2 & 0 & 0 \end{bmatrix} \qquad (6.34) $$

The Jacobian matrix that relates the joint rates to the angular velocity of the end effector is the linear combination of all angular velocity vectors of revolute joints, which is given by,

$$\boldsymbol{\omega} = \begin{bmatrix} \boldsymbol{z}_0 & \boldsymbol{x}_2 & \mathbf{0} & \boldsymbol{y}_4 & \boldsymbol{x}_4 \end{bmatrix} \begin{bmatrix} \dot{\theta}_1 \\ \dot{\theta}_2 \\ \dot{d}_3 \\ \dot{\theta}_4 \\ \dot{\theta}_5 \end{bmatrix} = \mathbf{J}_\omega \begin{bmatrix} \dot{\theta}_1 \\ \dot{\theta}_2 \\ \dot{d}_3 \\ \dot{\theta}_4 \\ \dot{\theta}_5 \end{bmatrix} \tag{6.35}$$

where the Jacobean matrix for the angular velocity is,

$$\mathbf{J}_\omega = \begin{bmatrix} \boldsymbol{z}_0 & \boldsymbol{x}_2 & \mathbf{0} & \boldsymbol{y}_4 & \boldsymbol{x}_4 \end{bmatrix} = \begin{bmatrix} 0 & \mathrm{c}\,\theta_1 & 0 & -\mathrm{c}\,\theta_2\mathrm{s}\,\theta_1 & -\mathrm{c}\,\theta_1\mathrm{c}\,\theta_3 + \mathrm{s}\,\theta_1\mathrm{s}\,\theta_2\mathrm{s}\,\theta_3 \\ 0 & \mathrm{s}\,\theta_1 & 0 & \mathrm{c}\,\theta_2\mathrm{c}\,\theta_1 & -\mathrm{c}\,\theta_3\mathrm{s}\,\theta_1 - \mathrm{c}\,\theta_1\mathrm{s}\,\theta_2\mathrm{s}\,\theta_3 \\ 1 & 0 & 0 & \mathrm{s}\,\theta_2 & \mathrm{c}\,\theta_2\mathrm{s}\,\theta_3 \end{bmatrix}. \tag{6.36}$$

Writing Eqs. (6.34) and (6.36) in a matrix form yields the derivative method based Jacobian, which is given by,

$$\mathbf{J}_\mathrm{D} = \begin{bmatrix} 0 & \mathrm{c}\,\theta_1 & 0 & -\mathrm{c}\,\theta_2\mathrm{s}\,\theta_1 & -\mathrm{c}\,\theta_1\mathrm{c}\,\theta_3 + \mathrm{s}\,\theta_1\mathrm{s}\,\theta_2\mathrm{s}\,\theta_3 \\ 0 & \mathrm{s}\,\theta_1 & 0 & \mathrm{c}\,\theta_2\mathrm{c}\,\theta_1 & -\mathrm{c}\,\theta_3\mathrm{s}\,\theta_1 - \mathrm{c}\,\theta_1\mathrm{s}\,\theta_2\mathrm{s}\,\theta_3 \\ 1 & 0 & 0 & \mathrm{s}\,\theta_2 & \mathrm{c}\,\theta_2\mathrm{s}\,\theta_3 \\ as\theta_1 - (l+d_3)c\theta_2c\theta_1 & (l+d_3)s\theta_2\mathrm{s}\,\theta_1 & -c\theta_2\mathrm{s}\,\theta_1 & 0 & 0 \\ -ac\theta_1 - (l+d_3)c\theta_2s\theta_1 & -(l+d_3)s\theta_2\mathrm{c}\,\theta_1 & c\theta_2\mathrm{c}\,\theta_1 & 0 & 0 \\ 0 & (l+d_3)c\theta_2 & \mathrm{s}\,\theta_2 & 0 & 0 \end{bmatrix} \tag{6.37}$$

Substituting Eq.(6.25) into Eq. (6.14) and replacing $\boldsymbol{r}_{\mathrm{OB}}$ with ${}^0\boldsymbol{P}_{O_5}$ derived in Eq. (6.32) generates the derivative method based Jacobian, which is equal to $\mathbf{J}_\mathrm{D}$ in Eq. (6.34). The

transformation of the screw based Jacobian and derivative method based Jacobian is verified.

6.5 Conclusions

This chapter revealed the interrelation of the screw-based Jacobian and derivative method-based Jacobian through investigating the geometrical meaning of a twist of a rigid body and the velocity of a reference point on this rigid body. Reconciliation of these two methods was formulated by using an adjoint transformation acting on a twist obtained by screw algebra.

Exampled by a planar 3R serial manipulator, the reconciliation was coordinated and interrelation was exposed. Further, velocity analysis of a more complicated spatial serial manipulator was studied by screw algebra and Denvit-Hartenberg method with the interrelation of Jacobian matrices verified.

Chapter 7 Screw Jacobian Analysis of a Reconfigurable Platform-Based Parallel Mechanism

7.1 Introduction

Parallel mechanisms, in general, have a rigid base and a moving platform connected by several limbs. For achieving higher mobility and dexterity, more degrees of freedom are introduced to the limbs. However, very few researchers focus on changing the design of the rigid base and making it foldable and reconfigurable to improve the performance of the mechanism.

Inspired by manipulating an object with a metamorphic robotic hand, this chapter presents a parallel mechanism with a reconfigurable base. This novel spherical-base integrated parallel mechanism has an enlarged workspace compared with traditional parallel manipulators. Evolution and structure of the proposed parallel mechanism is introduced and the geometric constraint of the mechanism is investigated based on mechanism decomposition. Further, kinematics of the proposed mechanism is reduced to the solution of a univariate polynomial of degree 8. Moreover, screw theory based Jacobian[64] is presented followed by the velocity analysis of the mechanism.

7.2 A Spherical-Base Integrated Parallel Mechanism

7.2.1 From Manipulation with a Metamorphic Hand to a Parallel Mechanism with a Reconfigurable Base

Figure 7.1 illustrates a three-fingered metamorphic robotic hand grasping and manipulating a disk. The metamorphic robotic hand contains a reconfigurable palm and three two-phalanx fingers. The reconfigurable palm is formed by a spherical five-bar linkage, with link AE as a grounded link, and the other four links are symmetrically arranged with respect to link AE such that links AB and ED are of the same length and so do links BC and DC. The three fingers are respectively mounted on link AE at point A_1, on link DC at point A_2 and on link BC at point A_3. When the palm is in a configuration that all the links are in the same plane, the three points A_1, A_2 and A_3 are evenly distributed about point O, i.e. centre of the spherical five-bar linkage. The 2-DOF reconfigurable palm changes configuration of the whole hand, and increases workspace, dexterity and manipulability of the hand[60,61]. The idea of equivalence about considering the multi-fingered hand with a grasped object as a parallel mechanism was put forward by Borras-Sol and Dollar[62,63]. When the hand is used to grasp and manipulate an object such as a disk as shown in Fig. 1, if the contact points between the object and the fingertips are thought of as spherical joints, an equivalent parallel mechanism with a reconfigurable base can be intuitively generated as illustrated in Fig. 2. This parallel mechanism is coined in this chapter *spherical-base integrated parallel mechanism*.

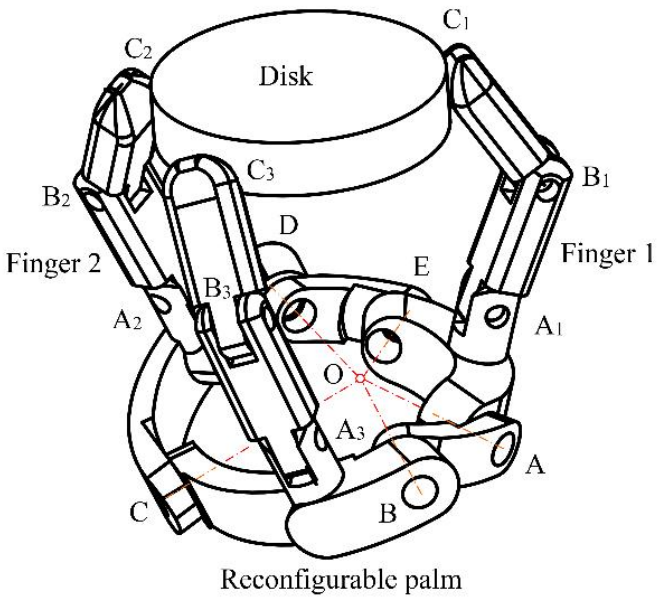

Figure 7.1 Object manipulated by a three-fingered Metamorphic hand

7.2.2 Structure of the Spherical-Base Integrated Parallel Mechanism

As shown in Fig. 7.2, the spherical-base integrated parallel mechanism is composed of a spherical reconfigurable base, a moving platform and three identical revolute-revolute-spherical chains connecting them. The reconfigurable base consists of five links which connect to each other forming a spherical five-bar linkage. In this design, link AE is fixed and joints A and E are assumed to be active joints to change the configurations of the base, and joints B, C and D are passive joints. The axes of these five joints always intersect at point O. The angles covered by links AB, BC, CD, DE and EA are denoted as φ_1 to φ_5 separately, and the sum of which satisfies $\varphi_1 + \varphi_2 + \varphi_3 + \varphi_4 + \varphi_5 = 2\pi$. There are three identical limbs mounted at point A_i (i = 1, 2 and 3), and the angles between OA_1 and OA, OB and OA_2, OA_3 and OD are indicated as δ_1, δ_2 and δ_3. The angle between any two limbs is 120° in the initial configuration of the mechanism when the five links of the reconfigurable base are located in the same plane.

However, one has to clarify that this initial state of the mechanism as a singular configuration is suitable for theoretical computations rather than a starting configuration for practical applications. Each limb is made up of two linkages coupled by a revolute joint B_i (i = 1, 2 and 3). The limbs are connected to the reconfigurable base by revolute joints A_i (i = 1, 2 and 3) and the moving platform by spherical joints C_i (i = 1, 2 and 3). The length of link A_iB_i is denoted as l_{i1}, while that of link B_iC_i is denoted as l_{i2} (i = 1, 2 and 3).

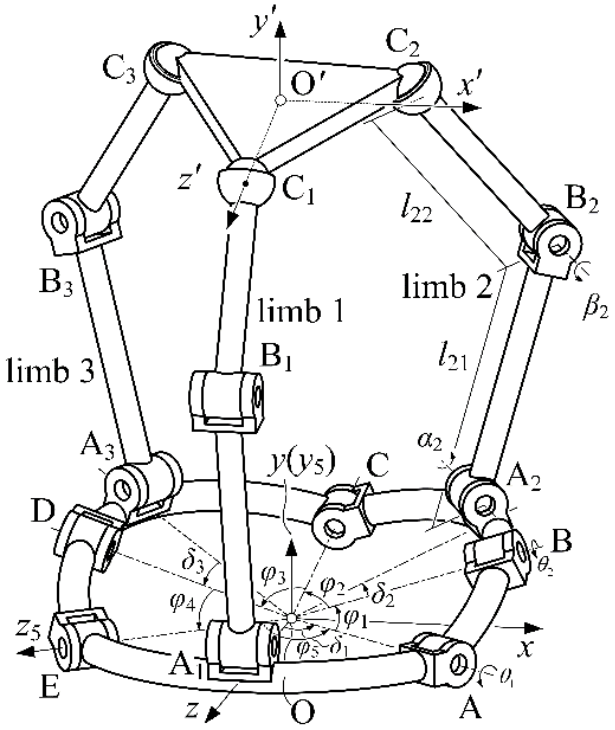

Figure 7.2 Structure of the spherical-base integrated parallel mechanism

7.3 Mechanism Decomposition and Geometric Constraints of the Spherical-Base Integrated Parallel Mechanism

The spherical-base integrated parallel mechanism, as the combination of a five-bar spherical base and a typical three-limb parallel mechanism, is a hybrid mechanism and

it is complicated to analyse its kinematics directly. Therefore, using mechanism decomposition, analysis of the geometry constraint of the mechanism can be separated as that of the reconfigurable base and that of the normal parallel mechanism first and then combine them together.

7.3.1 Constraint Equations of the Reconfigurable Base

As shown in Fig. 7.2, a global coordinate system F {O-*xyz*} is attached to the reconfigurable base with point O as the origin and its *y*-axis directed towards the upper platform and perpendicular to the plane formed by the axes of joints A and E. The *z*-axis of the coordinate system lies along OA_1. The radius of the spherical base is set at 1 for simplifying the calculation. For solving the geometric relationship of the reconfigurable base, local coordinate systems M_i {O-$x_iy_iz_i$ (i = 1 to 5)} are created at point O with the z_i-axis aligned the joint axis (joint A, B, C, D and E respectively) and the y_i-axis perpendicular to $z_i \times z_{i+1}$ (if i = 5, z_{i+1}-axis represents z_1-axis). The coordinate system M_5 {O-$x_5y_5z_5$} is taken as an example indicated in Fig. 3. In this local coordinate system, the position vectors of point A, B, C, D and E can be calculated as

$$\boldsymbol{P}_{\mathrm{A}} = \mathbf{R}(y_5, \varphi_5)\, \boldsymbol{P}_{\mathrm{E}} = \begin{bmatrix} s\varphi_5 \\ 0 \\ c\varphi_5 \end{bmatrix} = \begin{bmatrix} x_{\mathrm{A}} \\ y_{\mathrm{A}} \\ z_{\mathrm{A}} \end{bmatrix} \tag{7.1}$$

$$\boldsymbol{P}_{\mathrm{B}} = \mathbf{R}(y_5, \varphi_5)\mathbf{R}(z_1, \theta_1)\mathbf{R}(y_1, \varphi_1)\boldsymbol{P}_{\mathrm{E}} = \begin{bmatrix} c\varphi_1 s\varphi_5 + s\varphi_1 c\varphi_5 c\theta_1 \\ s\varphi_1 s\theta_1 \\ c\varphi_1 c\varphi_5 - s\varphi_1 s\varphi_5 c\theta_1 \end{bmatrix} = \begin{bmatrix} x_{\mathrm{B}} \\ y_{\mathrm{B}} \\ z_{\mathrm{B}} \end{bmatrix} \tag{7.2}$$

$$\begin{aligned}\boldsymbol{P}_{\mathrm{C}} &= \mathbf{R}(z_5,-\theta_5)\mathbf{R}(y_4,-\varphi_4)\mathbf{R}(z_4,-\theta_4)\mathbf{R}(y_3,-\varphi_3)\boldsymbol{P}_{\mathrm{E}} \\ &= \begin{bmatrix} s\varphi_3\left(s\theta_4 s\theta_5 - c\varphi_4 c\theta_4 c\theta_5\right) - c\varphi_3 s\varphi_4 c\theta_5 \\ c\varphi_3 s\varphi_4 s\theta_5 + s\varphi_3\left(s\theta_4 c\theta_5 + c\varphi_4 c\theta_4 s\theta_5\right) \\ c\varphi_3 c\varphi_4 - s\varphi_3 s\varphi_4 c\theta_4 \end{bmatrix} = \begin{bmatrix} x_{\mathrm{C}} \\ y_{\mathrm{C}} \\ z_{\mathrm{C}} \end{bmatrix}\end{aligned} \tag{7.3}$$

$$\boldsymbol{P}_{\mathrm{D}} = \mathbf{R}(z_5,-\theta_5)\mathbf{R}(y_4,-\varphi_4)\boldsymbol{P}_{\mathrm{E}} = \begin{bmatrix} -s\varphi_4 c\theta_5 \\ s\varphi_4 s\theta_5 \\ c\varphi_4 \end{bmatrix} = \begin{bmatrix} x_{\mathrm{D}} \\ y_{\mathrm{D}} \\ z_{\mathrm{D}} \end{bmatrix} \tag{7.4}$$

where *s* and *c* denote the sine and cosine functions, θ_1 to θ_5 are the rotation angles of joints A to E**,** and $\boldsymbol{P}_{\mathrm{E}} = (0,0,1)^{\mathrm{T}}$.

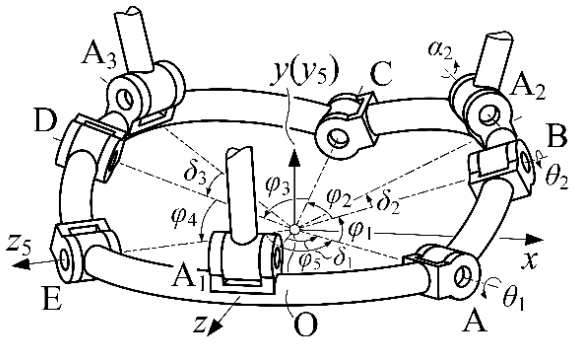

Figure 7.3 The reconfigurable base of the spherical-base integrated parallel mechanism

Due to the geometric constraints of the spherical base, the position vectors of its joints have to satisfy the following equations,

$$\boldsymbol{P}_{\mathrm{C}}^{\mathrm{T}} \cdot \boldsymbol{P}_{\mathrm{B}} = c\varphi_2 \tag{7.5}$$

$$\boldsymbol{P}_{\mathrm{C}}^{\mathrm{T}} \cdot \boldsymbol{P}_{\mathrm{D}} = c\varphi_3 \tag{7.6}$$

$$\boldsymbol{P}_{\mathrm{C}}^{\mathrm{T}} \cdot \boldsymbol{P}_{\mathrm{C}} = 1 \tag{7.7}$$

Substituting Eqs. (7.2), (7.3) and (7.4) into Eqs. (7.5) and (7.6) leads to the coordinate of x_C and y_C represented in terms of z_C as

$$x_C = P + Qz_C \tag{7.8}$$

$$y_C = M + Nz_C \tag{7.9}$$

where $P = \frac{y_D c\varphi_2 - y_B c\varphi_3}{x_B y_D - y_B x_D}, Q = \frac{y_B z_D - z_B y_D}{x_B y_D - y_B x_D}, M = \frac{x_B c\varphi_3 - x_D c\varphi_2}{x_B y_D - y_B x_D}, N = \frac{z_B x_D - x_B z_D}{x_B y_D - y_B x_D}$.

Substituting Eqs. (7.8) and (7.9) into Eq. (7.7) results in a quadratic equation as

$$S_1 z_C^2 + S_2 z_C + S_3 = 0 \tag{7.10}$$

where $S_1 = Q^2 + N^2 + 1, S_2 = 2(PQ + MN)$ and $S_3 = P^2 + M^2 - 1$.

Solving Eq. (7.10), the coordinate of z_C can be obtained as

$$z_C = \frac{-S_2 \pm \sqrt{S_2^{\,2} - 4S_1 S_3}}{2S_1} \tag{7.11}$$

.

Thus, the value of joint angle θ_4 is obtained by substituting Eq.(7.11) into z_C of Eq. (7.3) as

$$\theta_4 = -\arccos\left(\cot\varphi_3 \cot\varphi_4 - z_C / s\varphi_3 s\varphi_4\right) \tag{7.12}$$

The two possible values of z_C result in two joint angle θ_4, leading to two configurations of ΔBCD, one of which represents the case that the triangle vertex C appears above BD and the other indicates the case when vertex C is below BD.

Apart from Eq. (7.3), the position vector of point C can be expressed in another form as

$$\boldsymbol{P}_{\mathrm{C}} = \mathbf{R}(y_5, \varphi_5)\mathbf{R}(z_1, \theta_1)\mathbf{R}(y_1, \varphi_1)\mathbf{R}(z_2, \theta_2)\mathbf{R}(y_2, \varphi_2)\boldsymbol{P}_{\mathrm{E}} \tag{7.13}$$

which leads to another expression of z_{C} as

$$z_{\mathrm{C}} = c\varphi_2\left(c\varphi_1 c\varphi_5 - s\varphi_1 s\varphi_5 c\theta_1\right) - s\varphi_2\left(\left(s\varphi_1 c\varphi_5 + c\varphi_1 s\varphi_5 c\theta_1\right)c\theta_2 - s\varphi_5 s\theta_1 s\theta_2\right) \tag{7.14}$$

Substituting Eq. (7.14) into Eq. (7.11) and rearranging the equation yields

$$T_1 c\theta_2 + T_2 s\theta_2 - T_3 = 0 \tag{7.15}$$

where,

$T_1 = s\varphi_2\left(s\varphi_1 c\varphi_5 - c\varphi_1 s\varphi_5 c\theta_1\right)$, $T_2 = s\varphi_2 s\varphi_5 s\theta_1$ and

$T_3 = c\varphi_5(c\varphi_1 c\varphi_5 + s\varphi_1 s\varphi_5 c\theta_1) + \left(S_2 \mp \sqrt{S_2{}^2 - 4S_1 S_3}\right)\Big/2S_1$.

Solving Eq. (7.15) gives the joint angle θ_2 as

$$\theta_2 = \arctan\frac{T_2}{T_1} \pm \operatorname{arccot}\left(\frac{T_3}{\sqrt{T_1^2 + T_2^2}}\right) \tag{7.16}$$

The above equation indicates two solutions for θ_2, one of which implies the triangle vertex B locates below AC, and the other represents vertex B above AC. Because the reconfigurable base is a closed chain, the joint value θ_1 and θ_5 are not totally

independent. When assigning the value of angle θ_5, the spherical five-bar linkage mechanism degenerates to a spherical four-bar linkage mechanism. At that time, rotating joint A will make the spherical four-bar linkage mechanism reach its limited positions when point B, C and D lie in the same plane, thus it has,

$$\boldsymbol{P}_{\mathrm{D}} \cdot (\boldsymbol{P}_{\mathrm{B}} \times \boldsymbol{P}_{\mathrm{C}}) = 0 \tag{7.17}$$

$$\boldsymbol{P}_{\mathrm{B}} \cdot (\boldsymbol{P}_{\mathrm{D}} \times \boldsymbol{P}_{\mathrm{C}}) = 0 \tag{7.18}$$

The mechanism has two limited positions as the link AD can rotate on both sides with respect to link DC. Thus, the value θ_5 decides the range of that of θ_1, the relation between the two angles can be obtained as

$$\boldsymbol{P}_{\mathrm{B}}{}^{\mathrm{T}} \cdot \boldsymbol{P}_{\mathrm{A}} = c\varphi_1 \tag{7.19}$$

$$\boldsymbol{P}_{\mathrm{B}}{}^{\mathrm{T}} \cdot \boldsymbol{P}_{\mathrm{D}} = c(\varphi_2 + \varphi_3) \tag{7.20}$$

$$\boldsymbol{P}_{\mathrm{B}}{}^{\mathrm{T}} \cdot \boldsymbol{P}_{\mathrm{B}} = 1 \tag{7.21}$$

Substituting Eqs. (7.1), (7.2), (7.3) into Eqs. (7.19) throughout (7.21) and solving the latter gives the two limited values of angle θ_1 as

$$\theta_{1\mathrm{lim}} = \arctan(\frac{U_2}{U_1}) \pm \arccos(\frac{-U_3}{\sqrt{U_1{}^2 + U_2{}^2}}) \tag{7.22}$$

where $U_1 = -s\varphi_4 c\theta_5 c\varphi_5 \,\mathrm{s}\,\varphi_1 - s\varphi_1 c\varphi_4 s\varphi_5$, $U_2 = s\varphi_1 s\varphi_4 s\theta_5$ and

$U_3 = c(\varphi_2 + \varphi_3) - c\varphi_1 c\varphi_4 c\theta_5 + s\varphi_4 c\varphi_1 c\theta_5 s\varphi_5$.

Hence the range of θ_1 with respect to θ_5 is

$$V_1 \le \theta_1 \le V_2 \tag{7.23}$$

where $\mathrm{V}_1 = \arctan(\frac{U_2}{U_1}) - \arcsin(\frac{-U_2}{\sqrt{U_1^2 + U_2^2}})$ and $\mathrm{V}_2 = \arctan(\frac{U_2}{U_1}) + \arccos(\frac{-U_3}{\sqrt{U_1^2 + U_2^2}})$.

Based on the above analysis, it can be found that given a pair of θ_1 and θ_5, there are four groups of solution for θ_2, θ_3 and θ_4 resulting in four different configurations of the base. Motion planning is needed when controlling this mechanism because the configuration of the spherical base is considered by the order of its inputs.

7.3.2 Position of the 3-RRS Parallel Mechanism in a Particular Configuration of the Reconfigurable Base

A local coordinate system M′{O′-*x*′*y*′*z*′} is attached to the upper moving platform with the origin O' coincided with the centroid of the equilateral triangle $\Delta C_1C_2C_3$ and the *z*′-axis directed to point C_1. The coordinates of A_i (i = 1, 2 and 3) in the global coordinate system are given by,

$$^{\mathrm{F}}\boldsymbol{P}_{\mathrm{A}_1} = \begin{bmatrix} 0 & 0 & 1 \end{bmatrix}^{\mathrm{T}} \tag{7.24}$$

$$^{\mathrm{F}}\boldsymbol{P}_{\mathrm{A}_2} = \mathbf{R}(y, \delta_1)\mathbf{R}(z_1, \theta_1)\mathbf{R}(y_1, \varphi_1)\mathbf{R}(z_2, \theta_2)\mathbf{R}(y_2, \delta_2)\ ^{\mathrm{F}}\boldsymbol{P}_{\mathrm{A}_1} \tag{7.25}$$

$$^{\mathrm{F}}\boldsymbol{P}_{\mathrm{A}_3} = \mathbf{R}(y, -\delta_1)\mathbf{R}(z_5, -\theta_5)\mathbf{R}(y_4, -\varphi_4)\mathbf{R}(z_4, -\theta_4)\mathbf{R}(y_3, -\delta_3)\ ^{\mathrm{F}}\boldsymbol{P}_{\mathrm{A}_1} \tag{7.26}$$

The coordinates of C_i in the coordinate system M′ can be obtained as

$$^{M'}\boldsymbol{P}_{C_1} = \begin{bmatrix} 0 & 0 & r \end{bmatrix}^T \tag{7.27}$$

$$^{M'}\boldsymbol{P}_{C_2} = \begin{bmatrix} \frac{\sqrt{3}}{2}r & 0 & -\frac{r}{2} \end{bmatrix}^T \tag{7.28}$$

$$^{M'}\boldsymbol{P}_{C_3} = \begin{bmatrix} -\frac{\sqrt{3}}{2}r & 0 & -\frac{r}{2} \end{bmatrix}^T \tag{7.29}$$

The upper moving platform $C_1C_2C_3$ is an equilateral triangle as $|O'C_1| = |O'C_2| = |O'C_3| = 3r^2$. The position vector $^{F}\boldsymbol{P}_{Ci}$ of C_i (i = 1, 2 and 3) with respect to global coordinate frame F is given by the transformation as follows,

$$^{F}\boldsymbol{P}_{Ci} = {}^{F}\boldsymbol{P}_{OO'} + {}^{F}\mathbf{R}_{M'}\,{}^{M'}\boldsymbol{P}_{Ci}, \ (i = 1, 2 \text{ and } 3), \tag{7.30}$$

where $^{F}\boldsymbol{P}_{OO'}$ is the position vector of O′ expressed in the global coordinate frame F and $^{F}\mathbf{R}_{M'}$ is the rotation matrix indicating the rotation of coordinates from coordinate frame M′ to the global coordinate frame F.

7.3.3 Forward Kinematics of the Spherical-base Integrated Parallel Mechanism

The sequence of calculating the forward kinematics of the spherical-base integrated mechanism is to take the configuration of the base into consideration primarily as a way to degenerate the whole mechanism into a 3-RRS mechanism with a confirmed base configuration, then apply the way to formulating forward kinematics of a parallel mechanism to this simplified parallel mechanism, which is well presented in the

reference[66-68]. For each limb in this proposed mechanism, the local limb coordinate system K_i {O-$x_{Ki}y_{Ki}z_{Ki}$} (i =1, 2 and 3) is established with the origin O, z_{Ki}-axis directed to point A_i and y_{Ki}-axis perpendicular to the plane formed by the linkage of the reconfigurable base. In terms of Fig. 7.4, the y_{K2}-axis is perpendicular to the plane constructed by ΔCOD.

The position vector of point C_i in the global coordinate frame can be described as

$$\boldsymbol{k}_i = \mathbf{R}_{\mathbf{K}i}\begin{bmatrix} 0 \\ l_i s\alpha_i \\ 1 - l_i c\alpha_i \end{bmatrix}, i = 1, 2, 3 \tag{7.31}$$

where $\boldsymbol{k}_i$ is the position vector of point C_i expressed in the local coordinate system M_5 {O-$x_5y_5z_5$}, $\mathbf{R}_{\mathbf{K}i}$ describes the transformation from the local limb coordinate system to the coordinate system M_5 {O-$x_5y_5z_5$} as

$$\mathbf{R}_{\mathbf{K}i} = \begin{bmatrix} u_{xi} & v_{xi} & w_{xi} \\ u_{yi} & v_{yi} & w_{yi} \\ u_{zi} & v_{zi} & w_{zi} \end{bmatrix} = \begin{cases} \mathbf{R}(y, \delta_1), & i = 1 \\ \mathbf{R}(y, \varphi_5)\mathbf{R}(z, \theta_1)\mathbf{R}(y, \varphi_1)\mathbf{R}(z, \theta_2)\mathbf{R}(y, \delta_2), & i = 2 \\ \mathbf{R}(z, -\theta_5)\mathbf{R}(y, -\varphi_4)\,\mathbf{R}(z, -\theta_4)\mathbf{R}(y, -\delta_3), & i = 3 \end{cases} \tag{7.32}$$

The values of θ_2 and θ_4 can be obtained through Eqs. (7.16) and (7.12) according to the geometry constraints of the reconfigurable base. So $\boldsymbol{k}_i$ is computed by substituting θ_2 and θ_4 together with Eq. (7.32) into Eq. (7.31) as

$$\boldsymbol{k}_1 = \begin{bmatrix} (1 - l_1 c\alpha_1) s\delta_1 \\ l_1 s\alpha_1 \\ (1 - l_1 c\alpha_1) c\delta_1 \end{bmatrix}, \boldsymbol{k}_i = \begin{bmatrix} w_{xi}(1 - l_i c\alpha_i) + l_i v_{xi}\, \mathrm{s}\alpha_i \\ w_{yi}(1 - l_i c\alpha_i) + l_i v_{yi}\, \mathrm{s}\alpha_i \\ w_{zi}(1 - l_i c\alpha_i) + l_i v_{zi}\, \mathrm{s}\alpha_i \end{bmatrix},\ i = 2 \text{ and } 3 \tag{7.33}$$

For calculating the forward kinematics, the angle value of joint B_i is given, hence the length between point A_i and C_i is introduced by the following equation,

$$l_i = \sqrt{l_{i1}^2 + l_{i2}^2 - 2l_{i1}l_{i2}c\beta_i} \ , \ i = 1,2 \text{ and } 3 \tag{7.34}$$

Thus, the upper moving platform, which is connected to the limbs by spatial joints, restricts the position of point C_i ; that is

$$\left(\boldsymbol{k}_i - \boldsymbol{k}_{i+1}\right)^{\mathrm{T}} \left(\boldsymbol{k}_i - \boldsymbol{k}_{i+1}\right) = 3r^2, \ i = 1,2 \text{ and } 3 \tag{7.35}$$

Equation (7.35) describes the geometrical relation between the endpoints of any two limbs. So if $i = 3$, then $i + 1$ is equal to 1. By utilizing the way to calculating forward kinematics of the parallel mechanism introduced by Merlet [66], we can see that there are up to 16 solutions for the fixed-base parallel mechanism. However, in this spherical-base integrated mechanism, the number doubles as the reconfigurable base provides two configurations for given inputs investigated in Section 7.3.1. Path planning is necessary to get a desired configuration of the base and the moving platform.

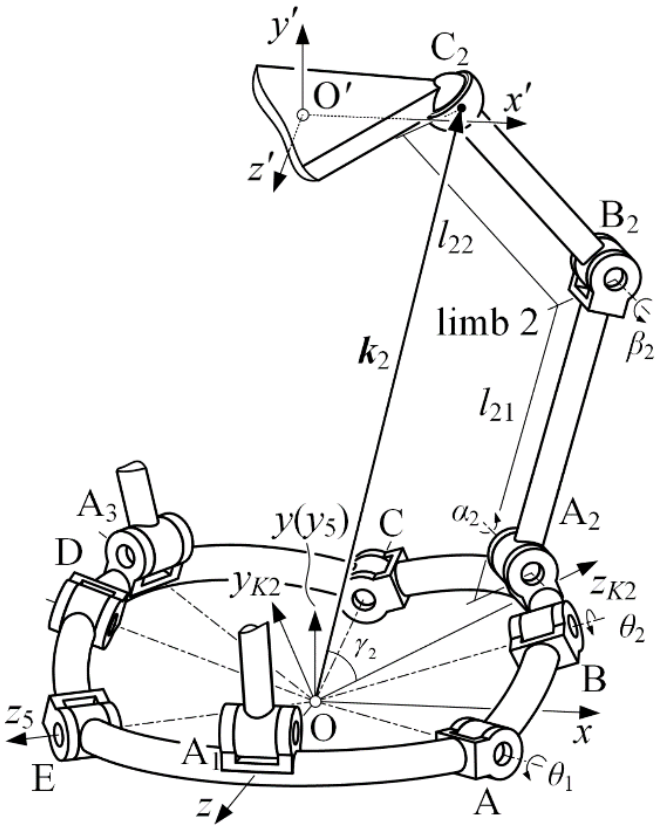

Figure 7.4 Kinematic analysis for limb 2 of the spherical-base integrated parallel mechanism

The workspace of the spherical-base integrated parallel mechanism proposed in this work is larger than that of the 3-RRS parallel mechanism with same limb and platform constructions and parameters. To make the comparison fairly, the base of the 3-RRS parallel mechanism is designed as the same of the initial configuration of the proposed mechanism (stated in Section 7.2.2.) Under this definition, the workspace of this proposed mechanism is enlarged compared with the 3-RRS fixed-base parallel mechanism. By locking the base of this proposed mechanism in its initial state, it shares the same workspace of the 3-RRS parallel mechanism. When the joints of the base are released, it will contribute to a larger workspace as you can always lock the base during its motion in where the mechanism degenerates to a 3-RRS mechanism as a

consequence. In other words, the workspace of the spherical-base integrated parallel mechanism is the sum of the workspaces of its degenerated 3-RRS parallel mechanisms with all possible base configurations.

7.4 Inverse Kinematics of the Spherical-Base Integrated Parallel Mechanism

The inverse kinematic problem can be described as giving the position and orientation of the upper moving platform to acquire the rotation angle of each active joint. For simplifying the model, we assume that point A_i (i = 1, 2 and 3) is on the links of the reconfigurable base. By decomposing the hybrid mechanism into a spherical five-bar linkage and a 3-RRS parallel mechanism where its three limbs are mounted on the former, the inverse kinematics of each linkage is investigated and then integrated through the instinct geometry when connecting them. As the configurations of the reconfigurable five-bar base play a vital role in deciding the position and orientation of the platform, it has to be primarily considered. In this case, the procedures of obtaining the inverse kinematics of this mechanism are divided into the following two steps:

a. Find all possible configurations of the base relying on its geometric constraints with the platform when the position and orientation of the latter are given.

b. For considering the mechanism as a whole after decouple, the length of each limb has to be achievable which it lies in the certain boundary.

For every possible configuration of the spherical base, it has to satisfy the geometric condition that the plane constructed by ΔOA_iB_i (i = 1, 2 or 3) is perpendicular to its

corresponding plane constructed by the linkage of the reconfigurable base. As shown in Fig. 7.4, ΔOA_2B_2 is orthogonal to ΔOBC. Denote C'_i the intersection between OC_i and the surface of the sphere constructed by the spherical mechanism. In this way, the coordinates of C'_3 can be written as,

$$\boldsymbol{P}_{C'_3} = \frac{1}{\sqrt{x_{C_3}^2 + y_{C_3}^2 + z_{C_3}^2}} \begin{bmatrix} x_{C_3} & y_{C_3} & z_{C_3} \end{bmatrix}^{\mathrm{T}} = \begin{bmatrix} x_{C'_3} & y_{C'_3} & z_{C'_3} \end{bmatrix}^{\mathrm{T}}$$

The coordinates of C'_3 can be acquired in another way by multiplying the rotation matrices from the point E as,

$$\begin{aligned} \boldsymbol{P}_{\mathrm{C}} &= \mathbf{R}(z_5, -\theta_5)\mathbf{R}(y_4, -\varphi_4)\mathbf{R}(z_4, -\theta_4)\mathbf{R}(y_3, -\delta_3)\mathbf{R}(x_3, -\gamma_3)\boldsymbol{P}_{\mathrm{E}} \\ &= \begin{bmatrix} c\gamma_3(s\delta_3(s\theta_4 s\theta_5 - c\varphi_4 c\theta_4 c\theta_5) - c\delta_3 c\theta_5 s\varphi_4) + s\gamma_3(c\theta_4 s\theta_5 + c\varphi_4 c\theta_5 s\theta_4) \\ c\gamma_3(s\delta_3(s\theta_4 c\theta_5 + c\varphi_4 c\theta_4 s\theta_5) + c\delta_3 s\theta_5 s\varphi_4) + s\gamma_3(c\theta_4 c\theta_5 - c\varphi_4 s\theta_4 s\theta_5) \\ c\gamma_3(c\delta_3 c\varphi_4 - s\delta_3 c\theta_4 s\varphi_4) + s\gamma_3 s\varphi_4 s\theta_4 \end{bmatrix} = \begin{bmatrix} x_{C'_3} \\ y_{C'_3} \\ z_{C'_3} \end{bmatrix} \end{aligned} \tag{7.36}$$

As there are only three unknowns θ_4, θ_5 and r_3 in Eq. (7.36), the standard trigonometric substitutions are adopted to estimate these unknown variables,

$$\begin{cases} s\gamma_3 = \dfrac{2u_1}{1+u_1^2},\ c\gamma_r = \dfrac{1-u_1^2}{1+u_1^2} \\ s\theta_4 = \dfrac{2u_2}{1+u_2^2},\ c\theta_4 = \dfrac{1-u_1^2}{1+u_1^2} \\ s\theta_5 = \dfrac{2u_3}{1+u_3^2},\ c\theta_5 = \dfrac{1-u_3^2}{1+u_3^2} \end{cases} \tag{7.37}$$

In order to estimate u_2, substituting Eq. (7.38) into the equations in Eq. (7.37) results in three quadratic equations in u_2

$$E_1 u_2^2 + E_2 u_2 + E_3 = 0 \tag{7.38}$$

$$F_1 u_2^2 + F_2 u_2 + F_3 = 0 \tag{7.39}$$

$$G_1 u_2^2 + G_2 u_2 + G_3 = 0 \tag{7.40}$$

where E_i and F_i are second-degree polynomials in u_3 and u_1 and G_i (i = 1, 2, 3) is the second-degree polynomials in u_1, shown in Appendix B. Sylvester Dialytic Elimination Method [38] can be utilized here to estimate u_2 from these equations. Taking Eq. (7.38) × G_1 − Eq. (7.40) × E_1 and Eq. (38) × G_3 − Eq. (7.40) × E_3 respectively, the two linear equation in u_3 are obtained as

$$\left(E_1 G_2 - E_2 G_1\right) u_2 + \left(E_1 G_3 - E_3 G_1\right) = 0 \tag{7.41}$$

$$\left(E_3 G_1 - E_1 G_3\right) u_2 + \left(E_3 G_2 - E_2 G_3\right) = 0 \tag{7.42}$$

Combining Eq. (7.41) and Eq. (7.42) to estimate u_2, we obtain,

$$\left(E_1 G_3 - E_3 G_1\right)^2 + \left(E_1 G_2 - E_2 G_1\right)\left(E_3 G_2 - E_2 G_3\right) = 0 \tag{7.43}$$

A fourth-degree polynomial in u_3 can be derived from substituting E_i and G_i (i = 1, 2, 3) into Eq. (7.43); that is,

$$J_1 u_3^4 + J_2 u_3^3 + J_3 u_3^2 + J_4 u_3 + J_5 = 0 \tag{7.44}$$

where J_i (i = 1 to 5) is eighth-degree polynomials in u_1. Taking the same method for Eqs. (7.39) and (7.40), and writing it in the similar form with Eq. (44) as,

$$H_1 u_3^4 + H_2 u_3^3 + H_3 u_3^2 + H_4 u_3 + H_5 = 0 \tag{7.45}$$

where H_i (i = 1 to 3) is eighth-degree polynomials in u_1. For estimating the term u_3^4, we multiply Eq. (7.44) by H_1 and Eq. (7.45) by J_1, and then take the subtraction of the two to obtain the third-degree polynomial in u_3, as follows,

$$\left(H_2 J_1 - H_1 J_2\right) u_3^3 + \left(H_3 J_1 - H_1 J_3\right) u_3^2 + \left(H_4 J_1 - H_1 J_4\right) u_3 + \left(H_5 J_1 - H_1 J_5\right) = 0 \tag{7.46}$$

Another equation of u_3 can be derived from multiplying Eq. (7.44) by H_2 and Eq. (7.45) by J_2, and subtracting, which yields,

$$\left(H_2 J_1 - H_1 J_2\right) u_3^4 + \left(H_2 J_3 - H_3 J_2\right) u_3^2 + \left(H_2 J_4 - H_4 J_2\right) u_3 + \left(H_2 J_5 - H_5 J_2\right) = 0 \tag{7.47}$$

Multiplying Eq. (7.45) by u_3 leads to

$$\left(H_2 J_1 - H_1 J_2\right) u_3^4 + \left(H_3 J_1 - H_1 J_3\right) u_3^3 + \left(H_4 J_1 - H_1 J_4\right) u_3^2 + \left(H_5 J_1 - H_1 J_5\right) u_3 = 0 \tag{7.48}$$

We write Eqs. (7.44) throughout (7.48) in matrix form as

$$\mathbf{M} \cdot \left[u_3^4, u_3^3, u_3^2, u_3, 1\right]^T = \mathbf{0} \tag{7.49}$$

Where

$$\mathbf{M} = \begin{bmatrix} H_1 & H_2 & H_3 & H_4 & H_5 \\ J_1 & J_2 & J_3 & J_4 & J_5 \\ H_2 J_1 - H_1 J_2 & H_3 J_1 - H_1 J_3 & H_4 J_1 - H_1 J_4 & H_5 J_1 - H_1 J_5 & 0 \\ H_2 J_1 - H_1 J_2 & 0 & H_2 J_3 - H_3 J_2 & H_2 J_4 - H_4 J_2 & H_2 J_5 - H_5 J_2 \\ 0 & H_2 J_1 - H_1 J_2 & H_3 J_1 - H_1 J_3 & H_4 J_1 - H_1 J_4 & H_5 J_1 - H_1 J_5 \end{bmatrix}$$

Equation (7.49) is valid if and only if the determinant of **M** is equal to zero, which results in a thirty-second-degree polynomial in the square of u_1, as follow,

$$\sum_{i=0}^{64} N_i u_1^i = 0 \tag{7.50}$$

In Eq. (7.50), N_i is only decided by the structure of the hybrid mechanism. Solving Eq. (7.50) will obtain at most 32 pairs of solutions for u_1, with each pair containing one positive and one negative solution. The other two parameters u_2 and u_3 can be calculated by substituting u_1 into Eqs. (7.45) and (7.40) separately, which overall results in 64 groups of solution for u_2 and u_3. Thus, θ_4, θ_5 and r_3 are solved in the Eq. (7.38) by substituting the above parameter into these trigonometric functions. Once θ_4 and θ_5 are obtained, the configuration of the spherical base is confirmed. The next step is to solve the configuration for the limbs based on the known base configuration and moving platform.

With explicit expressions of $\boldsymbol{P}_{\mathrm{Ai}}$ and $\boldsymbol{k}_{\mathrm{i}}$ (i = 1, 2 or 3), we can move forward to obtain the length of each limb so as to get the value of β_i (i = 1, 2 or 3) in the $\Delta A_iB_iC_i$ and complete to solve the inverse kinematics, by the following equation,

$$c\beta_i = \left(l_{i1}^2 + l_{i2}^2 - l_i^{\,2}\right) \Big/ 2l_{i1}l_{i2}, \quad i = 1,2 \text{ and } 3 \tag{7.51}$$

Two solutions of β_i (i = 1, 2 or 3) exist for non-singular configurations of each limb that contribute to 8 possible states for a specific base configuration, which leads to at most 512 different configurations for the whole mechanism theoretically. The quantity of

possible configurations is much smaller that the theoretical number because the solutions of the spherical base only consider the geometrical constraint of limb 3, and these solutions need to be verified to satisfy the corresponding geometrical constraint of limb 2, which will significantly decrease the number of solutions.

7.5 Screw Theory based Jacobian Analysis

As aforementioned, since the parallel mechanism consists of three limbs mounted on a reconfigurable base, structure decomposition of the mechanism can be applied to analysing the Jacobian matrix of the whole mechanism, the Jacobian analysis of the reconfigurable base can be completed first followed by that of the parallel mechanism.

7.5.1 Jacobian Analysis for the Reconfigurable Base

The velocity of point C can be expressed as a linear combination of angular velocity of axis OA and OB or the other linear combination of angular velocity of axis OE and OD,

$$\boldsymbol{v}_{\mathrm{C}} = \dot{\theta}_1(\boldsymbol{P}_{\mathrm{A}} \times \boldsymbol{P}_{\mathrm{C}}) + \dot{\theta}_2(\boldsymbol{P}_{\mathrm{B}} \times \boldsymbol{P}_{\mathrm{C}}) \tag{7.52}$$

$$\boldsymbol{v}_{\mathrm{C}} = \dot{\theta}_5(\boldsymbol{P}_{\mathrm{E}} \times \boldsymbol{P}_{\mathrm{C}}) + \dot{\theta}_4(\boldsymbol{P}_{\mathrm{D}} \times \boldsymbol{P}_{\mathrm{C}}) \tag{7.53}$$

Since $\boldsymbol{v}_{\mathrm{C}}$ is a passive variable, it should be estimated from Eqs. (7.52) and (7.53). Thus we take right inner product on both sides of Eqs. (7.52) and (7.53) with $\boldsymbol{P}_{\mathrm{D}}$, it has

$$\boldsymbol{P}_{\mathrm{D}} \cdot \boldsymbol{v}_{\mathrm{C}} = \dot{\theta}_1 \boldsymbol{P}_{\mathrm{D}} \cdot (\boldsymbol{P}_{\mathrm{A}} \times \boldsymbol{P}_{\mathrm{C}}) + \dot{\theta}_2 \boldsymbol{P}_{\mathrm{D}} \cdot (\boldsymbol{P}_{\mathrm{B}} \times \boldsymbol{P}_{\mathrm{C}}) \tag{7.54}$$

$$\boldsymbol{P}_{\mathrm{D}} \cdot \boldsymbol{v}_{\mathrm{C}} = \dot{\theta}_5 \boldsymbol{P}_{\mathrm{D}} \cdot (\boldsymbol{P}_{\mathrm{E}} \times \boldsymbol{P}_{\mathrm{C}}) \tag{7.55}$$

Substituting Eq. (7.55) into Eq. (7.54) yields,

$$\dot{\theta}_2 = -\frac{\boldsymbol{P}_{\mathrm{D}} \cdot (\boldsymbol{P}_{\mathrm{A}} \times \boldsymbol{P}_{\mathrm{C}})}{\boldsymbol{P}_{\mathrm{D}} \cdot (\boldsymbol{P}_{\mathrm{B}} \times \boldsymbol{P}_{\mathrm{C}})} \dot{\theta}_1 + \frac{\boldsymbol{P}_{\mathrm{D}} \cdot (\boldsymbol{P}_{\mathrm{E}} \times \boldsymbol{P}_{\mathrm{C}})}{\boldsymbol{P}_{\mathrm{D}} \cdot (\boldsymbol{P}_{\mathrm{B}} \times \boldsymbol{P}_{\mathrm{C}})} \dot{\theta}_5 \tag{7.56}$$

Similarly, the angular velocity $\dot{\theta}_4$ can be obtained and expressed as,

$$\dot{\theta}_4 = \frac{\boldsymbol{P}_{\mathrm{B}} \cdot (\boldsymbol{P}_{\mathrm{A}} \times \boldsymbol{P}_{\mathrm{C}})}{\boldsymbol{P}_{\mathrm{B}} \cdot (\boldsymbol{P}_{\mathrm{D}} \times \boldsymbol{P}_{\mathrm{C}})} \dot{\theta}_1 - \frac{\boldsymbol{P}_{\mathrm{B}} \cdot (\boldsymbol{P}_{\mathrm{E}} \times \boldsymbol{P}_{\mathrm{C}})}{\boldsymbol{P}_{\mathrm{B}} \cdot (\boldsymbol{P}_{\mathrm{D}} \times \boldsymbol{P}_{\mathrm{C}})} \dot{\theta}_5 \tag{7.57}$$

The Eqs. (7.56) and (7.57) can be expressed in matrix form as,

$$\begin{bmatrix} \dot{\theta}_2 \\ \dot{\theta}_4 \end{bmatrix} = \boldsymbol{J}_{\varphi} \begin{bmatrix} \dot{\theta}_1 \\ \dot{\theta}_5 \end{bmatrix} = \begin{bmatrix} -\dfrac{\boldsymbol{P}_{\mathrm{D}} \cdot (\boldsymbol{P}_{\mathrm{A}} \times \boldsymbol{P}_{\mathrm{C}})}{\boldsymbol{P}_{\mathrm{D}} \cdot (\boldsymbol{P}_{\mathrm{B}} \times \boldsymbol{P}_{\mathrm{C}})} & \dfrac{\boldsymbol{P}_{\mathrm{D}} \cdot (\boldsymbol{P}_{\mathrm{E}} \times \boldsymbol{P}_{\mathrm{C}})}{\boldsymbol{P}_{\mathrm{D}} \cdot (\boldsymbol{P}_{\mathrm{B}} \times \boldsymbol{P}_{\mathrm{C}})} \\ \dfrac{\boldsymbol{P}_{\mathrm{B}} \cdot (\boldsymbol{P}_{\mathrm{A}} \times \boldsymbol{P}_{\mathrm{C}})}{\boldsymbol{P}_{\mathrm{B}} \cdot (\boldsymbol{P}_{\mathrm{D}} \times \boldsymbol{P}_{\mathrm{C}})} & -\dfrac{\boldsymbol{P}_{\mathrm{B}} \cdot (\boldsymbol{P}_{\mathrm{E}} \times \boldsymbol{P}_{\mathrm{C}})}{\boldsymbol{P}_{\mathrm{B}} \cdot (\boldsymbol{P}_{\mathrm{D}} \times \boldsymbol{P}_{\mathrm{C}})} \end{bmatrix} \begin{bmatrix} \dot{\theta}_1 \\ \dot{\theta}_5 \end{bmatrix} \tag{7.58}$$

Thus the angular velocity of passive joints B and D is calculated through that of active joints A and E based on the geometric constraints of the spherical mechanism.

7.5.2 Screw-based Jacobian Analysis for the Spherical-Base Integrated Parallel Mechanism

The screw algebra is introduced in this section for analysing the velocity of the spherical-base integrated parallel mechanism. A screw $\boldsymbol{S}$ is a six-dimensional vector representing instantaneous kinematic properties of a rigid body, commonly expressed as,

$$\boldsymbol{S} = \begin{bmatrix} \boldsymbol{s} \\ \boldsymbol{s}_0 \end{bmatrix} = \begin{bmatrix} \boldsymbol{s} \\ \boldsymbol{r} \times \boldsymbol{s} + h\boldsymbol{s} \end{bmatrix} = \begin{bmatrix} s_x, s_y, s_z, s_{x0}, s_{y0}, s_{z0} \end{bmatrix}^{\mathrm{T}} \tag{7.59}$$

The first three components consist of a unit vector $\boldsymbol{s}$ directing along the screw axis, as well as the joint axis when describing a rotation. The last elements constitute $\boldsymbol{s}_0$ representing the moment of the vector $\boldsymbol{s}$ about the origin of the reference frame, and h expresses the screw pitch, which is equal to 0 for revolute joints and ∞ for prismatic joints, $\boldsymbol{r}$ is the position vector from the origin of the reference coordinate system to an arbitrary point on the screw axis $\boldsymbol{s}$.

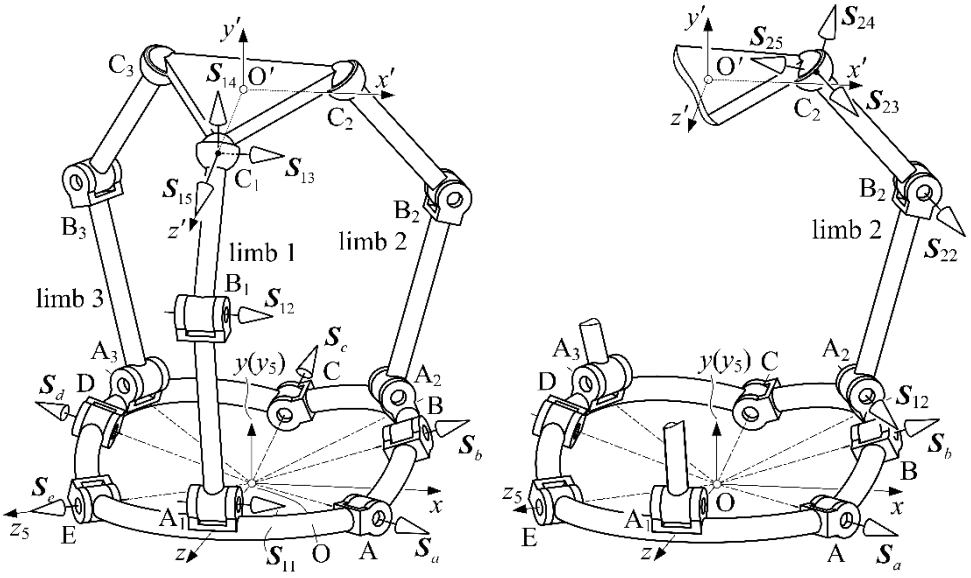

(a) (b)

Figure 7.5 Motion screw of the spherical-base integrated parallel mechanism

The whole mechanism Jacobian can be derived from the twist of the mechanism based on screw system notation. Fig. 7.5(a) illustrates motion screws of the spherical-base integrated parallel mechanism. We can assume each limb as an open-loop chain connecting the end-effector to the base, as shown in Fig. 7.5 (b). Defining $\boldsymbol{S}_p$ as the instantaneous motion of the moving platform, the twist $\boldsymbol{S}_p$ can be derived from the linear

combination of each joint's twist within the loop. Referring to Fig. 7.5(a), twist $\boldsymbol{S}_p$ can be obtained in terms of limb 1, 2 and 3 separately as

$$\boldsymbol{S}_p = \sum_{i=1}^{5} \dot{\theta}_{1i} \boldsymbol{S}_{1i} \tag{7.60}$$

$$\boldsymbol{S}_p = \dot{\theta}_1 \boldsymbol{S}_a + \dot{\theta}_2 \boldsymbol{S}_b + \sum_{i=1}^{5} \dot{\theta}_{2i} \boldsymbol{S}_{2i} \tag{7.61}$$

$$\boldsymbol{S}_p = \dot{\theta}_4 \boldsymbol{S}_d + \dot{\theta}_5 \boldsymbol{S}_e + \sum_{i=1}^{5} \dot{\theta}_{3i} \boldsymbol{S}_{3i} \tag{7.62}$$

Substituting Eqs. (7.56) and (7.57) into Eqs. (7.61) and (7.62) respectively leads to,

$$\boldsymbol{S}_p = \dot{\theta}_1 \left(\boldsymbol{S}_a - m_1 \boldsymbol{S}_b \right) + m_2 \dot{\theta}_5 \boldsymbol{S}_b + \sum_{i=1}^{5} \dot{\theta}_{2i} \boldsymbol{S}_{2i} \tag{7.63}$$

$$\boldsymbol{S}_p = m_3 \dot{\theta}_1 \boldsymbol{S}_d + \dot{\theta}_5 \left(\boldsymbol{S}_e - m_4 \boldsymbol{S}_d \right) + \sum_{i=1}^{5} \dot{\theta}_{2i} \boldsymbol{S}_{2i} \tag{7.64}$$

where $m_1 = \dfrac{\boldsymbol{P}_{\mathrm{D}} \cdot (\boldsymbol{P}_{\mathrm{A}} \times \boldsymbol{P}_{\mathrm{C}})}{\boldsymbol{P}_{\mathrm{D}} \cdot (\boldsymbol{P}_{\mathrm{B}} \times \boldsymbol{P}_{\mathrm{C}})}$, $m_2 = \dfrac{\boldsymbol{P}_{\mathrm{D}} \cdot (\boldsymbol{P}_{\mathrm{E}} \times \boldsymbol{P}_{\mathrm{C}})}{\boldsymbol{P}_{\mathrm{D}} \cdot (\boldsymbol{P}_{\mathrm{B}} \times \boldsymbol{P}_{\mathrm{C}})}$, $m_3 = \dfrac{\boldsymbol{P}_{\mathrm{B}} \cdot (\boldsymbol{P}_{\mathrm{A}} \times \boldsymbol{P}_{\mathrm{C}})}{\boldsymbol{P}_{\mathrm{B}} \cdot (\boldsymbol{P}_{\mathrm{D}} \times \boldsymbol{P}_{\mathrm{C}})}$ and $m_4 = \dfrac{\boldsymbol{P}_{\mathrm{B}} \cdot (\boldsymbol{P}_{\mathrm{E}} \times \boldsymbol{P}_{\mathrm{C}})}{\boldsymbol{P}_{\mathrm{B}} \cdot (\boldsymbol{P}_{\mathrm{D}} \times \boldsymbol{P}_{\mathrm{C}})}$.

According to [65], we know that the revolute-spherical screws dyad locate in a four-dimensional vector space. So the reciprocal screws form a two-system with zero pitch. Let $\boldsymbol{S}_{i1}^{r}$ and $\boldsymbol{S}_{i2}^{r}$ (i = 1, 2 and 3) denote a two-system of screws that is reciprocal to the four-system of screws $\boldsymbol{S}_{i2}$ to $\boldsymbol{S}_{i5}$ (i = 1, 2 and 3) of the ith limb. Performing the reciprocal product of both sides of Eqs. (7.60), (7.63) and (7.64) with reciprocal screw $\boldsymbol{S}_{i1}^{r}$ and $\boldsymbol{S}_{i2}^{r}$ gives six linear equations, which can be expressed in matrix form as,

$$\mathbf{J}_q{}^{\mathrm{T}}\Delta\boldsymbol{S}_p = \mathbf{J}_\theta\dot{\boldsymbol{\theta}}_a \tag{7.65}$$

where $\dot{\boldsymbol{\theta}}_a = \left[\dot{\theta}_1\ ,\ \dot{\theta}_5\ ,\ \dot{\theta}_{11}\ ,\ \dot{\theta}_{21}\ ,\ \dot{\theta}_{31}\right]^{\mathrm{T}}$ $\mathbf{J}_q{}^{\mathrm{T}} = \begin{bmatrix} \boldsymbol{S}_{11}^{r\,\mathrm{T}} \\ \boldsymbol{S}_{12}^{r\,\mathrm{T}} \\ \vdots \\ \boldsymbol{S}_{32}^{r\,\mathrm{T}} \end{bmatrix}$, $\mathbf{J}_\theta = \begin{bmatrix} \mathbf{J}_{\theta 1} \\ \mathbf{J}_{\theta 2} \\ \mathbf{J}_{\theta 3} \end{bmatrix}$ and Δ denotes the reciprocal operator expressed as $\Delta = \begin{bmatrix} \mathbf{0} & \mathbf{I} \\ \mathbf{I} & \mathbf{0} \end{bmatrix}$.

The term $\mathbf{J}_{\theta i}$ is derived in detail in Appendix B, and $\mathbf{J}_q{}^{\mathrm{T}}$, in general, is a 6×6 nonsingular matrix. Thus, multiplying both sides of Eq. (7.65) by the inverse of $\mathbf{J}_q{}^{\mathrm{T}}$ gives the twist of the moving platform as,

$$\Delta\boldsymbol{S}_p = \left[\mathbf{J}_q{}^{\mathrm{T}}\right]^{-1}\mathbf{J}_\theta\dot{\boldsymbol{\theta}}_a \tag{7.66}$$

where $\Delta\boldsymbol{S}_p$ is the twist of the moving platform with interchange of its primary part and secondary part comparing to $\boldsymbol{S}_p$. The left-hand side and right-hand side of equation (7.65) gives the power of the platform and the actuated joints respectively, which provides background for dynamic analysis of the proposed parallel mechanism based on the concept of kinetic energy.

7.5.3 Velocity of the Spherical-Base Integrated Parallel Mechanism

The spherical-base integrated parallel mechanism can be decomposed as three closed-loop mechanisms between any two of three limbs and an additional closed-loop of the five-bar reconfigurable base. The instantaneous motion of each link can be described

as its instantaneous twist, and all the links' motion in a closed-loop form a linear combination of all the instantaneous twists within the loop. Let twist $\boldsymbol{S}_{ij}$ denote the instantaneous motion along the jth joint in the ith limb and twist $\boldsymbol{S}_a$, $\boldsymbol{S}_b$, $\boldsymbol{S}_c$, $\boldsymbol{S}_d$ and $\boldsymbol{S}_e$ denote that along the joints of the reconfigurable base. Define variable $\dot{\theta}_{ij}$ and $\dot{\theta}_k$ as the velocity of the jth joint in the ith limb and the velocity of the kth joint in the reconfigurable base. Based on the notations introduced above, twists of three closed-loop-mechanisms are expressed as separately as follows.

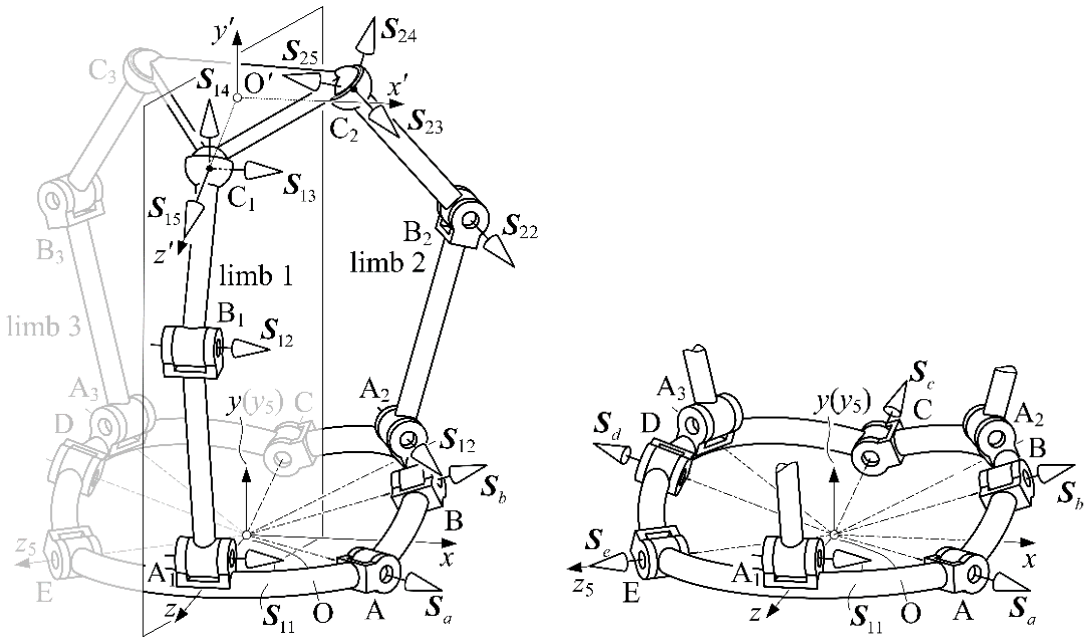

(a) (b)

Figure 7.6 Motion screw of closed-loop mechanism decomposed from the parallel mechanism

For the closed-loop composed of limb 1 and 2, shown in Fig. 7.6(a), the closed-loop-twist is

$$\dot{\theta}_1\boldsymbol{S}_a + \dot{\theta}_2\boldsymbol{S}_b + \sum_{i=1}^{5}\dot{\theta}_{1i}\boldsymbol{S}_{1i} - \sum_{i=1}^{5}\dot{\theta}_{2i}\boldsymbol{S}_{2i} = \boldsymbol{0} \tag{7.67}$$

For limb 2 and 3, the closed-loop-twist is

$$\dot{\theta}_3 \boldsymbol{S}_c + \sum_{i=1}^{5} \dot{\theta}_{2i} \boldsymbol{S}_{2i} - \sum_{i=1}^{5} \dot{\theta}_{3i} \boldsymbol{S}_{3i} = \boldsymbol{0} \tag{7.68}$$

And for limb 3 and 1, the closed-loop-twist is

$$\dot{\theta}_4 \boldsymbol{S}_d + \dot{\theta}_5 \boldsymbol{S}_e + \sum_{i=1}^{5} \dot{\theta}_{3i} \boldsymbol{S}_{3i} - \sum_{i=1}^{5} \dot{\theta}_{1i} \boldsymbol{S}_{1i} = \boldsymbol{0} \tag{7.69}$$

Further, the closed-loop-twist of the reconfigurable base, shown in Fig. 7.6(b) is

$$\dot{\theta}_1 \boldsymbol{S}_a + \dot{\theta}_2 \boldsymbol{S}_b + \dot{\theta}_3 \boldsymbol{S}_c + \dot{\theta}_4 \boldsymbol{S}_d + \dot{\theta}_5 \boldsymbol{S}_e = \boldsymbol{0} \tag{7.70}$$

In each decomposed closed-loop-mechanism, only part of all the joints are active, which can be separated from the rest passive joints in the twists given in Eqs. (7.67) throughout (7.70) as,

$$\dot{\theta}_1 \boldsymbol{S}_a + \dot{\theta}_{11} \boldsymbol{S}_{11} - \dot{\theta}_{21} \boldsymbol{S}_{21} = -\dot{\theta}_2 \boldsymbol{S}_b - \sum_{i=2}^{5} \dot{\theta}_{1i} \boldsymbol{S}_{1i} + \sum_{i=2}^{5} \dot{\theta}_{2i} \boldsymbol{S}_{2i} \tag{7.71}$$

$$\dot{\theta}_{21} \boldsymbol{S}_{21} - \dot{\theta}_{31} \boldsymbol{S}_{31} = -\dot{\theta}_3 \boldsymbol{S}_c - \sum_{i=2}^{5} \dot{\theta}_{2i} \boldsymbol{S}_{2i} + \sum_{i=2}^{5} \dot{\theta}_{3i} \boldsymbol{S}_{3i} \tag{7.72}$$

$$\dot{\theta}_5 \boldsymbol{S}_e + \dot{\theta}_{31} \boldsymbol{S}_{31} - \dot{\theta}_{11} \boldsymbol{S}_{11} = -\dot{\theta}_4 \boldsymbol{S}_d - \sum_{i=2}^{5} \dot{\theta}_{3i} \boldsymbol{S}_{3i} + \sum_{i=2}^{5} \dot{\theta}_{1i} \boldsymbol{S}_{1i} \tag{7.73}$$

$$\dot{\theta}_1 \boldsymbol{S}_a + \dot{\theta}_5 \boldsymbol{S}_e = -\dot{\theta}_2 \boldsymbol{S}_b - \dot{\theta}_3 \boldsymbol{S}_c - \dot{\theta}_4 \boldsymbol{S}_d \tag{7.74}$$

The Eqs. (7.71) to (7.74) can be expressed in a matrix form that indicates the relationship between velocity of the active joints and that passive joints as,

$$\mathbf{J}_a\dot{\boldsymbol{\theta}}_a = \mathbf{J}_p\dot{\boldsymbol{\theta}}_p \tag{7.75}$$

where $\dot{\boldsymbol{\theta}}_a$ and $\dot{\boldsymbol{\theta}}_p$ denote the velocity vectors of active joints and passive joints as, $\dot{\boldsymbol{\theta}}_P = \left[\dot{\theta}_2\ ,\dot{\theta}_3\ ,\dot{\theta}_4\ ,\dot{\theta}_{12}\ ,\dot{\theta}_{13}\ ,\dot{\theta}_{14}\ ,\dot{\theta}_{15}\ ,\ \ldots\ ,\dot{\theta}_{35}\ \right]^{\mathrm{T}}$, $\mathbf{J}_a$ and $\mathbf{J}_p$ denote the active-Jacobian matrix and passive-Jacobian matrix respectively as

$$\mathbf{J}_a = \left[\begin{array}{cc|ccc} \boldsymbol{S}_1 & \boldsymbol{0} & \boldsymbol{S}_{11} & -\boldsymbol{S}_{21} & \boldsymbol{0} \\ \boldsymbol{0} & \boldsymbol{0} & \boldsymbol{0} & \boldsymbol{S}_{21} & -\boldsymbol{S}_{31} \\ \boldsymbol{0} & \boldsymbol{S}_5 & -\boldsymbol{S}_{11} & \boldsymbol{0} & \boldsymbol{S}_{31} \\ \boldsymbol{S}_1 & \boldsymbol{S}_5 & \boldsymbol{0} & \boldsymbol{0} & \boldsymbol{0} \end{array}\right] \text{ and } \mathbf{J}_p = \left[\begin{array}{ccc|ccc} -\boldsymbol{S}_2 & \boldsymbol{0} & \boldsymbol{0} & -\mathbf{J}_{p1} & \mathbf{J}_{p2} & \boldsymbol{0} \\ \boldsymbol{0} & -\boldsymbol{S}_3 & \boldsymbol{0} & \boldsymbol{0} & -\mathbf{J}_{p2} & \mathbf{J}_{p3} \\ \boldsymbol{0} & \boldsymbol{0} & -\boldsymbol{S}_4 & \mathbf{J}_{p1} & \boldsymbol{0} & -\mathbf{J}_{p3} \\ -\boldsymbol{S}_2 & -\boldsymbol{S}_3 & -\boldsymbol{S}_4 & \boldsymbol{0} & \boldsymbol{0} & \boldsymbol{0} \end{array}\right]$$

where $\mathbf{J}_{pi} = \left[\boldsymbol{S}_{i2}\quad \boldsymbol{S}_{i3}\quad \boldsymbol{S}_{i4}\quad \boldsymbol{S}_{i5}\right]$, $i = 1\ ,\ 2$ and 3.

The above Jacobian matrixes can be used for singularity and dexterity analysis of the proposed integrated parallel mechanism.

7.6 Conclusions

In this chapter, a parallel mechanism with a reconfigurable base was for the first time presented based on the manipulation of rigid objects using a Metamorphic hand. The structure of the proposed mechanism was presented followed by the geometric constraint analysis.

Through decomposing the mechanism into a typical 3RRS parallel mechanism and a spherical five-bar linkage, the kinematics was investigated, leading to closed-form

solutions for forward and inverse kinematics. Then, the screw-based Jacobian was utilized to establish the relationship between active joints and passive joints through the reciprocal product of twists and wrenches. The kinematics study demonstrated that this novel spherical-base integrated parallel manipulator had an enlarged workspace compared with conventional parallel mechanisms.

Chapter 8 Screw Embedded Jacobian and Exponential Mapping of Grasp Affordability with a Reconfigurable Palm

8.1 Introduction

This chapter presents the kinematics and grasp constraint and affordance of a newly designed mobile manipulator with a three-fingered Metamorphic robotic hand. Structure design of the mobile manipulator, which contains a Robotino 3.0, a customised robot arm and a three-fingered Metamorphic hand, is presented. Using mechanism decomposition, kinematics of the manipulator is formulated based on product-of-exponentials method and kinematics of the Metamorphic hand is investigated leading to the construction of grasp constraint providing a theoretical background for measuring grasp quality of the grasps predicted by the grasp-affordance model.

Further, the relation of the grasp-affordance model to the manipulator and hand kinematics with the associated grasp constraint are indicated linking the manipulator kinematics with the grasp-affordance model for object manipulation. The mobile manipulator proposed in this work is to be used for toys tidying up in a child's room with extended applications to the field of service robot in clutter clearing.

8.2 Structure of a Mobile Manipulator with a Metamorphic Robotic Hand

A low cost customised mobile manipulator is designed in this work as illustrated in Fig. 8.1. It contains a mobile platform, i.e. Robotino 3.0 developed by Festo^{TM}, a customised 5-DOF robot arm, a customized 2-DOF wrist and a three-fingered Metamorphic robotic hand. The commercialized mobile robot Robotino 3.0 forms the base of the manipulator permitting it to move, normally translations along and directions and rotation about Z-axis (see Fig. 8.1), freely around specified working environment and locate the manipulator at a desired task position. It contains a vision system and a collision-avoiding contour controller consisting of nine distance sensors. The 5-DOF robot arm is a light-weight arm which is specially designed for the purpose of carrying the proposed Metamorphic hand with an additional 2-DOF wrist. The wrist inherits the structure of a universal joint, and connects the three-fingered Metamorphic hand to the robot arm. The Metamorphic robotic hand consists of a reconfigurable palm and three fingers which are evenly distributed around the palm. Each of the three fingers has two phalanges connected by two parallel revolute joints providing two degrees of freedom.

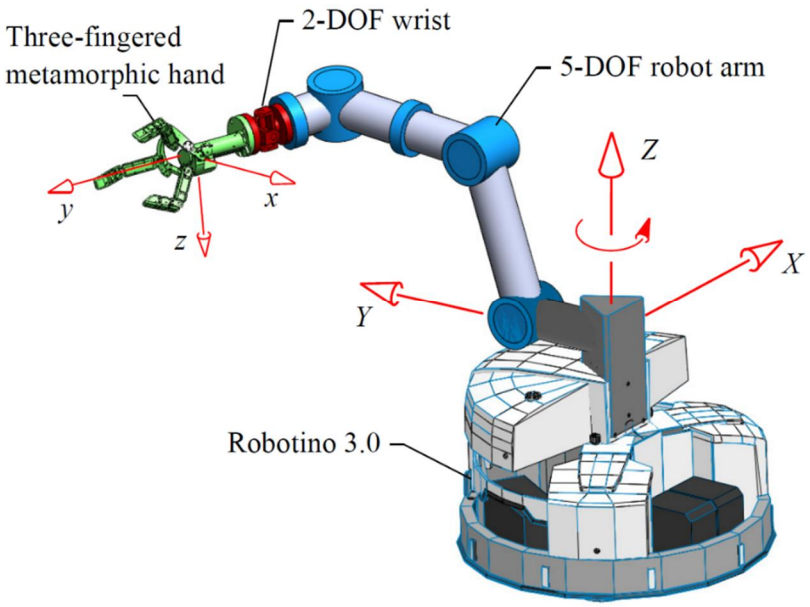

Figure 8.1 Structure of a mobile manipulator with a Metamorphic robotic hand

The articulated reconfigurable palm is formed by a spherical five-bar linkage consisting of five links 1 to 5 with the base link 5 connected to the wrist. The palm has two degrees of freedom and it is actuated by two gear-motor sets respectively at joints A and E as illustrated in Fig. 8.2. The two actuators are utilized to adjust configurations of the palm with either one of them being in particular used to change the structure of the reconfigurable palm by rotating the crank, i.e. link 1 or link 4, to make it overlap link 5 so as to form a four-bar linkage in an innate metamorphic phase. Then, locking either actuator, the palm evolves into a one degree-of-freedom four-bar mode. And if both actuators are locked, the palm becomes rigid. Thus, the palm can change its mobility from two to one, to zero and contrarily from zero to one, to two. In this design, the structure of the palm is symmetric such that the length of link 1 equals the length of link 4 and lengths of links 2 and 3 are of the same. The three two-phalanx fingers are evenly mounted at points F_1, F_2 and F_3 respectively. It should be pointed out that each finger contains only two parallel joints that provide only flexion/extension motions but

no adduction/abduction motion. It is expected that the introducing of the reconfigurable palm will compensate the absence of adduction/abduction motions of the three fingers and provide dexterous manipulation and grasp by adapting configurations of the palm for various tasks and different environment.

Further, in order to secure the innate metamorphic phases, rotatability criterion of spherical linkage [107]from the kinematics of mechanism point of view is considered and the angles corresponding to links 1 to 5 are assigned as $\alpha_1 = \alpha_4 = 35°$, $\alpha_2 = \alpha_3 = 90°$, and such that $\alpha_1 + \alpha_2 + \alpha_3 + \alpha_4 + \alpha_5 = 2\pi$.The angles comply with the condition presented in [107] so that $\alpha_1 + \alpha_2 + \alpha_4 = \alpha_3 + \alpha_5$ leading to the desired property that excluding the indeterminate position where all links fall on a great circle, all joints have full rotatability except for the joint between link 2 and link 3.

8.3 Kinematics of the Metamorphic Hand and the Serial Manipulator

From the mechanism point of view, the whole manipulator is constructed by a complex hybrid mechanism containing a 7-DOF serial arm and a Metamorphic robotic hand which itself is composed of an articulated palm and three open-chain fingers. Using mechanism decomposition, kinematics of the whole manipulator can be achieved by analysing kinematics of the palm, the fingers and the 7- DOF serial arm respectively and then combining and integrating the results leading to the full kinematics of the manipulator.

8.3.1 Geometry and Kinematics of the Articulated Reconfigurable Palm

In this section, kinematics of the articulated reconfigurable palm is investigated first which is to be used as a bridge to connect kinematics of the manipulator with that of the fingers. Fig. 8.2 shows the detailed geometry of the articulated reconfigurable palm which is formed by a spherical five-bar linkage.

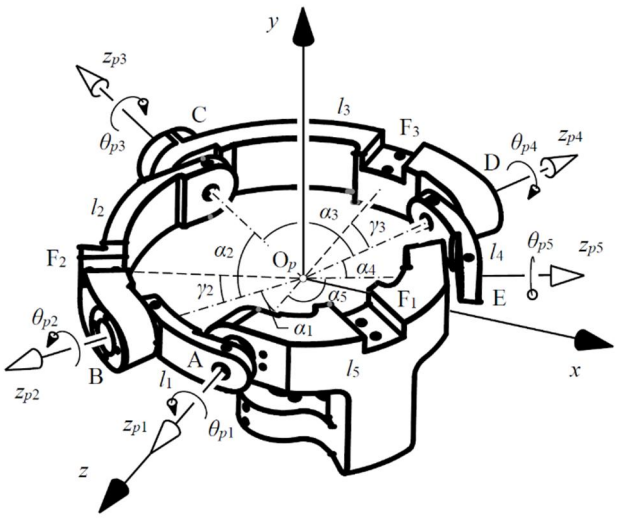

Figure 8.2 The articulated reconfigurable palm and its geometry

In the spherical five-bar linkage, joints A and E are active joints with joint angles denoted as θ_{p1} and θ_{p5}, and joints B, C and D are passive joints with their joint angles respectively denoted as θ_{p2}, θ_{p3}, and θ_{p4}. In order to investigate kinematics of the reconfigurable palm, coordinate systems are set up in Fig. 8.2 in such a way that, for all the body-attached coordinate systems for links 1 to 5, their origins are all located at point O_p with z_{pi}-axis collinear with axis of the proximal joint of the link i, y_{pi}-axis directed along $\boldsymbol{z}_{pi+1} \times \boldsymbol{z}_{\mathrm{pi}}$ for i = 1, 2, 3 and 4, and x_{Pi}-axis determined by y_{pi} and z_{pi} with

the right-hand rule. A global coordinate system is established at point O_p and has its z -axis aligned with the axis of joint A and its y-axis directed along $\boldsymbol{z}_{pi} \times \boldsymbol{z}_{p5}$, coinciding with y_{p5}. Based on this, given the values of angles θ_{p1} and θ_{p5}, according to the calculations in [61], with the relations that $\alpha_4 = \alpha_1$ and $\alpha_3 = \alpha_3$, the passive joint angles θ_{p2}, θ_{p3} and θ_{p4} can be obtained as

$$\theta_{p2} = \cos^{-1}(\cot\alpha_1\cot\alpha_2 - z_C / s\alpha_1 s\alpha_2) \tag{8.1}$$

where $z_C = \dfrac{-B \pm \sqrt{B^2 - 4AC}}{2A}$ with $A = V^2 + Q^2 + 1$, $B = 2(UV + PQ)$ and $C = U^2 + P^2 - 1$. The terms U, V, P, and Q are,

$$U = c\alpha_2(y_D - y_B)/(x_B y_D - y_B x_D),\ V = (y_B z_D - z_B y_D)/(x_B y_D - y_B x_D),$$
$$P = c\alpha_2(x_B - x_D)/(x_B y_D - y_B x_D),\ Q = (z_B x_D - x_B z_D)/(x_B y_D - y_B x_D).$$

In which, the coordinates x_B , y_B , z_B and x_D , y_D , z_D can be derived from the global reference frame as $(x_B, y_B, z_B) = (-s\alpha_1 c\theta_{p1}, -s\alpha_1 s\theta_{p1}, c\alpha_1)$ and $(x_D, y_D, z_D) = (c\alpha_1 s\alpha_5 + s\alpha_1 c\alpha_5 c\theta_{p5}, s\alpha_1 s\theta_{p5}, c\alpha_1 c\alpha_5 - s\alpha_1 s\alpha_5 c\theta_{p5})$.

$$\theta_{p3} = \arctan\frac{F}{E} \pm \arccos\left(\frac{G}{\sqrt{E^2 + F^2}}\right), \tag{8.2}$$

where $E = s\alpha_2(c\alpha_1 s\alpha_2 + s\alpha_1 c\alpha_2 c\theta_{p2})$, $F = -s\alpha_2 s\alpha_1 s\theta_{p2}$ and $G = c\alpha_2(c\alpha_1 c\alpha_2 - s\alpha_1 s\alpha_2 c\theta_{p2}) - c\alpha_1 c\alpha_5 + s\alpha_1 s\alpha_5 c\theta_{p5}$.

$$and \quad \theta_{p4} = \arctan\frac{M}{L} \pm \arccos\left(\frac{N}{\sqrt{M^2 + L^2}}\right). \tag{8.3}$$

with $L = s\alpha_2(s\alpha_1 s\alpha_5 + c\alpha_1 s\alpha_5 c\theta_{p5})$, $M = -s\alpha_2 s\alpha_5 s\theta_{p5}$ and

$N = c\alpha_2(c\alpha_1 c\alpha_5 - s\alpha_1 s\alpha_5 c\theta_{p5}) + (B \mp \sqrt{B^2 - 4AC}) / 2A$.

Thus this section presents geometry and kinematics of the articulated reconfigurable palm which lays a foundation for linking the kinematics of the robot arm and the fingers leading to the full kinematics of the whole manipulator.

8.3.2 Kinematics of the 7-DOF Serial Robot

Treating the robot arm and wrist together as a 7-DOF serial robot, its kinematics can be formulated with product-of-exponentials representation as follows.

The geometry of the serial robot is shown in Fig. 8.3. Lengths of the links are denoted as α_i (i = 1, 2, …, 6) and let θ_i (i = 1, 2, …, 7) corresponds to the fully extended configuration in which zero position (or reference configuration) of the 7-DOF serial robot is defined together with a fixed reference frame $\{O_\mathrm{m}\}$ and an end-effector frame $\{O_\mathrm{p}\}$ attached respectively to the Robotino and the palm of the Metamorphic robotic hand. Further, the direction of positive rotation for each joint is defined as indicated in Fig. 8.3.

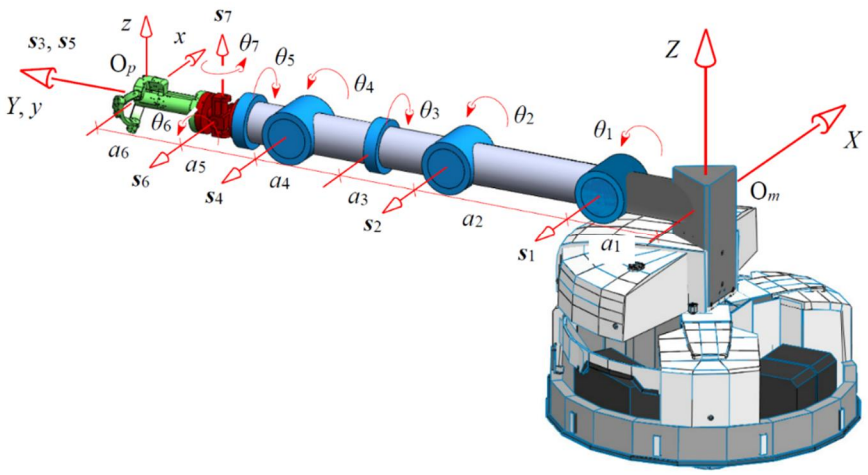

Figure 8.3 Geometry of the mobile manipulator in the reference position.

Using product-of-exponential formula [96][108], the forward kinematics of the proposed 7-DOF serial Robot has the form,

$$\mathbf{T}_{O_m O_p} = e^{[\boldsymbol{S}_1]\theta_1} e^{[\boldsymbol{S}_2]\theta_2} e^{[\boldsymbol{S}_3]\theta_3} e^{[\boldsymbol{S}_4]\theta_4} e^{[\boldsymbol{S}_5]\theta_5} e^{[\boldsymbol{S}_6]\theta_6} e^{[\boldsymbol{S}_7]\theta_7} \mathbf{M}_{O_p}, \tag{8.4}$$

where $\boldsymbol{S}i = (\boldsymbol{\omega}_i, \boldsymbol{v}_i)$ (i = 1, 2, …, 7) is the twist of the i^{th} joint and $\mathbf{M}_{O\text{p}}$ is the position vector of point O_p, both presented in the zero configuration in the fixed frame. The term $\mathbf{M}_{O\text{p}}$ can be directly obtained from Fig. 8.3 as

$$\mathbf{M}_{Op} = \begin{bmatrix} 1 & 0 & 0 & 0 \\ 0 & 1 & 0 & \sum_{i=1}^{6} a_i \\ 0 & 0 & 1 & 0 \\ 0 & 0 & 0 & 1 \end{bmatrix}. \tag{8.5}$$

Referring to Fig. 8.3, in the reference configuration, screw axis of joint 1 is $\boldsymbol{\omega}_1 = \boldsymbol{s}_1 = (-1, 0, 0)$. To determine $\boldsymbol{v}_1$, we pick any arbitrary point $\boldsymbol{r}_1$ that lies on the axis

of joint 1; the most convenient choice is the point $r_1 = (0, a_1, 0)$. Since all the joints in the serial robot are revolute joints, their corresponding pitches are zero, and hence it has $v_1 = r_1 \times \omega_1 = (0, 0, a_1)$. The screw axis of joint 2 is $\omega_2 = s_2 = (-1, 0, 0)$, selecting $r_2 = (0, a_1 + a_2, 0)$, it yields $v_2 = (0, 0, a_1 + a_2)$. The screw axis of joint 3 is in the Y direction of the fixed frame, thus $\omega_3 = s_3 = (0, 1, 0)$, choosing $r_3 = (0, 0, 0)$ results in $v_3 = (0, 0, 0)$. The screw axis of joint 4 is $\omega_4 = s_4 = (-1, 0, 0)$, choosing $r_4 = (0, a_1 + a_2 + a_3 + a_4, 0)$ leads to $v_4 = (0, 0, a_1 + a_2 + a_3 + a_4)$. The screw axis of joint 5 is $\omega_5 = s_5 = (0, 1, 0)$, choosing $r_5 = (0, 0, 0)$, it follows $v_5 = (0, 0, 0)$. The screw axis of joint 6 is $\omega_6 = s_6 = (-1, 0, 0)$, choosing $r_6 = (0, a_1 + a_2 + a_3 + a_4 + a_5, 0)$, it has $v_6 = (0, 0, a_1 + a_2 + a_3 + a_4 + a_5)$. And the screw axis of joint 7 is in the Z direction of the fixed frame, so $\omega_7 = s_7 = (0, 0, 1)$. Assigning $r_7 = (0, a_1 + a_2 + a_3 + a_4 + a_5, 0)$ yields $v_7 = (a_1 + a_2 + a_3 + a_4 + a_5, 0, 0)$. From the above, twists $S_i = (\omega_i, v_i)$ of the 7-DOF serial robot are summarized and listed in Table. 8.1.

Table 8.1 Joint twists of the 7-DOF serial robot

Joint i	$\boldsymbol{\omega}_i$	$\boldsymbol{v}_i$
1	$(-1, 0, 0)^T$	$(-1, 0, \alpha_1)^T$
2	$(-1, 0, 0)^T$	$(-1, 0, \alpha_1 + \alpha_2)^T$
3	$(0, 1, 0)^T$	$(0, 0, 0)^T$
4	$(-1, 0, 0)^T$	$(-1, 0, \alpha_1 + \alpha_2 + \alpha_5 + \alpha_4)^T$
5	$(0, 1, 0)^T$	$(0, 0, 0)^T$
6	$(-1, 0, 0)^T$	$(-1, 0, \alpha_1 + \alpha_2 + \alpha_5 + \alpha_4 + \alpha_5)^T$
7	$(0, 0, 1)^T$	$(\alpha_1 + \alpha_2 + \alpha_5 + \alpha_4 + \alpha_5, 0, 0)^T$

Since the manipulator presented in this chapter contains only revolute joint, each term $e^{[s_i]\theta_i}$ in Eq. (8.4) has the form

$$e^{[s_i]\theta_i} = \begin{bmatrix} e^{[\omega_i]\theta_i} & \left(\mathbf{I} - e^{[\omega_i]\theta_i}\right)(\boldsymbol{\omega}_i \times \boldsymbol{v}_i) \\ \mathbf{0} & 1 \end{bmatrix}. \tag{8.6}$$

where, $e^{[\omega_i]\theta_i} = \mathbf{I} + \sin\theta_i [\boldsymbol{\omega}_i] + (1 - \cos\theta_i)[\boldsymbol{\omega}_i]^2$ with $\mathbf{I}$ being a 3 × 3 identity matrix.

Using Eq. (8.6) and substituting all structure parameters together with Eq. (8.5) into Eqn. (8.4), the full forward kinematics of the 7-DOF serial robot can be obtained as,

$$\mathbf{T}_{O_m O_p} = \begin{bmatrix} \mathbf{R}_{O_m O_p} & \boldsymbol{p}_{O_m O_p} \\ \mathbf{0} & 1 \end{bmatrix}. \tag{8.7}$$

where $\mathbf{R}_{O_m O_p} = \begin{bmatrix} r_{11} & r_{12} & r_{13} \\ r_{21} & r_{22} & r_{23} \\ r_{31} & r_{32} & r_{33} \end{bmatrix}$ and $\boldsymbol{p}_{O_m O_p} = [p_1 \quad p_2 \quad p_3]^{\mathrm{T}}$. Using the notations that $c_i = \cos\theta_i$, $s_i = \sin\theta_i$, $c_{ij} = \cos(\theta_i + \theta_j)$ and $s_{ij} = \sin(\theta_i + \theta_j)$, elements in $\mathbf{R}_{O_m O_p}$ and $\boldsymbol{p}_{O_m O_p}$ are derived as listed in Appendix C.

Equation (8.7) explicitly gives the forward kinematics of the robot arm and based on this inverse kinematics of the manipulator can be solved with the method presented by Gan et al. [109].

8.3.3 Palm Integrated Kinematics of the Metamorphic Hand and the Manipulator

Figure 8.4 shows the design of a three-fingered Metamorphic robotic hand with three two-phalanx fingers integrated to the articulated palm. As aforementioned, the three fingers are evenly distributed around the palm at points F_1, F_2 and F_3, respectively. As indicated in Fig. 8.2, the point F_1 lies at the middle point of link 5, the angle between O_pB and O_pF_2 is γ_2, and the angle between O_pD and O_pF_3 is γ_3, the three fingers are identical and lengths of the proximal phalanx and distal phalanx are respectively a_{f1} and a_{f2}. In order to integrate kinematics of the palm with the kinematics of the fingers, adjoint frames $\{F_i\}$ are established at point F_i with z_{i1} directed along O_pF_i, y_{11}directed along the y-axis of the global reference frame, y_{12} directed along $\boldsymbol{z}_{p3} \times \boldsymbol{z}_{p2}$, and y_{13} directed along $\boldsymbol{z}_{p4} \times \boldsymbol{z}_{p3}$, x_{i1} are determined by right-hand rule.

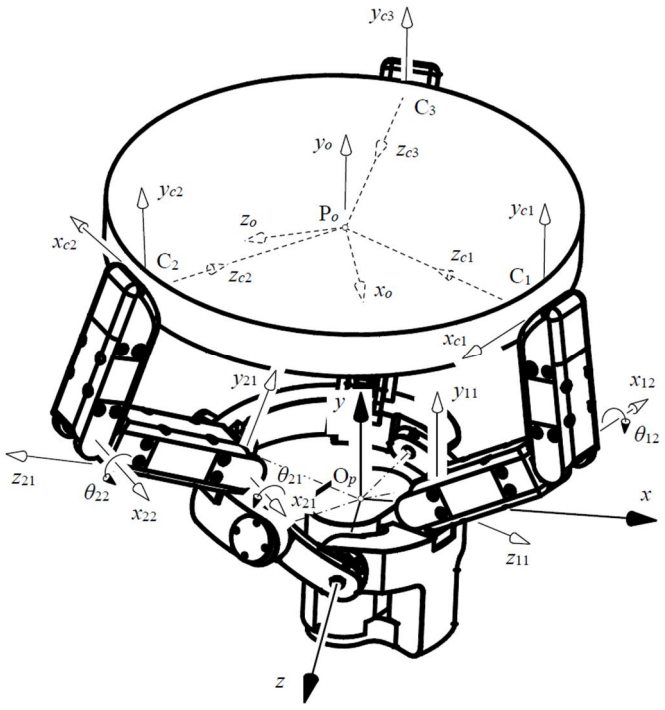

Figure 8.4 Grasp a disk with the three-fingered Metamorphic hand

Based on the above structure parameters and coordinate systems, we first present the finger-base frames in the hand global coordinate system. In which, orientation of the finger-base frame can be expressed with respect to frame {O_p} as

$$\begin{cases} \mathbf{R}_{O_pF_1} = \mathbf{R}(y, \alpha_5 / 2) \\ \mathbf{R}_{O_pF_2} = \mathbf{R}(z_{p1}, \theta_{p1})\mathbf{R}(y_{p1}, -\alpha_1)\mathbf{R}(z_{p2}, \theta_{p2})\mathbf{R}(y_{p2}, -\delta_2) \\ \mathbf{R}_{O_pF_3} = \mathbf{R}(y, \alpha_5)\mathbf{R}(z_{p5}, \theta_{p5})\mathbf{R}(y_{p4}, \alpha_4)\mathbf{R}(z_{p4}, \theta_{p4})\mathbf{R}(y_{p3}, \delta_3) \end{cases} . \quad (8.8)$$

where, θ_{p2} and θ_{p4} can be found in Eqn. (8.1) and (8.3). With Eq. (.88), reference frames of the finger bases can be expressed in the global coordinate system as

$$\mathbf{T}_{O_pF_i} = \begin{bmatrix} \mathbf{R}_{O_pF_i} & \mathbf{R}_{O_pF_i}\boldsymbol{d} \\ \mathbf{0} & 1 \end{bmatrix} \ (i = 1, 2 \ and \ 3), \quad (8.9)$$

where $\boldsymbol{d} = [0, 0, R]^T$ and $\mathbf{R}_{O_pF_i}\boldsymbol{d}$ gives the position vector of point F_i in the global reference frame. R is the theoretical radius of a virtual sphere on which all the links lie. In the finger-base reference frames, coordinates of the fingertips are given as

$$\mathbf{T}_{F_iT_i} = e^{[\boldsymbol{S}_{i1}]\theta_{i1}} e^{[\boldsymbol{S}_{i2}]\theta_{i2}} \mathbf{M}_{F_iT_i}. \quad (8.10)$$

Where, with respect to the zero position of each finger in its corresponding finger-base reference frame, it has $\omega_{i1} = \omega_{i2} = (1, 0, 0)$, for the axis of joint i_1, choosing $r_{i1} = (0, 0, 0)$, it has $v_{i1} = r_{i1} \times \omega_{i1} = (0, 0, 0)$ which yields $S_{i1} = (\omega_{i1}, v_{i1})$. Similarly, for the axis of joint $i2$, selecting $r_{i2} = (0, 0, a_{f1})$ leads to $v_{i2} = r_{i2} \times \omega_{i2} = (0, a_{f1}, 0)$ and

further to $S_{i2} = (\omega_{i2}, v_{i2})$. Further, in the finger reference configuration, there is $M_{F_iT_i} = (I, p_{F_iT_i})$ with I being a 3 by 3 identity matrix and $p_{F_iT_i} = (0, 0, a_{f1} + a_{f2})$.

Integrating the finger kinematics with the palm kinematics, the full kinematics of the three-fingered Metamorphic robotic hand can be presented in the hand global coordinate system as

$$\mathbf{T}_{O_pT_i} = \mathbf{T}_{O_pF_i}\mathbf{T}_{F_iT_i}, (i = 1, 2 \; and \; 3), \tag{8.11}$$

and subsequently in the manipulator global coordinate system as

$$\mathbf{T}_{O_mT_i} = \mathbf{T}_{O_mO_p}\mathbf{T}_{O_pF_i}\mathbf{T}_{F_iT_i}, (i = 1, 2 \; and \; 3), \tag{8.12}$$

Eq. (8.12) presents the integrated full kinematics for the proposed manipulator and Eqs. (8.11) and (8.12) provides background for further workspace, manipulability and dexterity analysis of the proposed Metamorphic hand and the mobile manipulator. Inverse kinematics of the proposed Metamorphic hand can be solved with the method provided by Gao et al. [110]. Based on the hand kinematics, grasp constraint of the robotic hand can be constructed.

8.4 Metamorphic Hand based Grasp Constraints

Based on the above hand kinematics, grasp constraint of the Metamorphic hand is formulated in this section laying theoretical approach for measuring the grasps predicted by grasp-affordance model from learning processor in the virtual environment for a specified object.

8.4.1 Form of Grasp Map and Grasp Constraints

According to [96], grasp an object with *n* fingers contacting it, the grasp map with respect to the object reference has the form

$$\mathbf{G} = \begin{bmatrix} \mathbf{Ad}^{T}_{g^{-1}_{oc_1}} \mathbf{B}_{c_1} & \cdots & \mathbf{Ad}^{T}_{g^{-1}_{oc_n}} \mathbf{B}_{c_n} \end{bmatrix}, \tag{8.13}$$

with $\mathbf{B}_{ci}$ indicating the wrench basis corresponding to different contact type. And grasp constraint of a multifingered hand grasping has the form

$$\mathbf{J_h}(\theta, x_o)\dot{\boldsymbol{\theta}} = \mathbf{G}^T \boldsymbol{V}^b_{po}, \tag{8.14}$$

where matrix $J_h(\theta, x_o)$, hand Jacobian, has the form

$$\mathbf{J}_h(\theta, x_o) = \begin{bmatrix} \mathbf{B}^T_{c_1} \mathbf{Ad}^{-1}_{g_{s_1 c_1}} \mathbf{J}^s_{s_1 f_1}(\theta_{f_1}) & & 0 \\ & \ddots & \\ 0 & & \mathbf{B}^T_{c_n} \mathbf{Ad}^{-1}_{g_{s_n c_n}} \mathbf{J}^s_{s_n f_n}(\theta_{f_n}) \end{bmatrix},$$

with $\dot{\boldsymbol{\theta}} = (\dot{\theta}_{f1}, \cdots, \dot{\theta}_{fn})$ giving the joint velocities, and $\boldsymbol{V}^b_{po}$ is the body velocity of the object expressed in a global reference frame.

Considering the example illustrated in Fig. 8.4 with the proposed Metamorphic hand grasping a disk and assuming that the contact type between the fingertips and the disk

is point contact with friction, grasp constraint of the case is constructed and formulated in the following section.

8.4.2 Grasp Constraints of the Metamorphic Hand

Referring to Fig. 8.4, without loss of generality, it is assumed that the contact points between the four fingers and the disk lying on the same plane which passes through the centroid of the disk and parallel to its two facets. The object reference frame $\{P_o\}$ is set up at the centroid of the disk with its x_o-axis and z_o-axis lie on the same plane which is formed by the three contact points. Contact frames $\{C_i\}$, i = 1, 2 and 3 are located at the contact points with its z_{ci}-axis directing towards point P_o and y_{ci}-axis parallel to y_o-axis. Then, contact frames can be presented in the object frame as

$$\mathbf{R}_{P_oC_i} = \begin{bmatrix} c\varphi_i & 0 & -s\varphi_i \\ 0 & 1 & 0 \\ s\varphi_i & 0 & c\varphi_i \end{bmatrix} \text{ and } \boldsymbol{p}_{P_oC_i} = \begin{bmatrix} r_d s\varphi_i \\ 0 \\ r_d c\varphi_i \end{bmatrix}. \tag{8.15}$$

where φ_i denotes the angle between x_{ci}-axis and x_o-axis with i = 1, 2 and 3, and rd denotes the radius of the disk.

With Eq. (8.15), the grasp map for each finger can be constructed by transforming the standard wrench basis of point-contact-with-friction into the object reference frame as

$$\mathbf{G}_i = \begin{bmatrix} \mathbf{R}_{P_oC_i} & 0 \\ \left[\boldsymbol{p}_{P_oC_i}\right]\mathbf{R}_{P_oC_i} & \mathbf{R}_{P_oC_i} \end{bmatrix} \mathbf{B}_{c_i} = \begin{bmatrix} c\varphi_i & 0 & -s\varphi_i \\ 0 & 1 & 0 \\ s\varphi_i & 0 & c\varphi_i \\ 0 & -r_d c\varphi_i & 0 \\ r_d c(2\varphi_i) & 0 & -r_d s(2\varphi_i) \\ 0 & r_d s\varphi_i & 0 \end{bmatrix}, \tag{8.16}$$

where, the wrench basis for each finger is $\mathbf{B}_{c_i} = \left(\mathbf{I}_{3\times3}, 0_{3\times3}\right)$ for i = 1, 2 and 3.

Substituting Eq. (8.16) into Eq. (8.13), grasp map for the grasp case indicated in Fig.8.4 can be obtained as

$$\mathbf{G} = \begin{bmatrix} \mathbf{G}_1 & \mathbf{G}_2 & \mathbf{G}_3 \end{bmatrix}_{6\times9}. \tag{8.17}$$

The parameter φ_i can be determined in the object reference frame upon the grasp is formed and the contact points are identified. The force-closure property of this grasp can then be detected by convexity conditions.

Since each of the fingers is a RR open chain, its Jacobian with respect to the finger-base reference frame has the form

$$\mathbf{J}^s_{F_iT_i} = \begin{bmatrix} 0 & 0 & 0 & 1 & 0 & 0) \\ 0 & a_{f1}c\theta_{i1} & -a_{f1}s\theta_{i1} & 1 & 0 & 0 \end{bmatrix}^{\mathrm{T}}. \tag{8.18}$$

Further, referring to Eq. (8.14), in order to formulate grasp constraint for the grasp shown in Fig. 8.4, $\mathbf{Ad}^{-1}_{T_{F_iC_i}}$ needs to be constructed. According to the relations of the coordinate systems illustrated in Fig.8.4, following equation exists

$$\mathbf{Ad}^{-1}_{T_{F_iC_i}} = \mathbf{Ad}^{-1}_{T_{P_oC_i}} \mathbf{Ad}^{-1}_{T_{O_pP_o}} \mathbf{Ad}^{-1}_{T_{F_iP_o}}. \tag{8.19}$$

In the object reference frame, the first term on the right-hand side of Eq. (8.19) can be written as

$$\mathbf{Ad}^{-1}_{T_{P_oC_i}} = \begin{bmatrix} \mathbf{R}^T_{P_oC_i} & -\mathbf{R}^T_{P_oC_i}\left[\boldsymbol{p}_{P_oC_i}\right] \\ 0 & \mathbf{R}^T_{P_oC_i} \end{bmatrix}. \tag{8.20}$$

Substituting Eq. (8.15) into Eq. (8.20) yields

$$\mathbf{Ad}^{-1}_{T_{P_oC_i}} = \begin{bmatrix} c\varphi_i & 0 & s\varphi_i & 0 & r_d c(2\varphi_i) & 0 \\ 0 & 1 & 0 & -r_d c\varphi_i & 0 & r_d s\varphi_i \\ -s\varphi_i & 0 & c\varphi_i & 0 & -r_d s(2\varphi_i) & 0 \\ 0 & 0 & 0 & c\varphi_i & 0 & s\varphi_i \\ 0 & 0 & 0 & 0 & 1 & 0 \\ 0 & 0 & 0 & -s\varphi_i & 0 & c\varphi_i \end{bmatrix}. \tag{8.21}$$

We assume that with respect to the hand global reference frame $\{O_p\}$, orientation and position of the object reference frame, which can be obtained from the virtual environment of the grasp affordance model, are

$$\mathbf{R}_{O_pP_o} = \begin{bmatrix} c\phi c\theta & c\phi s\theta s\psi - s\phi c\psi & c\phi s\theta c\psi + s\phi s\psi \\ s\phi c\theta & s\phi s\theta s\psi + c\phi c\psi & s\phi s\theta c\psi - c\phi s\psi \\ -s\theta & c\theta s\psi & c\theta c\psi \end{bmatrix}, \tag{8.22}$$

and

$$\boldsymbol{p}_{O_pP_o} = \begin{bmatrix} x_{O_pP_o} \\ y_{O_pP_o} \\ z_{O_pP_o} \end{bmatrix}, \tag{8.23}$$

with ϕ, θ *and* ψ representing the Euler angles of the object coordinate with respect to the hand global coordinate system. Then, the second term on the right-hand side of Eq. (8.19) can be constructed as

$$\mathbf{Ad}^{-1}_{T_{O_pP_o}} = \begin{bmatrix} \mathbf{R}^T_{O_pP_o} & -\mathbf{R}^T_{O_pP_o}\left[p_{O_pP_o}\right] \\ \mathbf{0} & \mathbf{R}^T_{O_pP_o} \end{bmatrix}. \tag{8.24}$$

In addition, substituting terms $\mathbf{R}_{O_pF_i}$ and $p_{O_pF_i}$ in Eq. (8.9) into the following equation

$$\mathbf{Ad}^{-1}_{T_{F_iO_p}} = \mathbf{Ad}_{T_{O_pF_i}} = \begin{bmatrix} \mathbf{R}_{O_pF_i} & \left[\boldsymbol{p}_{O_pF_i}\right]\mathbf{R}_{O_pF_i} \\ \mathbf{0} & \mathbf{R}_{O_pF_i} \end{bmatrix}, \tag{8.25}$$

the third term on the right-hand side of Eq. (8.19) can be obtained.

Substituting Eqs. (8.18) and (19) into Eq. (8.14) results in the hand Jacobian for the case shown in Fig. 8.4 as

$$\mathbf{J}_h = \begin{bmatrix} \mathbf{J}_{11} & 0 & 0 \\ 0 & \mathbf{J}_{22} & 0 \\ 0 & 0 & \mathbf{J}_{33} \end{bmatrix}_{9\times 6}, \tag{8.26}$$

where, for i = 1, 2 and 3, the 3×2 sub-matrix $\mathbf{J}_{ii}$ has the form

$$\mathbf{J}_{ii} = \mathbf{B}_{C_i}^{T} \mathbf{Ad}_{T_{F_i}C_i}^{-1} \mathbf{J}_{F_iT_i}^{s},$$

which can be obtained through symbolic computer program system such as Matlab™ upon all the essential variables are given.

The grasp map and the grasp constraint derived above can be used to evaluate the properties of grasps performed by the Metamorphic hand and thus measures and verifies the grasp quality obtained through grasp-affordance model. Further, if for any object motion $\boldsymbol{V}_{O_pP_o}^{b}$ there exists $\dot{\boldsymbol{\theta}}$ which satisfies Eq. (8.14), the grasp executed by the Metamorphic hand is supposed to be manipulatable.

8.5 Grasp Affordance Related to the Manipulator Kinematics and Grasp Constraints

In order to investigate the performance of the proposed mobile manipulator in a virtual environment and providing joint space for the manipulator to implement a desired task, the concept of grasp affordance is introduced in this section together with its relation to the manipulator kinematics and the aforementioned grasp constraint.

8.5.1 Grasp Affordance based on Object Models

According to Gibson [111], gripper-dependent grasp parameters associated with object models [99] are commonly coined as grasp affordance. In the grasp-affordance model,

the 6D (3D rotations and 3D translations) pose $\mathbf{T}_{O_m O_p} = (\mathbf{R}_{O_m O_p}, \boldsymbol{p}_{O_m O_p})$, $\mathbf{R}_{O_m O_p} \in SO(3)$ and $\boldsymbol{p}_{O_m O_p} \in \mathbb{R}^3$ of the Metamorphic hand is defined as grasp pose, or simply grasp denoted as x_{T_g}, and a grasp x_{T_g} is successful if placing the Metamorphic hand at $\mathbf{T}_{O_m O_p}$ and closing its fingers leads the hand to firmly grasp and lift up the object. By introducing grasp density which consists of a probability density function defined on the group of 6D poses *SE*(3), the grasp density of an object with pose x_{T_o} is proportional, for any robotic hand pose x_{T_g}, to the probability of grasp success when x_{T_o} lies in a reference pose and the Metamorphic hand is brought and closed at x_{T_g}. Linking to visual percepts, grasp densities are registered to a visual object model so as to be aligned to arbitrary object poses by visual pose estimation which can be formulated by the kernel density estimation (KDE) method.

Grasp densities are defined on *SE*(3), and using the KDE method [101] each grasp x_{T_g} is factorized into two functions defined on $\mathbb{R}^3$ and *SO*(3). Presenting the segregation of $x_{T_g} \in SE(3)$ into a translation $\boldsymbol{p}_{O_m O_p}$ and a rotation $\mathbf{R}_{O_m O_p}$ by

$$x_{T_g} = T_{O_m O_p} = \left(\mathbf{R}_{O_m O_p}, p_{O_m O_p}\right), \mu = \left(\mu_t, \mu_r\right), \sigma = \left(\sigma_t, \sigma_r\right), \tag{8.27}$$

the kernel is defined as

$$\mathbf{K}_{\mu,\sigma}\left(x_{T_g}\right) = \mathbf{N}_{\mu_t,\sigma_t} \Theta_{\mu_r,\sigma_r}\left(\theta\right), \tag{8.28}$$

where μ is the kernel mean point, σ is the kernel bandwidth, **N** is a trivariate isotropic Gaussian kernel, and Θ is an orientation kernel defined on *SO*(3). The orientation kernel Θ is defined with the unit-quaternion representation of 3D rotations and the von-Mises Fisher distribution on the 3-sphere in $\mathbb{R}^4$.

With the above equation and using method and algorithm presented by Detry et al.[99,101], by integrating the robotic hand in the virtual environment in which the model of a specified object is established, the optimized grasp $x_{T_g} = (\mathbf{R}_{O_m O_p}, \boldsymbol{p}_{O_m O_p})$ can be identified so as to place the reference frame of the Metamorphic hand for performing a potential successful grasp.

Considering using the mobile manipulator presented in this chapter to grasp an object, based on the grasp-affordance model, the grasp x_{T_g} obtained through the above process gives the pose of reference frame $\{O_p\}$ which is determined by the joint space of the 5-DOF robot arm and 2-DOF wrist. Referring to Fig. 8.1, the robot arm together with the wrist form a 7-DOF redundant serial robot. If the coordinates of the reference frame $\{O_{OmOp}\}$ are given, inverse kinematics of the 7-DOF serial robot needs to be solved so as to identify the corresponding joint space of the robot arm and wrist leading the robot hand to the specified pose to complete the grasp of the object.

8.5.2 Relation of Grasp Affordance to the Manipulator Kinematics and Grasp Constraints

The object-based grasp-affordance model provides a method of finding appropriate poses for successful grasp through virtual environment and machine learning, and the

grasp constraint theoretically provides an approach for measuring and verifying the quality of thus a grasp. The relations of grasp affordance, manipulator kinematics, and hand kinematics and grasp constraint are illustrated in Fig. 8.5. Object based grasp-affordance model predicts optimized poses $\mathbf{T}_{O_m O_p} = \left(\mathbf{R}_{O_m O_p}, \boldsymbol{p}_{O_m O_p} \right)$ for placing a specified robotic end-effector to perform possible successful grasps and the inverse kinematics of the manipulator identifies appropriate joint space leading the Metamorphic hand to the predicted poses.

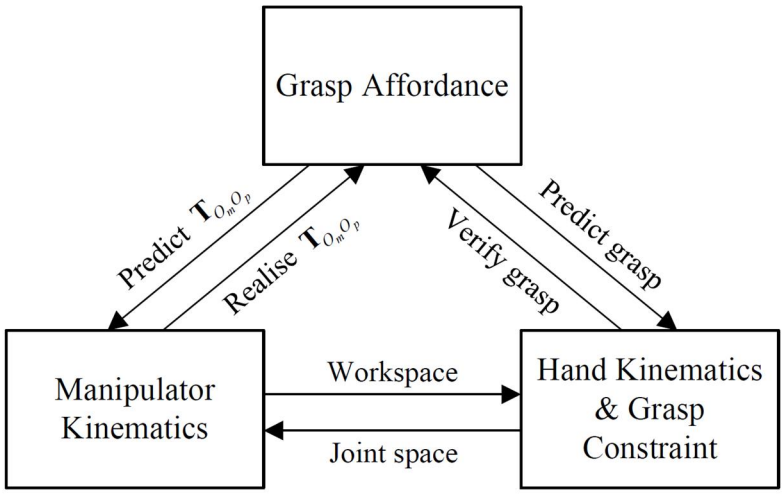

Figure 8.5 Relations of grasp affordance, manipulator kinematics and grasp constraint

Grasp-affordance model predicts divers kinematic possibilities for the robotic hand to grasp a specified object forming a grasp map **G** and the hand kinematics and grasp constraint verify the quality of an individual predicted grasp based on the hand Jacobian $\mathbf{J}_h$. Further, the hand kinematics lies in the range of workspace of the manipulator and the poses of the robotic and determined joint space of the manipulator. Integrating the manipulator kinematics and hand kinematics leads to the full kinematics of the proposed Metamorphic hand $\mathbf{T}_{O_m T_i}$.

8.6 Conclusions

In this chapter, a new and economic mobile manipulator was designed and developed by integrating a three-fingered Metamorphic hand and a customized 7-DOF arm-wrist set into a mobile platform–Robotino 3.0. The structure of the proposed mobile manipulator was presented and kinematics of the 7-DOF serial robot was investigated based on the product-of-exponential method in Lie displacement group providing background for leading the Metamorphic hand to the poses predicted with the grasp-affordance model. Based on mechanism decomposition, kinematics of the three-fingered Metamorphic robotic hand was subsequently implemented followed by the construction of grasp map and grasp constraint of the hand laying a theoretical foundation for measuring grasp quality for each individual grasp predicted by the grasp-affordance model.

Furthermore, relations of the grasp-affordance model, manipulator kinematics and hand kinematics with its associated grasp constraint were revealed and interpreted linking kinematics in robotics with machine learning in computer science. The flexible mobile manipulator presented in the chapter was developed for the application of clutter clearing with special scenarios for toys clearing up in child's room or in a nursery environment.

Chapter 9 Geometric Topology with Product Submanifolds on Metamorphic Hand Grasping

9.1 Introduction

When manipulating an object, a robotic hand system together with the object could be modelled by an equivalent parallel mechanism[64,112]. Grasp constraints that being applied to the object, performance analysis of the robotic hand, and further optimization design of the robotic hand can be implemented by using such methodology. All these modelling and analysis become more complicated immediately when doing manipulation with the Metamorphic hand since a reconfigurable palm is integrated. This chapter is to resolve the grasp constraints of an object manipulated by the Metamorphic hand. To bridge the gap between the mechanism principle and manipulation theory with the Metamorphic hand, an analytical method based on product submanifolds in the scope of Lie group $SE(3)$ is to be built and then to be applied to the grasp constraint analysis. This chapter then established a method of Lie group integrated topology diagram with reduction operations for analyzing complex parallel mechanisms and manipulation performance with the Metamorphic hand.

9.2 Product Submanifolds and its Tangent Space

9.2.1 Product Submanifolds of *SE*(3)

This section is to retrieve several fundamental concepts in Lie groups and product submanifolds from mathematical books[113,114], paving a way for using a product submanifold based approach in the scope of Lie group to perform kinematics analysis of the metamorphic hand with a reconfigurable palm.

A *complex* of the rigid motion group *SE*(3) can be defined as a subset of elements of *SE*(3) and coined $C \subseteq SE(3)$. With the concept of the complex of *SE*(3), a submanifold *M* of *SE*(3) can be regarded as a complex of *SE*(3) attached with the smooth group operations and we coin it $M \leq SE(3)$. If the closure property is satisfied for *M*, a subgroup *S* of *SE*(3) can be obtained and written as $S \leq SE(3)$. Alternatively, a subgroup of *SE*(3) can be directly obtained from a complex of *SE*(3) in the case the group axioms are fulfilled for the complex. The above relationship among the complex, submanifold, and subgroup of *SE*(3) is described in the following three definitions and is illustrated by the following commutative diagram in Fig. 9.1.

Definition 1. A *complex* of the rigid motion group *SE*(3) can be defined as a subset of elements of *SE*(3) and coined $C \subseteq SE(3)$.

Definition 2. A *submanifold* of *SE*(3) is a complex of *SE*(3) attached with the smooth group operations and designated as $M \leq SE(3)$.

Definition 3. A *subgroup* of *SE*(3) is identified by a submanifold of *SE*(3) when the *closure property* is satisfied for the submanifold and we described it $S \leq SE(3)$.

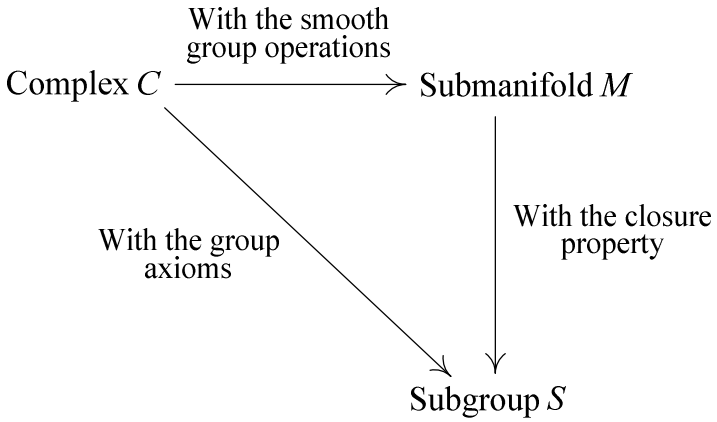

Figure 9.1 The relationship among the complex, submanifold, and subgroup of SE(3)

The product $C_1 \cdot C_2$ of two complexes C_1, C_2 of *SE*(3) is defined as the subset $C=\{c_1 \cdot c_2: c_1 \in C_1, c_2 \in C_2\}$ in which the product is the group multiplication of *SE*(3). Similar to the definition of the submanifold of *SE*(3) in the above, if integrating smooth group operations with the subset *C* attaining from the product of two complexes, the submanifold *M* of *SE*(3) can be obtained from the subset *C* and it is coined *product submanifold* in this chapter. It is not difficult to prove that *M* is the product of two submanifolds M_1, M_2 growing from the complexes C_1, C_2. It is noteworthy that the product operation in the product submanifold is distinctive with the product in the concept of product submanifold in the theory of differential manifolds. The former product is nothing more than the group multiplication of *SE*(3), while the latter product refers to the direct product or the Cartesian product of two submanifolds.

Definition 4. *The product $C_1 \cdot C_2$ of two complexes C_1, C_2*of $SE(3)$ is defined as the subset $C=\{c_1 \cdot c_2 : c_1 \in C_1, c_2 \in C_2\}$, in which the product is the group multiplication of $SE(3)$.

Definition 5. If integrating smooth group operations with the subset C attaining from the product of two complexes, the submanifold M of $SE(3)$ can be obtained from the subset C and, giving the *product submanifold of submanifolds* M_1, M_2 in which the two submanifolds grow from the complexes C_1, C_2. It is described as $M=M_1 \cdot M_2$.

If more strictly, let the two complexes C_1, C_2 fulfil the group axioms, then two subgroups S_1, S_2 are given. The product of subgroups S_1, S_2 of $SE(3)$ does not necessarily give another subgroup unless the closure property is satisfied for the resultant subset of the product, but usually gives a product submanifold according to the above definitions. In the same manner, we can derive the product of three or more submanifolds or subgroups to generate a product submanifold of $SE(3)$.

In kinematics, the product submanifold is, in fact, a mathematical representation of the well-known kinematic bond put forward by Hervé [115].

9.2.2 Tangent Spaces of Product Submanifolds

In certain instances, the tangent space of a product submanifold plays an essential role in mechanism analysis. From the differential geometry, the tangent space of a product submanifold is equivalent to the product of the tangent spaces of the submanifolds[114]. Let M_1, M_2, …, M_n be a sequence of differential manifolds of dimension d_1, d_2, …, d_n respectively, a product submanifold M of dimension $(d_1 + d_2 + \ldots + d_n)$ can be obtained

by taking the product of these manifolds and can be denoted as $M = M_1 \times M_2 \times \ldots \times M_n$. Hence, manifolds M_1, M_2, … , M_n come as submanifolds of M. As to the tangent spaces of product submanifold and its submanifolds, we have an isomorphism as follows

$$\phi: \mathrm{T}_p M \to \mathrm{T}_{p1} M_1 \times \mathrm{T}_{p2} M_2 \times \cdots \times \mathrm{T}_{pn} M_n \tag{9.1}$$

in which p_1, p_2, … , p_n are the projections of p on M_1, M_2, …, M_n respectively. That is to say, the tangent space of a product submanifold is equivalent to the product of the tangent spaces of the corresponding submanifolds. Considering the exponential map between a manifold with its tangent space, the relationship amongst the product submanifold of the submanifolds and the related tangent spaces can be described by a commutative diagram in Fig. 9.2.

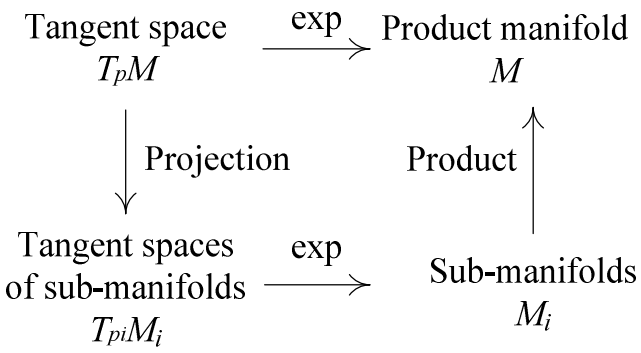

Figure 9.2 A commutative diagram for the product submanifold, the submanifolds, and the related tangent spaces

From Fig. 9.2, a submanifold of $SE(3)$ can be obtained through two approaches, in which one is to take the product of its submanifolds to gain a product submanifold, and

the other is to obtain its tangent space followed by taking the exponential map of the tangent space.

9.2.3 10 Lie Subgroups of *SE*(3)

In the rigid motion group *SE*(3), there exist 10 proper subgroups[118] in which smooth operations can be applied and hence form Lie subgroups[26,116,117]. These Lie subgroups, from dimension 1 to 4, are usually used to represent the motion generated by kinematic joints or kinematic bones. Table 9.1 lists these 10 proper subgroups with the corresponding motion types.

Table 9.1 Proper lie subgroups of *SE*(3) with motion types

Dimension	Lie subgroups
1	$\mathcal{T}$ (***u***), 1-dimensional translation $\mathcal{R}$ (P, ***u***), 1-dimensional rotation $\mathcal{H}$ (P, ***u***, *h*), Screw motion
2	$\mathcal{T}$ (2), Planar Cartesian motion C (P, ***u***), Cylindrical motion
3	$\mathcal{T}$ (3), Spatial Cartesian motion $\mathcal{G}$ (***u***), Planar motion $\mathcal{Y}$ (***w***, *h*), Pseudo-planar motion S (3), Rotational motion
4	$\mathcal{X}$ (***w***), SCARA motion

In parallel mechanisms, the above 10 proper Lie subgroups of *SE*(3) generate various product submanifolds by different combinations and it provides a compact representation of displacements generated by parallel mechanisms. The tangent spaces of these product submanifolds can be obtained by taking direct product of the

corresponding Lie algebras of the above 10 proper Lie subgroups. Such a representation is to be applied to the grasp constraint analysis of the Metahand in the following section.

9.3 Operation of Lie Group for Metamorphic Hand Grasping

9.3.1 Topology Diagram for the Metamorphic Hand

Figure 8.4 gives the structure of the three-fingered Metamorphic hand and the geometric model when it manipulates a cylindrical disk with a tripod grasping. More details of the description of the structure and its geometrical meanings refer to section 7.2.

Considering the geometrical structure of the above hand-object system and its kinematics property, we create a Lie group built-in topology diagram as illustrated in Fig. 9.3 below. In the topology diagram, each single vertex described by a circle represents a link in the above hand-object system, that is either a palm link or a finger phalange. Particularly, P_i (i=1, 2, …, 5) in Fig. 9.3 describes the five revolute joints on the reconfigurable palm and in such a case P_iP_j (j=1, 2, …, 5 and $i \neq j$) in the vertexes lying in the outer loop represents the link connecting any two palm joints. Similarly, A_i, B_i, C_i represents the revolute joints on the fingers, and A_kB_l, B_kC_l (k, l = 1, 2, …, 5 and $k \neq l$) locating in the inner vertexes represent the phalange connecting any two finger joints. Each single edge in the topology diagram presents the kinematic joint that connects two adjacent links fastened to the joint. We attach a Lie subgroup of $SE(3)$ in table 1 to each single edge to represent the motion space generated by the corresponding joint. The character F in the central circle presents the cylindrical disk.

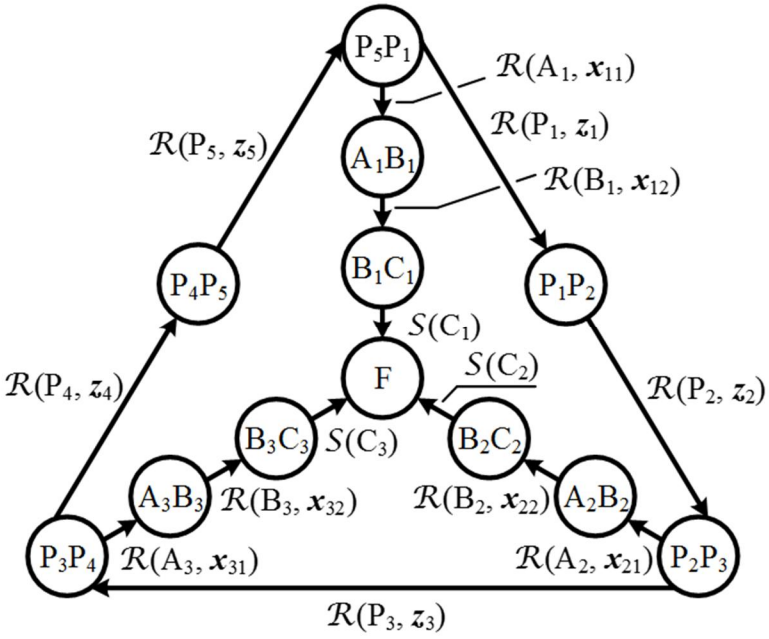

Figure 9.3 Lie group built-in topology diagram for the hand-object system with a reconfigurable base

9.3.2 Lie Group Operations on Hand-Object Model

Such a representation of the topology benefits the modelling and analysis of the hand-object system, especially the case that the robotic hand has a reconfigurable palm. It makes the operations much easier to be done and provides a compact representation of the operations, such as merging two adjacent edges or a series of connected edges, deducting the motions using equivalent product submanifolds. For example, in Fig. 9.3, if merging all the Lie subgroups from vertex P_5P_1 to F, the operation can be implemented by considering definition 5 to take the product of several Lie subgroups and the result can be obtained as

$$\mathcal{M}_1 = \mathcal{R}\left(\mathrm{A}_1, \boldsymbol{x}_{11}\right)\mathcal{R}\left(\mathrm{B}_1, \boldsymbol{x}_{12}\right)S\left(\mathrm{C}_1\right) \tag{9.2}$$

.

To calculate the displacement representation of vertex F with respect to the base P_5P_1, an iterative algorithm to deduct the above topology diagram is to be carried out by applying the following two operations:

1. Compute the intersection of product submanifolds of two adjacent fingers.
2. Compute the intersection of product submanifolds on outer edges of the diagram with restricted-displacement manifolds of the two related fingers.

From Fig. 9.3, the product submanifold for finger 2 and 3 can be presented respectively as,

$$\mathcal{M}_2 = \mathcal{R}\left(\mathrm{A}_2, \boldsymbol{x}_{21}\right)\mathcal{R}\left(\mathrm{B}_2, \boldsymbol{x}_{22}\right)S\left(\mathrm{C}_2\right) \tag{9.3}$$

$$\mathcal{M}_3 = \mathcal{R}\left(\mathrm{A}_3, \boldsymbol{x}_{31}\right)\mathcal{R}\left(\mathrm{B}_3, \boldsymbol{x}_{32}\right)S\left(\mathrm{C}_3\right) \tag{9.4}$$

Two product submanifolds can be substituted by each other if they generate the same Lie subgroup in table 1 or they are equivalent under group conjugation. Based on this proposition, when joint P_3 between fingers 2 and 3 are released and the other joints on the metamorphic palm are locked, the above first operation which resolves the intersection of product submanifolds of the two adjacent fingers can be achieved as below

$$\mathcal{M}_2 \cap \mathcal{M}_3 = \mathcal{T}\left(\boldsymbol{y}_0\right)S\left(\mathrm{P}_0\right) \tag{9.5}$$

The above result represents the displacement submanifold of the platform under the particular geometrical condition when only joint P_3 on the palm is released.

Further, the above second operation can be applied as follows

$$\left(\left(\mathcal{M}_2 \cup \mathcal{M}_3\right)/\left(\mathcal{M}_2 \cap \mathcal{M}_3\right)\right) \cap \mathcal{R}\left(\mathrm{P}_3, \boldsymbol{z}_3\right) = \varnothing \tag{9.6}$$

In such a case if only P_3 on the palm is released, the displacement submanifold of the platform that generated by fingers 2, 3 and the joint P_3 can be represented as

$$\mathcal{M}_{23} = \mathcal{T}\left(\boldsymbol{y}_0\right) S\left(\mathrm{P}_0\right) \tag{9.7}$$

From the above derivations, the topology diagram in Fig. 9.3 can be deducted to a simplified topology diagram as shown in Fig. 9.4.

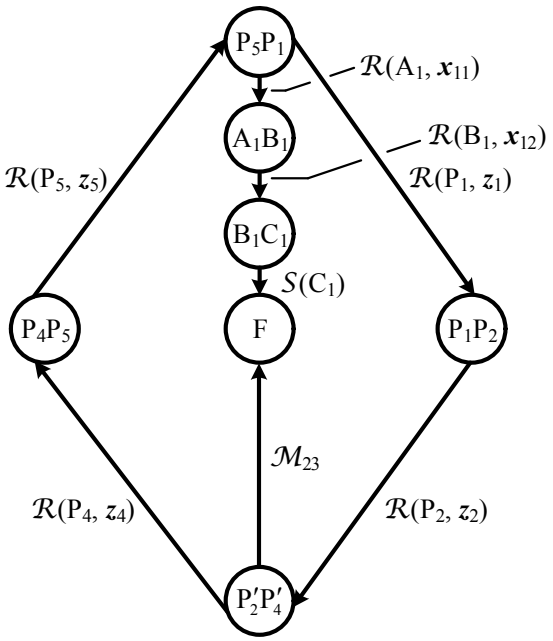

Figure 9.4 A simplified topology diagram by merging the subgroups of finger 2 and 3

From Fig. 9.3, when joints P_1, P_2 and P_3 are locked and the other joints on the metamorphic palm are released, applying the above two operations in the same manner, the displacement manifold of the platform which graph representation is shown in Fig. 9.4 can be derived as below

$$\mathcal{M}_1 \cap \mathcal{M}_{23} = \mathcal{T}(\boldsymbol{y}_0) S(\mathrm{P}_0) \tag{9.8}$$

$$\left((\mathcal{M}_1 \cup \mathcal{M}_{23})/(\mathcal{M}_1 \cap \mathcal{M}_{23})\right) \cap \left(\mathcal{R}(\mathrm{P}_1, \boldsymbol{z}_1)\mathcal{R}(\mathrm{P}_2, \boldsymbol{z}_2)\right) = \mathcal{T}(\rho_1 \boldsymbol{x}_0 + \rho_2 \boldsymbol{z}_0) \tag{9.9}$$

$$\mathcal{M}_{123} = \mathcal{T}(\boldsymbol{y}_0) S(\mathrm{P}_0) \mathcal{T}(\rho_1 \boldsymbol{x}_0 + \rho_2 \boldsymbol{z}_0) \tag{9.10}$$

Then the topology diagram can be deducted to the following diagram by merging all the Lie subgroups produced by the kinematic joints on fingers as shown in Fig. 9.5.

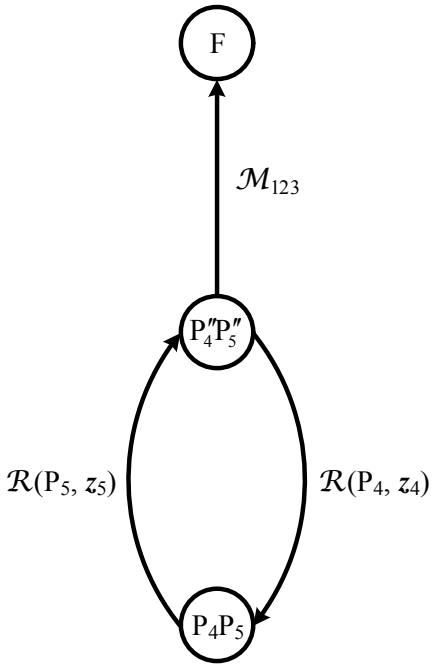

Figure 9.5 A simplified topology diagram by merging all the subgroups of finger 1, 2 and 3

Hence, the grasp constraints of the cylindrical disk with respect to the base P_5P_1 can be expressed by the displacement submanifold of the platform as

$$\mathcal{R}(\mathrm{P}_4, \boldsymbol{z}_4) \cap \mathcal{R}(\mathrm{P}_5, \boldsymbol{z}_5) = \varnothing \tag{9.11}$$

$$\mathcal{M} = \mathcal{M}_{123} = \mathcal{T}(\boldsymbol{y}_0) S(\mathrm{P}_0) \mathcal{T}(\rho_1 \boldsymbol{x}_0 + \rho_2 \boldsymbol{z}_0) \tag{9.12}$$

and the final topology diagram can be deducted as below in Fig. 9.6.

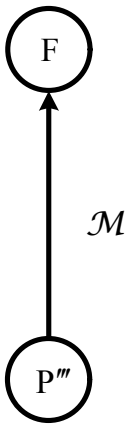

Figure 9.6 The final deducted topology diagram of the Metamorphic hand with grasped object

9.4 Conclusions

In this chapter, a Lie group built-in topology diagram together with its deduction operations was proposed for the first time for analyzing the grasp constraints of a cylindrical disk manipulated by the Metamorphic hand. The diagram and the deduction methodology was established on bridging the gap between product submanifolds in mathematical books and kinematics analysis of parallel mechanisms, particularly of complex parallel mechanisms with a reconfigurable base. The topology representation for the Metamorphic hand with manipulating a cylindrical disk was presented based on a proposed iterative algorithm. More details about the kinematics analysis of the hand-object system for the Metamorphic hand can refer to Chapter 8.

Chapter 10 Geometry Variation Entailed Metamorphic Hand Benchmarking and Anthropomorphism Index

10.1 Introduction

The mechanical system of a robotic hand closely relates to its behaviours in grasping and manipulation scenarios. The structure of a robotic hand consists of the architecture of the palm and the arrangement of fingers. Instead of an inflexible palm, the Metamorphic hand adopts a reconfigurable linkage mechanism as the palm with four fingers attached on it. Hence the motion of fingers depends on the palm geometry variation that awards fingers the additional capability to move in space in such a way to enhance the performance in comparison to the conventional rigid-palm robotic hands.

This chapter proposes a new evaluation method based on the transverse metacarpal arch to assess the palmar shape modulation of the Metamorphic hand. This method investigates the palmar motion during the robot hand grasping. It is hypothesized that the value of the arch indicates the closeness of the relative position of fingers. The posture of the Metamorphic hand is related to both the kinematic transverse arch and the rotation of the thumb base, which is different from human hands whose posture changes are dominated by the palmar motion. The functional workspace is proposed as

an indicator to evaluate the precision grasp of the Metamorphic hand and demonstrate the impact of the palm arch on grasp performance.

Gaussian Process Latent Variable Model[119] (GPLVM) is applied to evaluating the four-fingered Metamorphic hand, and comparing its result to other robotic hands and grippers with rigid palms. The area of hand workspace projected by GPLVM illustrates its dexterity, namely the larger size of the projected area, the more dexterous of the evaluated hand. The Metamorphic hand is evaluated in this way, and the result is analysed in the light of various sampling sizes of actuated joints and configurations of the palms.

10.2 Kinematic Transverse Arch of the Metamorphic Palm

10.2.1 The Kinematic Transverse Arch of Human Hands

The metamorphic palm is comprised of a five-bar spherical metamorphic mechanism. The angular displacement of the closed-loop links is a way to mimic human palm changes but its influence is not straight forward. In order to assess the change objectively, we introduce a new description method called kinematic transverse arch to evaluate the palmar shape modulations.

Anatomically, the human palm is described as two transverse metacarpal arches and five longitudinal metacarpal arches shown in Fig.10.1(a) [120]. The palm arches encompass a hollow cavity that changes its shape during pre-shaping and grasping according to the geometry of the object. Sangole and Levin [121] gave a new formulation about the transverse metacarpal arch called kinematic transverse arch when studying the biomechanics of human palms. More specifically, the kinematic transverse

arches are made up of three planes: thenar, middle, and hypothenar. The thenar arch is formed by the articulation of the thenar and middle planes. The hypothenar arch is formed by the articulation of the hypothenar and the middle plane shown in Fig.10.1(b).

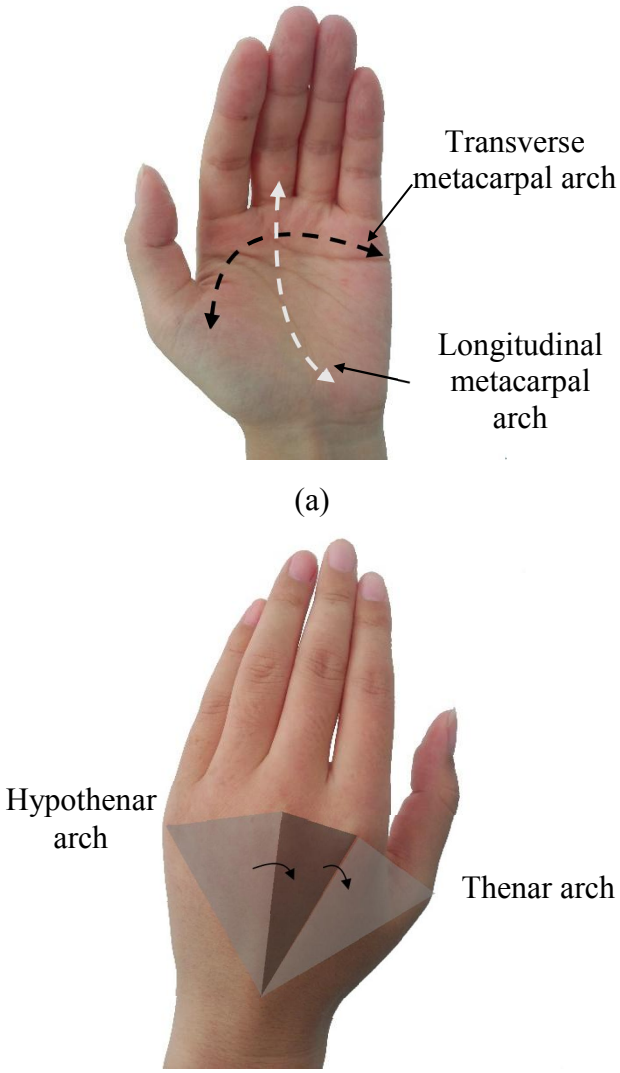

Figure 10.1 Arches of human hand, (a) Human palm arches, (b) The kinematic transverse arches

10.2.2 Transverse Arch Inspired Palm Geometry Variation Analysis

The ideas of kinematic transverse arches are applied to the motion analysis of the metamorphic palm, shown in Fig.10.2. The thenar and hypothenar arch angles are computed and the contribution of each to the arch formation will be expressed as a percentage of the total angle. The kinematic transverse arch shows the palmar shape modulation intuitively, the larger the value of the arch, the closer the relative position of the fingers, especially among the thumb, the index finger and the middle finger, on where most crawling actions and delicate operations mainly depend.

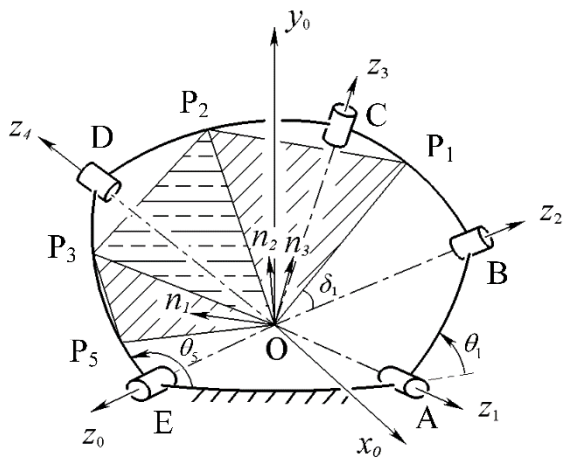

Figure 10.2 The kinematic transverse arch of the metamorphic palm

As shown in Fig.10.2, point P_1 to P_5 are the intersections between five fingers and the reconfigurable palm. $\boldsymbol{n}_1$, $\boldsymbol{n}_2$ and $\boldsymbol{n}_3$ are the normals of planes P_1OP_2, P_2OP_3 and P_3OP_5 which express the thenar, middle, and hypothenar planes respectively. The equations of these planes can be written as

$$\sum : \boldsymbol{n}_i \bullet (\boldsymbol{r} - \boldsymbol{r}_0) = 0 , \tag{10.1}$$

where, $\boldsymbol{r}_0$ is the vector directing to a fixed point and $\boldsymbol{r}$ is an arbitrary vector in the plane, $\boldsymbol{op}_i$ is the position vector that locates the *i*th finger with respect to the fixed coordinate frame $\{O-x_0y_0z_0\}$ that can be acquired as,

$$\begin{aligned} \boldsymbol{op}_i &= {}^0\boldsymbol{R}_j\, {}^j\boldsymbol{op}_i \\ {}^j\boldsymbol{op}_i &= \begin{bmatrix} s\delta_i & 0 & c\delta_i \end{bmatrix}^{\mathrm{T}} \end{aligned} \tag{10.2}$$

Where *j* indicates the number of the link connected to the *i*th finger and ${}^0\mathbf{R}_j$ is the rotation matrix of *j*th link with respect to the fixed frame. Thus, $\boldsymbol{n}_1$ to $\boldsymbol{n}_3$ can be obtained by following equations,

$$\boldsymbol{n}_1 = \frac{\boldsymbol{op}_1 \times \boldsymbol{op}_2}{\| \boldsymbol{op}_1 \times \boldsymbol{op}_2 \|}, \boldsymbol{n}_2 = \frac{\boldsymbol{op}_2 \times \boldsymbol{op}_3}{\| \boldsymbol{op}_2 \times \boldsymbol{op}_3 \|}, \boldsymbol{n}_3 = \frac{\boldsymbol{op}_3 \times \boldsymbol{op}_5}{\| \boldsymbol{op}_3 \times \boldsymbol{op}_5 \|}. \tag{10.3}$$

The thenar arch and hypothenar arch labeled as ϕ_1 and ϕ_2 are computed as,

$$\phi_1 = arc\cos(\boldsymbol{n}_1 \bullet \boldsymbol{n}_2),\ \ \phi_2 = arc\cos(\boldsymbol{n}_2 \bullet \boldsymbol{n}_3). \tag{10.4}$$

10.2.3 The Palm Geometry Variation related Actuation Constraints

The Metamorphic hand, shown in Fig. 10.3, is made up of a foldable palm and four actuated fingers, i.e. a four-DOF thumb, an index finger, a middle finger and a ring finger with three-DOF respectively. The little finger is omitted for simplifying the complexity of design and control as it is less important than other fingers in terms of functionality. The reconfigurable palm consists of five links which connect to each other to form a spherical five-bar linkage mechanism. In order to maximize the

rotatability of the spherical five-bar linkage, the angles of link 1 to link 5 are considered as $\alpha_1 = 20°$, $\alpha_2 = 40°$, $\alpha_3 = 70°$, $\alpha_4 = 112°$ and $\alpha_5 = 113°$, which need to satisfy the conditions $\alpha_1 + \alpha_2 + \alpha_3 + \alpha_4 + \alpha_5 = 360°$ and $\alpha_1 + \alpha_2 + \alpha_5 = \alpha_3 + \alpha_4$, presented in [107].

A thumb is mounted to link 2 by a revolute joint, which is similar to the CMC joint of human hands. An index finger is installed on link 3, and the middle finger and ring finger are mounted at link 4. All the fingers have three phalanxes that are connected by revolute joints in parallel and follow the same design. Different from fingers mounted at a fix palm, the Metamorphic hand has the capability to provide the adduction/abduction motions for fingers so as to expand their workspace and increase dexterity. Further, the maximum radius of the spherical linkage palm is designed at 50mm in the light of the size of an adult's hand.

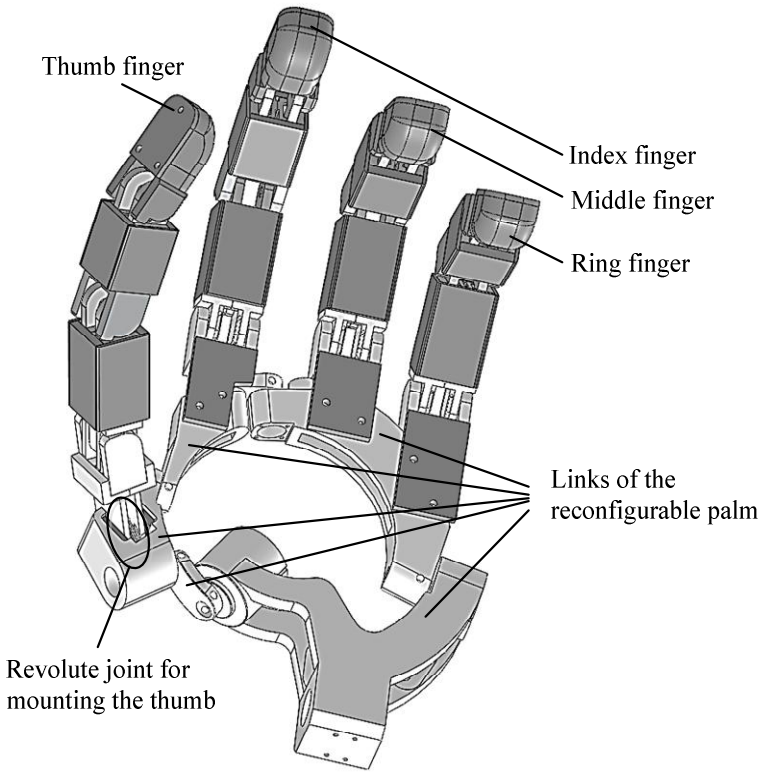

Figure 10.3 The Metamorphic hand with a reconfigurable palm

10.2.4 Geometric Constraints of the Metamorphic Palm

From the perspective of mechanism, the Metamorphic hand can be regarded as a hybrid mechanism consisting of a closed-chain palm and four open-chain fingers. The kinematics of the reconfigurable palm and fingers can be analyzed individually and then combined for the whole hand kinematics.

The kinematics of the Metamorphic palm was well presented in [61]. In the reference, joints A and E are treated as active joints of the palm, and joints B, C and D are passive joints whose motion depends on the input of joints A and E. In order to identify the geometric constraints of this reconfigurable palm, we use the same notions and coordinate frames set up in reference [61].

When assigning the value of angle θ_5, the spherical five-bar linkage mechanism degenerates to a spherical four-bar linkage mechanism. At that time, rotating link 1 will make the spherical four-bar linkage mechanism reach its limited positions when point B, C and D are in the same plane, which is given by,

$$\boldsymbol{P}_{\mathrm{D}} \cdot (\boldsymbol{P}_{\mathrm{B}} \times \boldsymbol{P}_{\mathrm{C}}) = 0\,, \tag{10.5}$$

$$\boldsymbol{P}_{\mathrm{B}} \cdot (\boldsymbol{P}_{\mathrm{D}} \times \boldsymbol{P}_{\mathrm{C}}) = 0\,. \tag{10.6}$$

The mechanism has two limited positions as the link 1 can rotate on both sides with respect to link 2. Thus, the value of θ_5 decides the range of θ_1, the relation between the two angles can be obtained as,

$$\boldsymbol{P}_B{}^{\mathrm{T}} \cdot \boldsymbol{P}_A = \cos\alpha_1, \tag{10.7}$$

$$\boldsymbol{P}_B{}^{\mathrm{T}} \cdot \boldsymbol{P}_D = \cos(\alpha_2 + \alpha_3), \tag{10.8}$$

$$\boldsymbol{P}_B{}^{\mathrm{T}} \cdot \boldsymbol{P}_B = 1. \tag{10.9}$$

Substituting $\boldsymbol{P}_{\mathrm{B}}$ and $\boldsymbol{P}_{\mathrm{D}}$ in [61] into Eq. (10.8) and solving the latter gives the two limiting value of angle θ_1 as

$$\theta_1^{'} = \arctan(\frac{Y}{X}) \pm \arccos(\frac{-Z}{\sqrt{X^2+Y^2}}) \tag{10.10}$$

where $X = \mathrm{s}\alpha_4\,\mathrm{c}\theta_5\,\mathrm{c}\alpha_5\,\mathrm{s}\alpha_1 + \mathrm{s}\alpha_1\,\mathrm{c}\alpha_4\,\mathrm{s}\alpha_5$, $Y = \mathrm{s}\alpha_1\,\mathrm{s}\alpha_4\,\mathrm{s}\theta_5$ and

$Z = \mathrm{c}(\alpha_2 + \alpha_3) - \mathrm{c}\alpha_1\,\mathrm{c}\alpha_4\,\mathrm{c}\theta_5 + \mathrm{s}\alpha_4\,\mathrm{c}\alpha_1\,\mathrm{c}\theta_5\,\mathrm{s}\alpha_5$.

So the range of θ_1 with a specified θ_5 is,

$$\arctan(\frac{Y}{X}) - \arccos(\frac{-Z}{\sqrt{X^2+Y^2}}) \le \theta_1 \le \arctan(\frac{Y}{X}) + \arccos(\frac{-Z}{\sqrt{X^2+Y^2}}) \tag{10.11}$$

Base on Eq. (10.11), the range of θ_1 can be calculated by rotating θ_5, whose value changes from -86° to 86° in terms of the palm design. Taking 1° as the spaced flexion value for θ_5, the range of θ_1 is shown in Fig. 10.4.

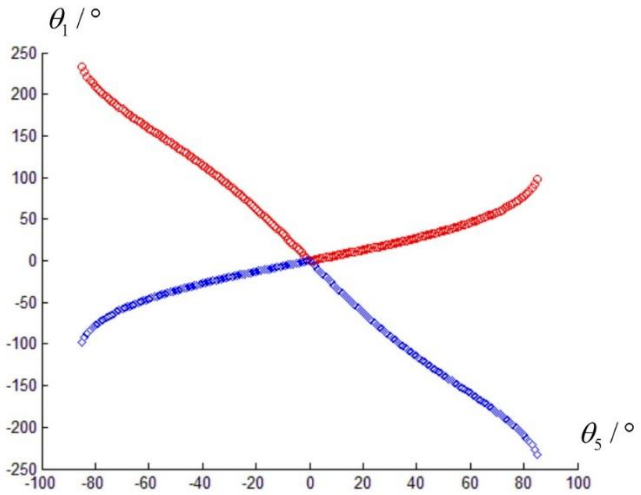

Figure 10.4 The range of θ_1 with respect to the changes of θ_5

It can be seen from the Fig. 10.4 that the singularity occurs when θ_1 and θ_5 are both 0; that is all the links locate in the same plane and the palm is not controllable at that moment. The joint space of the two active joints is symmetric about the singularity and follows the rule that the larger input of θ_5, the bigger range of θ_1.

10.3 Arch Measurement of the Metamorphic Palm

The kinematic transverse arch can be obtained by taking summation of ϕ_1 and ϕ_2. The contributions of the thenar arch and hypothenar arch are calculated as the percentage of the kinematic transverse arch. Fig.10.5 and Fig.10.6 show the kinematic transverse arch of the palm.

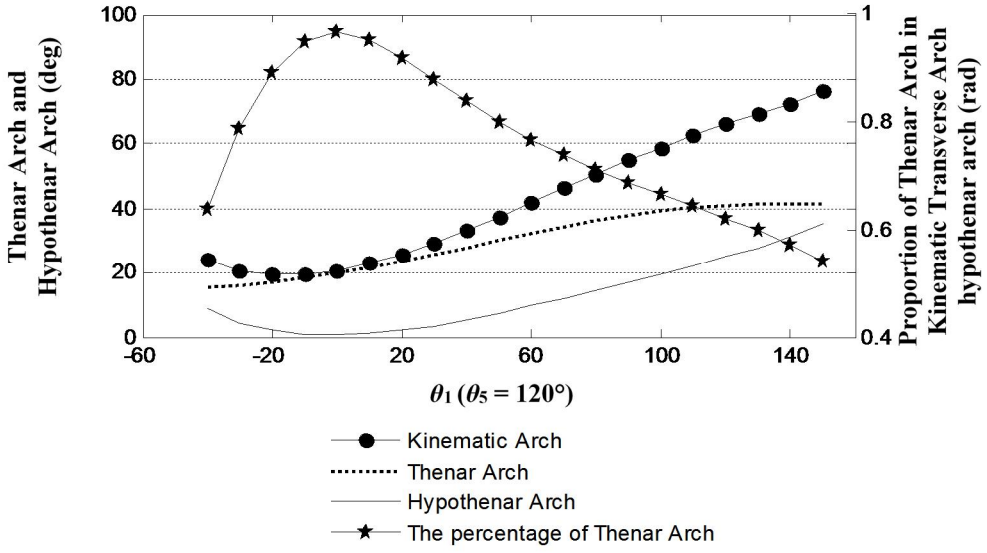

Figure 10.5 The contributions of the thenar arch, hypothenar arch in kinematic transverse arches at the change of θ_1 when $\theta_5 = 120°$

Fig.10.5 shows the palmar shape modulation described with the kinematic transverse arch when $\theta_5 = 120°$. The kinematic transverse arch angle decreases when θ_1 arises from -35° to 0, and then increases with θ_1 from 0 to 135°. The thenar arch contribution remains larger than 50% throughout the palm movement.When $\theta_1 = 120°$, the kinematic transverse arch reaches the maximum ($\phi = 75.8°$), and the contributions of the thenar arch and hypothenar halve.

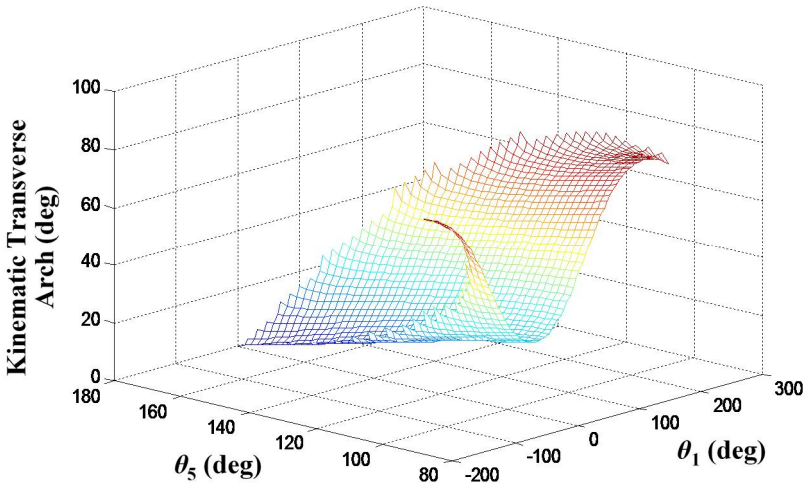

Figure 10.6 The kinematic transverse arch of the reconfigurable palm

The kinematic transverse arch angles for the metamorphic palm are given in Fig.10.6. The maximal palmar arch angle is 79.44°, and the corresponding thenar and hypothenar contributions are 49.1% and 51.9%. In this circumstance, the driving angles θ_5 and θ_1 are 90° and 170°, respectively. Inspecting the movement of dexterous hands, most of the palmar arches lie in 30° to 70°.

The palmar concavity shape variations of human hands for cylindrical (8.5cm diameter can, height 14cm) and spherical (10.5cm diameter ball) grasping were tested by Archana P. Sangole, etc[121]. The overall range of absolute angles for the two types of grasping was from 100° to 120°. Individual contributions of the thenar and hypothenar movement to palmar arch formation are approximately 55% and 45%[121], respectively.

Comparing with the palmar arch angles of human hands, the modulations of the Metamorphic hand are a little smaller. The difference between the Metamorphic hand and the human hands is the construction of the thumb. For human palms, the thumb is contacted to the thenar plane of the kinematic transverse arch that can rotate 0 to 90° around the MPJ of the index finger, which establishes a surjection between the posture of the thumb and the thenar arch. However, the thumb of the Metamorphic hand is contacted to the palm link with an additional revolute joint that could produce a rotation of the thumb itself from 0 to 90°. Thus the posture of the thumb is not only related to the kinematic transverse arch, but also to the rotation of the thumb base.

10.4 Palm Geometry Variation based Workspace of the Metamorphic Hand

The analysis in Section 10.3 shows that the palm arch is closely related to the relative position of the fingers, and the values of the arch indicate the closeness of their relative position. However, different from the human hands whose posture changes mainly depend on the palmar motion, the posture of the Metamorphic hand partially depends on the palm modulation because the thumb could rotate itself around the base with an additional revolute joint. So an indicator considering both the palm geometry and posture of the fingers is needed for measuring the precision graspability of the hand.

The functional workspace[122] is an indicator to evaluate the precision graspability of a multifingered hand, which is calculated by the overlapped volume constructed by maximal workspace of thumb-tip and that of each fingertip. The trajectory of each finger itself can be obtained through successive screw displacement method. After

interpolating points inside the boundary and processing them with Delaunay triangulation method, the workspace of the fingers can be obtained as Fig.10.7.

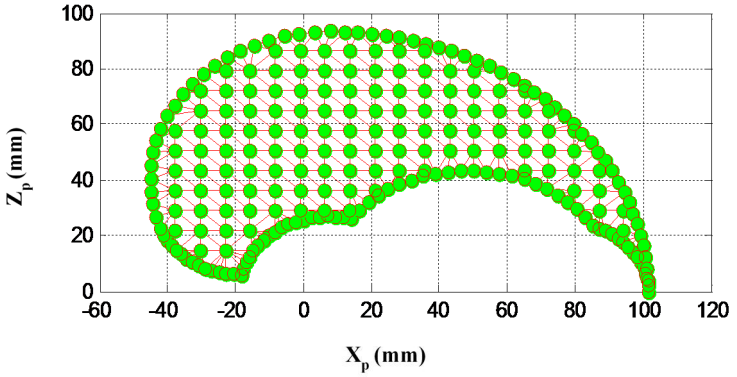

(a)

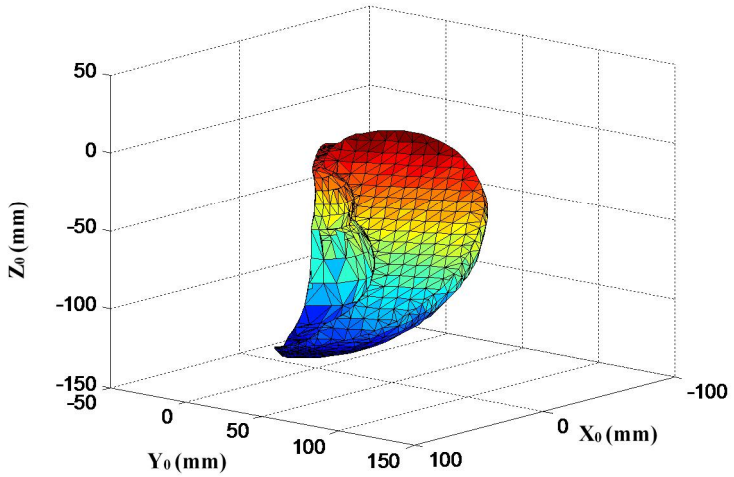

(b)

Figure 10.7 The workspace of the thumb and other fingers processed with Delaunay triangulation method. (a) The workspace of index finger, middle finger, ring finger and little finger. (b) The workspace of the thumb

The workspace of index finger forms a plane shown in Fig.10.7(a) as its base is fixed with the palm link, leading to the motion restricted in the finger working plane, which is the same as the workspaces of the middle finger, ring finger and little finger. The

thumb has an additional revolute joint between its base and the palm link, so its workspace is much larger shown in Fig.10.7(b). Except for the thumb, the workspaces of other fingers are divided into a total of *n* triangles and these triangles are labeled by *i* in turn. So the whole workspace of the fingers is acquired by,

$$MW = \sum_{i=1}^{n} S_i \tag{10.12}$$

where S_i is the area of the *i*th triangle. Substituting n = 379 into Eq.(10.12), the workspace is obtained as

$$MW = 7170mm^2 \tag{10.13}$$

Fixing the two input of the palm as $\theta_5 = \pi/2$, $\theta_1 = -2\pi/3$, the workspace of the Metamorphic hand is visualized in Fig. 10.8.

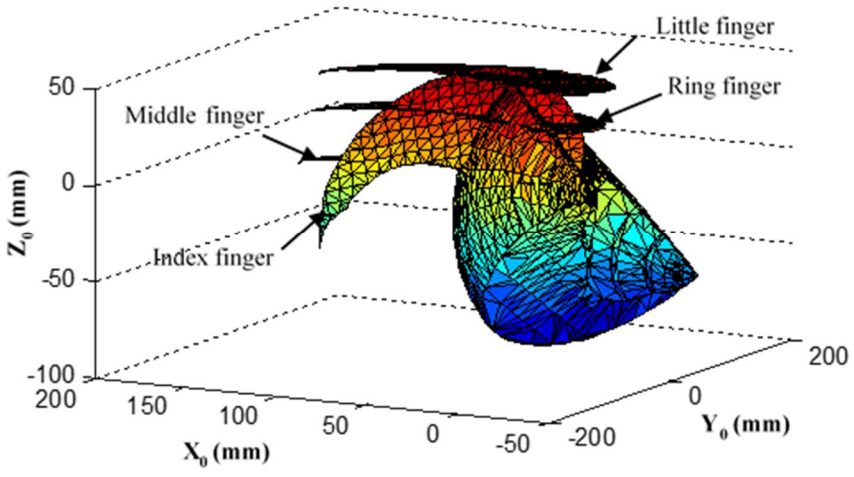

Figure 10.8 The workspace of the whole hand with two palm actuation angles as θ_5=π/2, θ_1=-2π/3

The functional workspace of each finger can be determined by adding all triangle areas of which the center points are in any one tetrahedron of the thumb motion area. As shown in Fig.10.9, the functional workspaces of four fingers are 1763.8 mm^2, 3470.3 mm^2, 1828.4 mm^2 and 0 mm^2 respectively.

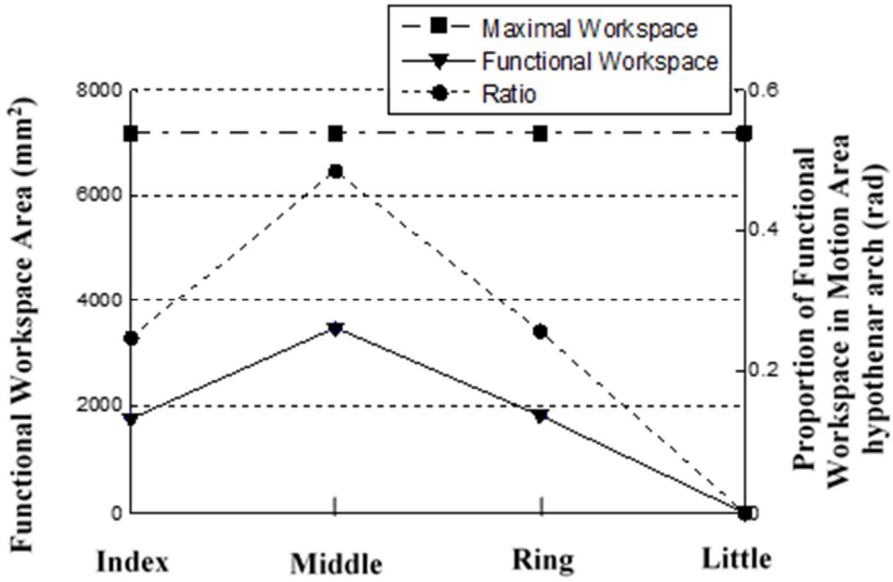

Figure 10.9 The functional workspace of each finger

We extended the functional workspace of a finger to the whole hand by the assembly of the weighted workspace of fingers. The functional workspace of the hand can be measured by following equation [123],

$$FW = \sum_{i=2}^{k} \omega_i v_i \tag{10.14}$$

where FW indicates the functional workspace of the robot hand, v_i is the functional workspace of the ith finger and ω_i is the percentage of v_i in the maximal workspace of ith finger. Considering the precision operations of the hand mainly depending on the

relative movement of the thumb, index finger and middle finger, the effect of the little finger will be ignored and the value of k is taken as 4. Then we can get the figure showing the functional workspace with the different input of φ_0 and φ_1 in Fig.10.10.

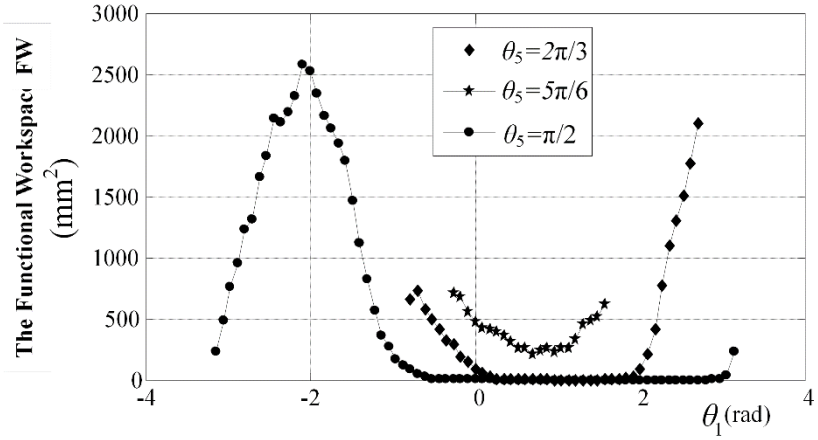

Figure 10.10 The functional workspace with different θ_1 when $\theta_0 = \pi/2$, $2\pi/3$ and $5\pi/6$

From Fig.(10.10), it is not hard to recognized that when the functional workspace reaches the maximum ($\theta_5 = \pi/2$, $\theta_1 = -2\pi/3$), the hand is in a good configuration shown in Fig.10.8, and the palm arch also has a big value shown in Fig.10.6. However, when the palm arch reaches the maximum ($\theta_5 = \pi/2$, $\theta_1 = 3\pi/4$), the functional workspace value is zero. This is because the four fingers have no overlapped region with the thumb, so the posture of the metamorphic hand is not natural or in a relative bad configuration to perform grasps. Similarly, the hand could not perform good performance on grasping when the hand is in a good posture but has a small palm arch. Therefore, only when both the palm arch and hand posture are in good status can the robot hand perform good performance on the precision grasp.

Having considered both the palm arch and hand posture, the functional workspace shows the precision graspability of the Metamorphic hand. With the functional workspace obtained above, fine palm configurations can be selected according to the geometry of the objects.

10.5 Hand Model Generation and Simplification for Benchmarking

10.5.1 Hand Model Generation

According to the requirement of the evaluation method, the metacarpophalangeal (MCP) joint of the middle finger has to be set as the origin. Thus, the link 4, on which the middle finger is located, is fixed to the base. The palm has two degrees of freedom and it is actuated by drive 4 and drive 3, shown in Fig. 10.3. The two actuated joints D and C can rotate by different angles to change the configurations of the palm. Specifically, the MCP joint of the index finger will change its position along with the rotation of link 3. Similarly, the coordinate of the carpometacarpal (CMC) joint of the thumb changes with the rotation applied to palm joints D and C. The value of the rotation angles, θ_4 and θ_1, can be calculated based on the rotation of θ_1 and θ_5.

Each finger of the hand has three parallel revolute joints but two active joints, the MCP joint and DIP joint. The PIP joint is coupled with the DIP joints via tendons and shares the same rotation angle. Therefore, the Metamorphic hand has 11 DOFs, which leads to a very large sample size. For instance, if selecting nine equally spaced flexion values

for each active joint, which will result in 9^{11} = 3.1381e+10 different hand postures. Obviously, it's impossible for PC to generate such vast amount points.

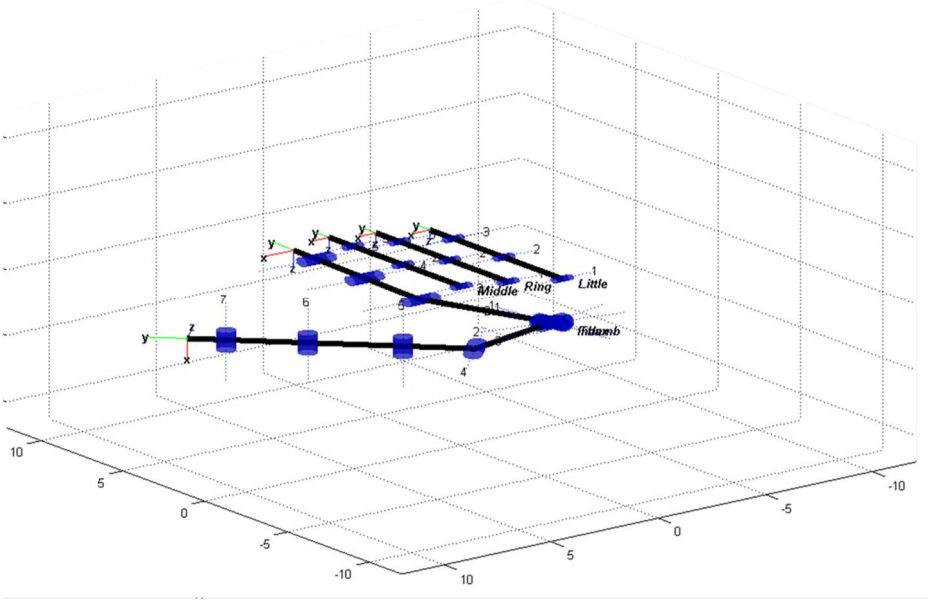

Figure 10.11 The model of the Metamorphic hand

10.5.2 Hand Model Simplification

To decrease the complexity and save computing cost, the Metamorphic hand is simplified by merging active joints, which results in decreasing the degree of freedom from 11 to 5. Finally, the five left active joints are two palm joints (θ_4 and θ_3), the CMC joint (θ_0) and the MCP joints of the thumb (θ_{11}) and the index finger (θ_{21}), while the other six joints become passive joints. More specifically, the DIP joint of the thumb (θ_{12}) is coupled with its MCP joints (θ_{11}); The DIP joint of index finger (θ_{22}), the MCP joints and DIP joints of the middle finger and the ring finger (θ_{31}, θ_{32}, θ_{41} and θ_{42} respectively) are all coupled with the MCP joint of the index finger (θ_{21}). The model of the Metamorphic hand is shown in Fig. 10.3.

10.6 Measurement Indexes and Criteria

10.6.1 Projection based Measurement Indexes

Projecting the movements of the Metamorphic hand onto the latent space and treating that of human hands as the evaluation criterion, the overlap is able to be calculated between to two, which shows the similarity of the two types of hand. Fig. 10.3 indicates the overlap area and the relative coverage of the Metamorphic hand comparing to humans hand in latent space. The method about how to measure the area of overlap is to decompose the latent space into several regular grids and count the amount of the units and generate the relative coverage of the whole hand.

More specifically, it is easy to reveal the measurement mechanism when taking one grasp trajectory for example. At the time of generating human grasp dataset, the each experimenter will execute a unique grasp mode twice. However, the trajectory of the second trial cannot follow that of the first trial completely even if in the same grasping task, which leads to incomplete coincide of the projection in the latent space. Therefore, the slight difference of the projections between two trials needs to be taken into account. In other words, the tolerance of the projection of one group mode has to be preset before for not only recognizing the specific grasp mode but also distinguishing it from other postures.

That tolerance of one grasp mode will decide the resolution of the grid in latent space. The GP-LVM models provide a way to map grasp manifolds from the latent to high-dimensional space by a Gaussian process. The kernel width of the manifolds affects the

tolerance of one grasp, resulting in a different value of overlap area in the same set of hands postures.

10.6.2 Evaluation of the Metamorphic Hand based on AI[1]

Depending on the simplification mentioned above, the Metamorphic hand can be driven based on the reduced model. The strategy of how to select hand postures driven by five positive joints, θ_0, θ_{11}, θ_{21}, θ_3 and θ_4, is described as follows. The value of θ_0, θ_{11}, and θ_{21} ranges from 0 to 80° with 9 equally spaced samples taken from that range, where $\theta_{(1)} = 0$ is finger opened and $\theta_{(9)} = 80°$ is finger closed. For the two palm joints, θ_4 and θ_3, are assigned with 120 sets of value according to the geometric constraints of the palm. Overall, it generates $120 \times 9_3 = 87480$ different hand postures.

After projecting those hand poses onto the latent space, The AI is 12.69%, shown in Fig. 10.6 (a). Generally speaking, the value will be increased along with the extension of sample size. Thus, the actual value of 11-DOF Metamorphic hand must be higher than 12.69%.

10.6.3 The Improvement of AI with the Reconfigurable Palm

In order to indicate the affection of reconfigurable palm to AI, the properties of the Metamorphic hand can be updated as the fixed palm, and the influence on the latent space overlap can be analyzed. The angles of two palm joints are fastened at the initial state. So the value of θ_3 and θ_4 is zero. Give the same range and value of θ_0, θ_{11} and θ_{12}

[1] Anthropomorphism Index

so as to ensure the only possible factor to affect AI is whether leading in the palm motion. Thus, $9^3 = 729$ types of hand poses are generated and then projected onto the latent space, resulting 6.34% of coverage, shown in Fig.10.6 (b).

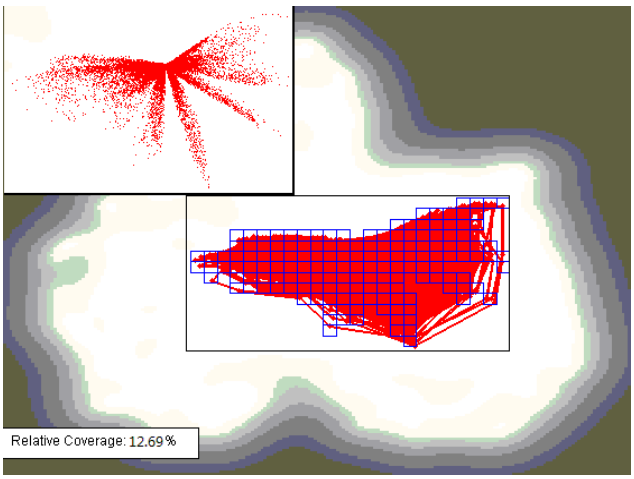

(a)

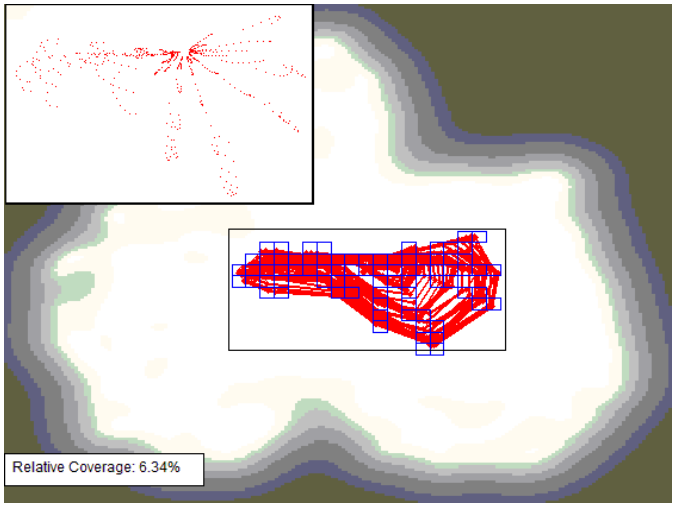

(b)

Figure 10.12 Projection of the Metamorphic hand to the latent space. (a) The projection of the Metamorphic hand with the reconfigurable palm; (b) The projection of the Metamorphic hand with the freezed reconfigurable palm ($\theta_3 = \theta_4 = 0$)

The AI corresponding to the Metamorphic hand with reconfigurable palm is twice as that with the fixed palm. The comparison proves that the reconfigurable palm of the Metamorphic hand improves the AI, as well as the graspability and dexterity.

10.7 Comparison of the Metamorphic Hand with Selected Robotic hands

10.7.1 The Effect of Number of DODs

The AI of the Metamorphic hand (12.69%) is much higher that of SensorHand [124] (0.25%), Michelangelo Hand [125] (2.8%) and FRH-4 Hand [126] (5.2%), illustrated in Form 1. The reasons why the evaluation system generated the very low value of AI of SensorHand and Michelangelo Hand mainly because they had few degree of freedoms. For the SensorHand, it just has one DOF and three fingers, in which most of the joints are rigid. Thus, there is no doubt that SensorHand produces such a low score and its graspability is obviously poor. While mentioning the Michelangelo hand, it has Two DOFs and five fingers. Although most of the joints are coupled, the value of AI is much higher than that of SensorHand relatively. Similarly, it shows the same results when comparing Michelangelo Hand to FRH-4 Hand and the Metamorphic hand.

These comparisons demonstrate that the number of DOFs is a critical factor affecting the score of the evaluation. So increasing the number of DOFs and bringing in more active joints can enhance the dexterity of the robotic hands.

10.7.2 The Effect of Distribution of DOFs

While analyzing the AI of FRH-4 Hand and the Metamorphic hand, the value of the latter is nearly 2.5 times as that of FRH-4 Hand on the basis of same number of DOFs but different in palms. Apart from the number of DOFs, the distribution of those is another crucial factor to affect the functionality of robotic hands.

Table 10.1 The AI of four robotic hands evaluated by the toolbox

Hand	Otto Bock SensorHand	Otto Bock Michelangelo Hand	FRH-4 Hand	The Metamorphic Hand
Picture	 [124]	 [125]	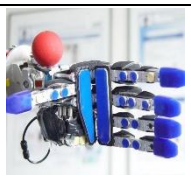 [126]	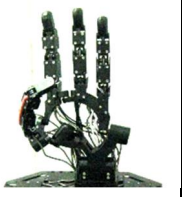
Fingers	3	5	5	4
Palm DOFs, (All DOFs)	0, (1)	0, (2)	1, (5)	2, (5[2])
Latent space projection	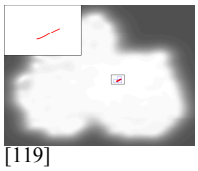 [119]	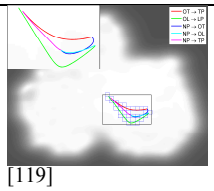 [119]	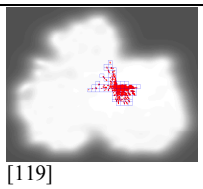 [119]	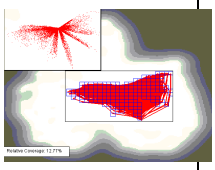
Coverage	0.25%[119]	2.8%[119]	5.2%[119]	12.69%

The palm of the Metamorphic hand has 2 DOFs and thus provides adduction/abduction motions for the fingers mounted on that, which enlarges the workspace of the fingers

[2] Considering the computing cost, the DOFs of the Metamorphic hand decreases from 11 to 5. The active joints are two palm joints, the CMC joint and the MCP joints of the thumb and the index finger.

significantly, leading to a high outcome of AI produced by the system. On the contrary, the palm of FRH-4 Hand only possesses one DOF, leading to less dexterity compared with the Metamorphic hand.

In sum, the number and distribution of DOFs are the two important parameters that have to be taken into consideration when designing the robotics hand. These parameters will contribute to arranging the DOFs to obtain a robotic hand with fewer DOFs but excellent performance.

10.7.3 The Influence of Sampling Density on AI

The data of the Metamorphic hand are generated by sampling its joint space and calculating the related fingertip poses via forward kinematics. So the sampling density and sample size are the two key factors affecting the value if AI if the number of drives and their range of motion are fixed. Fig. 10.5 shows the results of AI with different sample density and fixed sample size. The figure shows the changing trend clearly that the larger density of sampling, the higher value of AI. In particular, the increasing trend slows down with decreasing influence of sampling density. Finally, the value of AI reaches its upper limit at this sample size.

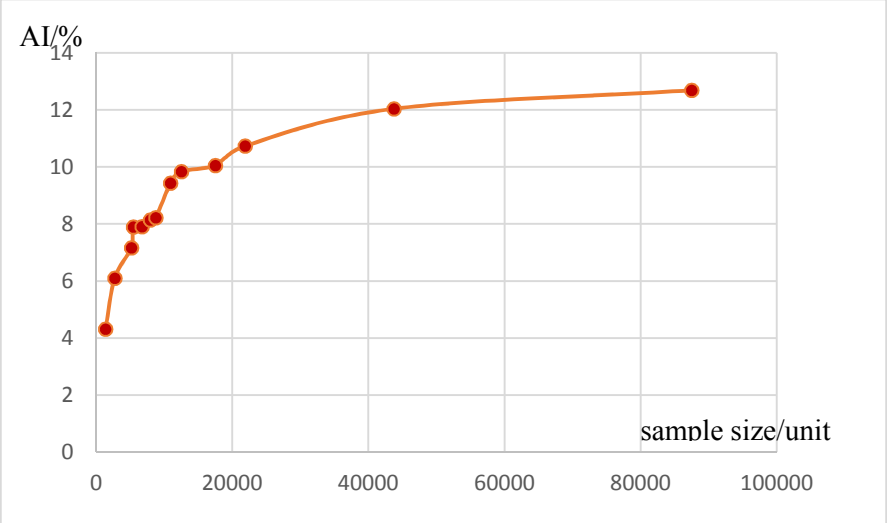

Figure 10.13 The value of AI with fixed sample size and various sampling density

10.7.4 AI Analysis According to Different Palm Configurations

Based on this dimensionality reduction method, the AI of different palm configurations is capable of being calculated, which contributes to evaluating the functionality of different palm pose and finding the best palm configuration. In the other words, the unique palm configuration, which produces the highest AI value, is regarded as the most similar configuring to human hands comparing with other palm poses. Fig. 5 illustrates the relation between the angles of two palm positive joints and the value of AI. The peak of AI value is 11.88% as $(\theta_4, \theta_3) \in \{(25.49°, 12.01°), (26.62°, 35.04°), (32.28°, 65.99°), \ldots\}$. That is to say, in such value of palm rotating angle, the Metamorphic hand has the largest graspability.

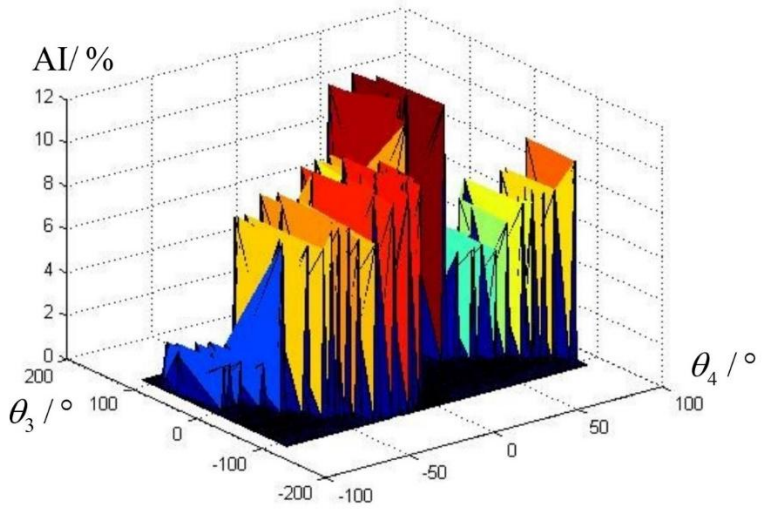

Figure 10.14 The value of AI with different palm configurations

10.8 Conclusions

In this chapter, the kinematic transverse arch was developed to evaluate the palm movement of the Metamorphic hand. It was a more intuitive description that establishes the relationship between human palm and the metamorphic palm. The functional workspace as an indicator considering both palm modulation and the relative posture of fingers showed the precision grip ability of the hand. By measuring the functional workspace value, the impacts of palm arch on the hand graspability was obtained and a suitable palm configuration was selected according to the object to be grasped. The Metamorphic hand obtained a good precision grasp when the palm arch had a large value. A suitable palm configuration was selected for the object grasping based on the functional workspace analysis of the Metamorphic hand.

Evaluation of the four-fingered Metamorphic hand based on a dimensionality reduction model (GP-LVM) was created with Anthropomorphism Index. The structure of the

Metamorphic hand was introduced which is regarded as a hybrid mechanism consisting of a closed-chain palm and four open-chain fingers. The actuation constraints of palm were reviewed through analysing the geometric constraints of the reconfigurable palm. Simplification for the Metamorphic hand was explained in consideration of the computation cost. Based on the reduced hand model, the Anthropomorphism Index of the Metamorphic hand was calculated by 12.69%, which was much higher than that of some selected robotic hands because of bringing in the palm variation. In addition, the sample density and distribution of DOFs that affected the results significantly were analysed for finding the most similar configuration to human hands. The Metamorphic hand demonstrated good graspability adaptability and manipulability comparing to other robotic hands with a fixed palm.

Chapter 11 Conclusions

11.1 General Conclusions

This thesis was dedicated to the study of the intrinsic connection between screw coordinates from the perspective of geometry, and its derived Jacobian in contrast with the derivative Jacobian, and their uses in velocity analysis and evaluation of the Metamorphic hand. The general conclusions of the thesis is stated as follows,

Chapter 1 introduced the problems, aims and objectives of the thesis.

Chapter 2 presented the background and prior knowledge used in the following chapters, specifically the line geometry, line coordinates, screw coordinates and its applications in the analysis of first-order kinematics, state-of-the-art of parallel mechanisms and dexterous hands and their latest development with the ideology of Metamorphosis which led to the reconfigurable base-integrated parallel mechanism and the Metamorphic hand.

Chapter 3 revealed the interconnection of screw coordinates from its original line coordinates, namely ray coordinates and axis coordinates. From the geometrical presentation of a line as a ray of two points, a triangle was constructed with its projection on three coordinate planes making up the secondary part of ray coordinates. Its counterpart, a reciprocal triangle was constructed for the first time by the plane normals to give the geometrical representation of axis coordinates. In this way, the geometrical meaning of axis coordinates was revealed with its primary part as the

vectors subtraction of the weighted plane normals and secondary part as their cross product.

Chapter 4 was the follow-on study on the screw coordinates and revealed their intrinsic connections from the perspective of geometry. The triangle derived from ray coordinates and its counterpart, the reciprocal triangle derived from axis coordinates were connected geometrically and algebraically, and then extended to conformability and duality of ray coordinates and its reciprocal, axis coordinates. The correlation was established with their correlated part ratios to relate the vector space to the dual vector space where the ray coordinates and axis coordinates were constructed. At last, the correlation operator that mapped the vector space to its dual vector was explained with a conformability graph.

Chapter 5 investigated the geometrical meaning of a twist and its decomposition into a rotation about an axis and a translation parallel to that axis. This chapter also presented the compound of twists of a serial manipulator and its generation, the resultant twist, geometrically and algebraically. Then the position vector of ISA of the resultant twist was formulated by weighted position vectors of joint screws. Further, the screw based Jacobian was proposed with the unit joint screws as its columns.

Chapter 6 was the further investigation based on chapter 5 and related the screw-based Jacobian to the derivative method based Jacobian of the same manipulator. The relation of a resultant twist and the end-effector velocity was formulated through an adjoint transformation acting on the twist. This study was then pushed to explore the reconciliation of Jacobians calculated by screw algebra and derivative method. Finally,

a planar 3R serial manipulator and a spatial serial manipulator examples varied this adjoint transformation of two methods.

Chapter 7 proposed a novel parallel mechanism with a reconfigurable base inspired by the manipulation of an object with a Metamorphic hand. The geometrical constraints of the base were investigated, followed by the kinematics analysis of the parallel mechanism. The forward and inverse kinematics solutions were calculated based on the mechanism decomposition principle together with screw-based Jacobian, which demonstrated the enlargement of the workspace of this reconfigurable base-integrated parallel mechanism.

Chapter 8 proposed the design of a 7-DOF serial manipulator with a Metamorphic hand attached at its distal end. The kinematics of the manipulator was investigated through a product-of-exponential method in Lie group, followed by the analysis of grasping constraints of the three-fingered Metamorphic hand. Grasp matrix of the flexible palm-integrated hand was presented with its application in the grasping affordance analysis.

Chapter 9 analyzed the grasping model of a three-fingered Metamorphic hand manipulating an object based on product submanifolds deduction method. 10 proper Lie submanifolds were reviewed. The construction of topological diagram of the hand-object system was proposed. The operation on Lie subgroups was carried out by merging the submanifolds of two adjacent fingers in turn, leading to a final deducted hand-object model.

Chapter 10 proposed assessment methods to evaluate robotic hands, particularly the Metamorphic hand, and identified the influence on the hand performance by involving the reconfigurable palm. The kinematic transverse arch model was utilized to assess the palm geometry variation according to human palm motion. Fine palm configurations were identified by measuring the functional workspace of the Metamorphic hand. Moreover, evaluation of the Metamorphic hand was conducted through Gaussian Process Latent Variable Model in such a way to measure the workspace of robotic hands in comparison to the human hand. The result was shown by criteria named Anthropomorphism Index. The AI of the Metamorphic hand was higher than that of other compared robotic hands as a result of introducing the flexible palm. Besides, the influence of sample size on the result was studied, and the best palm configuration was also discovered according to the evaluation results.

11.2 Contributions and Main Achievements of the Thesis

This thesis presented a comprehensive study on screw coordinates together with their geometrical interpretation and reconciliation. The theoretical exploration had been well used in the analysis of kinematics of serial types of robots, particularly the Jacobian analysis of serial manipulators, parallel mechanisms and multifingerd robotic hands. Several contributions and main achievements in this thesis were summarized in this section.

The intrinsic interrelationship of screw coordinates was revealed for the first time by giving the geometrical interpretation of ray coordinates and axis coordinates. Homogeneous coordinates of a point and a plane were converted to a set of homogeneous coordinates with the last component as 1 to present the geometrical

insight in Euclidean 3-space. Using these ratios of homogeneous coordinates, a triangle formed by ray coordinates was presented geometrically while its primary part was the subtraction of the two position vectors and secondary part was their cross product corresponding to the projection of this triangle on different coordinate planes. Accordingly, a reciprocal triangle was formed to relate the two weighted plane normals to axis coordinates with its primary part as the vectors subtraction and secondary part as the vectors cross product.

Relating the geometrical presentation to the algebraic presentation of screw coordinates, conformability and duality of ray coordinates and axis coordinates were revealed, and then extended to the vector space and dual vector space, and their interrelation with a correlation operator.

The presentation of a resultant twist was also investigated geometrically through the compound of twists of a serial manipulator. The ISA of the resultant twist was coordinated and its position vector was the assembly of weighted joint position vectors in this manipulator. The screw-based Jacobian and the derivative method-based Jacobian were reconciled through an adjoint transformation that related the twist derived from screw algebra to the end-effector velocity derived from the derivative method.

Then, a new type of parallel mechanism was proposed with its base as a reconfigurable mechanism. The kinematics of this novel parallel mechanism was investigated through mechanism decomposition with its forward and inverse kinematics solution acquired.

Screw algebra was used to form its Jacobian matrix, and enlargement of the workspace of this proposed mechanism was also varied mathematically.

The grasp matrix of the three-fingered Metamorphic hand was established by the product-of-exponential method. With the formulated grasping constraints, the preliminary study of grasping affordance of the Metamorphic hand with a reconfigurable palm was proposed. Based on the grasping model, Lie group based product submanifolds deduction was applied to analyzing of the motion of hand-object system. The topological diagrams were presented through the operation of submanifolds of adjacent fingers, in turn, leading to the final deducted hand-object model.

Evaluating the performance of the Metamorphic hand was proposed with Gaussian Process Latent Variable Model which mapped the high dimensional data composed of coordinates of finger position and orientation to a two-dimensional latent space. Anthropomorphism Index was put forward to measure the area projected in latent space of the robotic hands in comparison to that of the human hand, in such a way to evaluate the dexterity of a robotic hand to human hands. The Metamorphic hand demonstrated better performance than other robotic hands by a larger AI value. This was also verified by the kinematic transverse arch model, which adopted a palmar shape modulation to explain the advantages of the Metamorphic hand with a reconfigurable palm in contrast to other robotic hands with a fixed palm.

The novelties of this thesis are summarized as follows,

a) Depicted the geometrical meaning the screw coordinates and derived their interrelation geometrically and algebraically, leading to the intrinsic geometrical interpretation of the correlation operator widely used in screw algebra.
b) Revealed the duality and conformability of the screw coordinates and their corresponding representations in vector space and dual vector space for the first time.
c) Explained the geometrical meaning of a twist and the transformation between the screw-based Jacobian and derivative method-based Jacobian of serial manipulators through a geometrically based approach for the first time.
d) Analyzed the kinematics and Jacobian of a novel reconfigurable platform base integrated parallel mechanism through screw theory and verified the enlarged workspace of this hybrid mechanism.
e) Derived the grasping matrix of the Metamorphic hand by means of the product-of-exponential method, and the grasping affordance model for grasp analysis.
f) Established the topological model of the Metamorphic hand grasping object model, and simplified the model with product submanifolds operations.
g) Demonstrated the enhanced performance of the Metamorphic hand comparing to conventional fixed-palm robotic hands with a nonlinear data reduction method and a palmar shape modulation approach.

11.3 Future Works

This thesis investigated the geometrical interpretation and reconciliation of screw coordinates, accompanying with the screw based Jacobian analysis and its application in kinematics study of serial manipulators, parallel mechanisms and multifingerd

robotic hands. There still remains some problems that are worth further investigating in the follow aspects,

a) The application of the intrinsic connection of screw coordinates and how it can be utilized in the analysis of mechanics and mechanisms.
b) The physical meaning of inverse Jacobians derived from screw algebra and derivative method and their relationship.
c) The mobility analysis of the reconfigurable based integrated parallel mechanisms and the methodology of analysing the properties of generally complicated mechanisms.
d) Grasping stability analysis of the Metamorphic hand and how the reconfigurable palm can contribute to a more stable grasp.
e) Finger gaits planning based on the Metamorphic hand as well as the palm variation planning.
f) The dynamics analysis of the Metamorphic hand with the modelling of the reconfigurable palm.
g) Dimension synthesis of the Metamorphic hand and the methodology on the selection of key parameters to design palm.

List of Publications

Journal papers

- Sun, J., Zhang, X., Wei, G., & Dai, J. S. (2016). Geometry and kinematics for a spherical-base integrated parallel mechanism. *Meccanica*, 1-15.
- Sun, J & Dai, J. Geometrical interpretation of Jacobian based on screw theory and that on derivative principle. (to be submitted)
- Dai, J. & Sun, J. Geometrical presentation and correlated characteristics of ray and axis coordinates. (to be submitted)
- Cui L., Sun, J. & Dai, J. In-Hand Forward and Inverse Kinematics with Rolling Contact. *Robotica* (in review)

Conference papers

- Sun, J., Zhang, X., Wei, G. & Dai, J. Geometry and Kinematics of a Parallel Manipulator with a Reconfigurable Base. *the third Inter. Workshop on Fundamental Issues and Future Research Directions for Parallel Mechanisms and Manipulators,* Tianjin, China, July 7-8 2014
- Wei, G., **Sun, J**., Zhang, X., Pensky, D., Piater, J., & Dai, J. S. (2015). Metamorphic hand based grasp constraint and affordance. In *Proceedings of the American Society of Mechanical Engineers (ASME) 2015 International Design Engineering Technical Conferences & Computers and Information in Engineering Conference*. American Society of Mechanical Engineers (ASME).

EU project reports

- K. Zhang, J. Sun, J.S. Dai, H. Kjellstrom, D. Kragic, K. Pauwels, E. Ros, 2014, Metamorphic End-Effectors/Manipulator and Control Strategies for Dexterous Manipulation. EU FP7, TOMSY project final report.
- J. Sun, K. Zhang, J.S. Dai, H. Kjellstrom, D. Kragic, 2014, Benchmarking for the Metamorphic Hand based on a Dimensionality Reduction Model. EU FP7, TOMSY project technical report.

References

[1] Caylay, A. (1860) On a New Analytical Representation of Curves in Space, *Quarterly Mathematical Journal*, vol. **V**, pp. 81-86.

[2] Plücker, J. (1865). On a New Geometry of Space. *Philosophical Transactions of the Royal Society of London*, **155***,* pp. 725-791.

[3] Klein, A. (1893) *Einleitung in die höhere Geometrie*, Seminar, (1926) *Vorlesungen über Höhere Geometrie*, (ed. Blaschke), Die Grundlehren der Mathematischen Wissenschaften in Einzeldarstellungen, Verlag von Julius Springer, Berlin.

[4] Dai, J.S. (2006) A Historical Review of the Theoretical Development of Rigid Body Displacements from Rodrigues Parameters to the Finite Twist. *Mechanism and Machine Theory*, **41**(1)*,* pp. 41-52.

[5] Ball, R.S. (1876) *Theory of Screws: A Study in the Dynamics of a Rigid Body*, Hodges, Foster, and Co., Grafton-Street, Dublin.

[6] Hunt, K.H.（1978), *Kinematic Geometry of Mechanisms*. Clarendon Press, Oxford.

[7] Woods, F.S. (1922), *Higher Geometry, An Introduction to Advanced Methods in Analytic Geometry*, Ginn and Company, New York

[8] Klein, F. (1908), *Elementary Mathematics from an Advanced Standpoint: Geometry*, (Hedrick, E.R. and Noble, C.A. trans. from *Elementarmathematik vom höheren Standpunkte aus*, J. Springer, Berlin 1925), C.A. Macmillan (1939), Dover (2004), New York.

[9] Grassmann, H. (1862), *Extension Theory*, Translated by Kannenberg, L.C. (1999), *History of Mathematics*, vol **19**, American Mathematical Society, London Mathematical Society, London.

[10] Collins, J.V. (1899), An Elementary Exposition of Grassmann's "Ausdehnungslehre" or Theory of Extension. *The American Mathematical Monthly*. **6**(8/9):193-198.

[11] Ball, R.S. (1900), *A Treatise on the Theory of Screws*, Cambridge University Press, Cambridge.

[12] Duffy, J. (1996) *Statics and Kinematics with Applications to Robotics*, Cambridge University Press, New York.

[13] Lipkin, H. and Duffy, J. (1985) The Elliptic Polarity of Screws. *J. Mechanisms Transmissions, Automation Design Trans. ASME*, **107***,* pp. 377–387.

[14] Davidson, J.K. and Hunt, K.H. (2004), *Robots and Screw Theory: Applications of Kinematics and Statics to Robotics*, Oxford University Press, New York.

[15] McCarthy, J.M. (1990) *An Introduction to Theoretical Kinematics*, The MIT Press, London.

[16] Dai, J.S. (2014) *Geometrical Foundations and Screw Algebra for Mechanisms and Robotics*, Chinese translations, Higher Education Press, Beijing, ISBN: 9787040334838, (translated from Dai, J.S. 2016, *Screw Algebra and Kinematic Approaches for Mechanisms and Robotics*, to be published by Springer, London)

[17] Dai, J.S. and Rees Jones, J., (2002) Null-space construction using cofactors from a screw algebra context, *Proc Royal Soc Lond, Series A: Mathematical, Physical and Engineering Sciences*, **458** (2024), pp. 1845-1866.

[18] McCarthy, J.M. and Soh, G.S. (2011), *Geometric Design of Linkages*, 2nd ed., Springer, New York.

[19] Kong, X. and Gosselin, C.M, (2010), *Type Synthesis of Parallel Mechanisms*, Springer, New York.

[20] Su, H.-J. and Tari, H. (2011) On Line Screw Systems and Their Application to Flexure Synthesis. *J Mech Rob, Trans ASME*. **3**(1), 011009.

[21] Featherstone, R. (2008), *Rigid Body Dynamics Algorithms*, Springer, New York.

[22] Selig, J.M. (2000), *Geometric Fundamentals of Robotics*, Springer, New York.

[23] Yang, A.T. (1974), *Calculus of Screws*, in Basic Questions of Design Theory, North-Holland, Elsevier, New York.

[24] Bottema, O. and Roth, B. (1979) *Theoretical Kinematics*, North-Holland Series in Applied Mathematics and Mechanics, North-Holland, Amsterdam.

[25] Dai, J.S., Holland, N. and Kerr, D.R. (1995) Finite twist mapping and its application to planar serial manipulators with revolute joints. *Journal of Mechanical Engineering Science*, **209**(4), pp. 263 271.

[26] Dai, J.S. (2012) Finite displacement screw operators with embedded Chasles' motion. *Journal of Mechanisms and Robotics, Trans. ASME*. **4**(4), pp. 041002.

[27] Merlet, J.P. (1989) Singular Configurations of Parallel Manipulators and Grassmann Geometry. *Int J Rob Res*. **8**(5), pp. 45-56.

[28] Zhang, K. and Dai, J.S. (2014), A kirigami-inspired 8R linkage and its evolved overconstrained 6R linkages with the rotational symmetry of order two. *Journal of Mechanisms and Robotics, Trans. ASME*. **6**(2), pp. 021008, 2014.

[29] Bruyninckx, H., Demey, S., Dutre, S. and De Schutter, J. (1995) Kinematic Models for Model Based Compliant Motion in the Presence of Uncertainty. *International Journal of Robotics Research*. **14**(5), pp. 465-482.

[30] Shafarevich, I.R. and Remizov (2013), A. *Linear Algebra and Geometry*, Springer, ISBN 978-3-642-30993-9.

[31] Barali, D. (2011) How to Understand Grassmannians. *the Teaching of Mathematics*. vol. **XIV**, 2, pp. 147-157.

[32] Monsarrat, B., and Gosselin, C. M. (2003) Workspace analysis and optimal design of a 3-leg 6-DOF parallel platform mechanism. *Robotics and Automation, IEEE Transactions on*, 19(6): 954-966

[33] Gouttefarde, M., Merlet, J. P., & Daney, D. (2006). Determination of the Wrench-Closure Workspace of 6-DOF Parallel Cable-Driven Mechanisms. *Advances in Robot Kinematics* (Vol.22, pp.315-322).

[34] Dai, J. S., Huang, Z., and Lipkin, H. (2006) Mobility of overconstrained parallel mechanisms. *Journal of Mechanical Design*, 128(1): 220-229

[35] Huang, T., Tang, G., Li, S., Li, Y., Chetwynd, G. D., and Whitehouse, J. D. (2003) Kinematic calibration of a class of parallel kinematic machines (PKM) with fewer than six degrees of freedom. *Science in China Series E: Technological Sciences*, 46(5): 515-526

[36] Sun, T., Song, Y., Li, Y., and Zhang, J. (2010) Workspace decomposition based dimensional synthesis of a novel hybrid reconfigurable robot. *Journal of Mechanisms and Robotics*, *2*(3): 031009

[37] Gogu, G. (Ed.). (2009) Structural synthesis of parallel robots: part 1: methodology (Vol. 149). Springer.

[38] Chablat, D., & Wenger, P. (2007). Architecture optimization of a 3-dof translational parallel mechanism for machining applications, the orthoglide. *Robotics & Automation IEEE Transactions on, 19*(3), 403-410.

[39] Zhao, T. S., Dai, J. S., and Huang, Z. (2002). Geometric synthesis of spatial parallel manipulators with fewer than six degrees of freedom. *Proceedings of the*

Institution of Mechanical Engineers, Part C: Journal of Mechanical Engineering Science, *216*(12), 1175-1185.

[40] Zhao, T. S., Dai, J. S., and Huang, Z. (2002). Geometric Analysis of Overconstrained Parallel Manipulators with Three and Four Degrees of Freedom. *JSME International Journal Series C*, *45*(3), 730-740.

[41] Kong, X., and Gosselin, C. M. (2004) Type synthesis of 3-DOF translational parallel manipulators based on screw theory. *Journal of mechanical design*, 126(1): 83-92

[42] Xu, Q., and Li, Y. (2008) An investigation on mobility and stiffness of a 3-DOF translational parallel manipulator via screw theory. *Robotics and Computer-Integrated Manufacturing*, 24(3): 402-414

[43] Huda, S., and Takeda, Y. (2007) Kinematic analysis and synthesis of a 3-URU pure rotational parallel mechanism with respect to singularity and workspace. *Journal of Advanced Mechanical Design, Systems, and Manufacturing*, 1(1): 81-92

[44] Vischer, P., and Clavel, R. (2000) Argos: a novel 3-DoF parallel wrist mechanism. *The International Journal of Robotics Research*, 19(1): 5-11

[45] Di Gregorio, R. (2001) A new parallel wrist using only revolute pairs: the 3-RUU wrist. *Robotica*, 19(3): 305-309

[46] Gan, D., and Dai, J. S. (2013). Geometry Constraint and Branch Motion Evolution of 3PUP Parallel Mechanisms with Bifurcated Motion. *Mechanism and Machine Theory*, *61*, 168-183.

[47] Zhang, K., Dai, J. S., and Fang, Y. (2012). Constraint analysis and bifurcated motion of the 3PUP parallel mechanism. *Mechanism and Machine Theory*, *49*, 256-269.

[48] Wang, J., and Gosselin, C. M. (2004) Kinematic analysis and design of kinematically redundant parallel mechanisms. *Journal of Mechanical Design*, 126(1): 109-118

[49] Saglia, J. A., Tsagarakis, N. G., Dai, J. S. and Caldwell, G. D. (2009) A high performance redundantly actuated parallel mechanism for ankle rehabilitation. *The International Journal of Robotics Research*, 28(9): 1216-1227

[50] Dai, J. S., & Jones, J. R. (1999). Mobility in metamorphic mechanisms of foldable/erectable kinds. *Journal of Mechanical Design, 121*(3), 375-382.

[51] Gan, D., Dai, J. S., and Liao, Q. (2010) Constraint analysis on mobility change of a novel metamorphic parallel mechanism. Mechanism and Machine Theory, 45(12): 1864-1876

[52] Zhang, K., Dai, J. S., and Fang, Y. (2013) Geometric constraint and mobility variation of two 3SvPSv metamorphic parallel mechanisms. *Journal of Mechanical Design, 135*(1): 011001

[53] Wei, G., and Dai, J. S. (2014) Origami-inspired integrated planar-spherical overconstrained mechanisms. *Journal of Mechanical Design, 136*(5): 051003

[54] Yi, B. J., Na, H. Y., Lee, J. H., Hong, Y. S., Oh, S. R., Suh, I. H., and Kim, W. K. (2002) Design of a parallel-type gripper mechanism. *The International Journal of Robotics Research, 21*(7): 661-676

[55] Mohamed, M. G., & Gosselin, C. M. (2005). Design and analysis of kinematically redundant parallel manipulators with configurable platforms.*IEEE Transactions on Robotics, 21*(3), 277-287.

[56] Lambert, P. (2013) *Parallel Robots with Configurable Platforms* (Doctoral dissertation, TU Delft, Delft University of Technology).

[57] Dai, J.S. Robotic Hand with Palm Section Comprising Several Parts Able to Move Relative to Each Other, Patent: WO/2005/105391, 2005, International PCT: PCT/GB2005/001665, UK patent: GB04 095 48.5, 2004, Europe patent: EP05740527.6, US Patent process: US 11/587,766, China Patent: CN200580018189.6.

[58] Dai, J.S., Wei. G., Wang, S., Luo, H. and Li, J. (2011) An Anthropomorphic Hand with Reconfigurable Palm. China patent: No. 201110026001.X

[59] Wei, G., Gogu, G., Stephan, F., Aminzadeh, A., Wuerdemann, H., & Walker, R., et al. (2014). Dexdeb - application of dextrous robotic hands for deboning operation. *Springer Tracts in Advanced Robotics, 94*, 217-235.

[60] Cui, L., and Dai, J. S. (2011) Posture, workspace, and manipulability of the metamorphic multifingered hand with an articulated palm. *Journal of mechanisms and robotics*, *3*(2): 021001.

[61] Wei, G., Dai, J. S., Wang, S., and Luo, H. (2011) Kinematic analysis and prototype of a metamorphic anthropomorphic hand with a reconfigurable palm. *International Journal of Humanoid Robotics, 8(*3): 459-479

[62] Borras, J., and Dollar, A. M. (2014). Framework comparison between a multifingered hand and a parallel manipulator. In *Computational Kinematics* (pp. 219-227). Springer Netherlands.

[63] Borràs, J., and Dollar, A. M. (2013). A parallel robots framework to study precision grasping and dexterous manipulation. In *Robotics and Automation (ICRA), 2013 IEEE International Conference on* (pp. 1595-1601). IEEE.

[64] Dai, J. S. (2014) Screw Algebra and Lie Groups and Lie Algebras, Higher Education Press, Beijing, also Screw Algebra and Kinematic Approaches for Mechanisms and Robotics, Springer, london

[65] Tsai, L. W. (1999) Robot analysis: the mechanics of serial and parallel manipulators. John Wiley & Sons.

[66] Merlet, J. P. (2006). *Parallel robots* (Vol. 128). Springer Science & Business Media.

[67] Innocenti, C., and Parenti-Castelli, V. (1990). Direct position analysis of the Stewart platform mechanism. *Mechanism and machine theory*, *25*(6), 611-621.

[68] Raghavan, M. (1993). The Stewart platform of general geometry has 40 configurations. *Journal of Mechanical Design*, *115*(2), 277-282.

[69] Roth, B. (1993) Computations in kinematics. In *Computational Kinematics* (pp. 3-14). Springer Netherlands.

[70] Garcia-Cerezo, A., Mandow, A., Martinez, J. L., & Gomez-De-Gabriel, J. (2007). Development of ALACRANE: A Mobile Robotic Assistance for Exploration and Rescue Missions. *IEEE International Workshop on Safety, Security and Rescue Robotics* (pp.1-6).

[71] Hans, M., Graf, B., & Schraft, R. D. (2002). Robotic home assistant Care-O-bot: past-present-future. *IEEE International Workshop on Robot and Human Interactive Communication, 2002. Proceedings* (Vol.3, pp.380-385). IEEE.

[72] Exploration, H. M., Huntsberger, T., Rodriguez, G., & Schenker, P. S. (2014). Robotics challenges for robotic and human mars exploration.*American Society of Civil Engineers*.

[73] Matsuoka, Y. (1997). The mechanisms in a humanoid robot hand.*Autonomous Robots, 4*(2), 199-209.

[74] Angeles, J. (2002). *Fundamentals of robotic mechanical systems*.*Fundamentals of Robotic Mechanical Systems*. Springer-Verlag New York, Inc.

[75] Okada, T. (1982). Computer control of multijointed finger system for precise object-handling. *IEEE Transactions on Systems Man & Cybernetics, 12*(3), 289-299.

[76] Claudio Melchiorri, & Gabriele Vassura. (1994). Implementation of whole-hand manipulation capability in the ub hand system design. *Advanced Robotics, 9*(5), 547-560.

[77] Mason, M. T., & Salisbury, J. K. (1985). *Robot hands and the mechanics of manipulation*. MIT Press.

[78] Townsend, W. (2000). The barretthand grasper – programmably flexible part handling and assembly. *Industrial Robot, 27*(3), 181-188.

[79] Lotti, F., Tiezzi, P., & Vassura, G. (2004). UBH3: investigating alternative design concepts for robotic hands. *Automation Congress, 2004. Proceedings. World* (Vol.15, pp.135-140).

[80] Jacobsen, S. C., Wood, J. E., Knutti, D. F., & Biggers, B. (1984). The utah/mit dextrous hand work in progress. *International Journal of Robotics Research, 3*(4), 21-50.

[81] Lovchik, C. S., & Diftler, M. A. (1999). The Robonaut hand: a dexterous robot hand for space. *IEEE International Conference on Robotics and Automation, 1999. Proceedings* (Vol.2). IEEE.

[82] Lee, Y. K., & Shimoyama, I. (1999). A skeletal framework artificial hand actuated by pneumatic artificial muscles. *, 2*(3), 349-350.

[83] Tuffield, P., & Elias, H. (2003). The shadow robot mimics human actions.*Industrial Robot, 30*(1), 56-60.

[84] Mouri, T., Kawasaki, H., Yoshikawa, K., Takai, J., & Ito, S. (2002). Anthropomorphic robot hand: gifu hand iii. *Iccas, 2001*, 212-213.

[85] Liu, H., Wu, K., Meusel, P., Seitz, N., Hirzinger, G., & Jin, M. H., et al. (2008). Multisensory five-finger dexterous hand: The DLR/HIT Hand II.*Ieee/rsj International Conference on Intelligent Robots and Systems, September 22-26, 2008, Acropolis Convention Center, Nice, France*(pp.3692-3697).

[86] Zhang, Y., Han, Z., Zhang, H., Shang, X., Wang, T., & Guo, W., et al. (2001). Design And Control Of The Buaa Four-Fingered Hand. *IEEE International Conference on Robotics & Automation* (Vol.3, pp.2517 - 2522).

[87] Lovchik, C. S., & Diftler, M. A. (1999). The Robonaut hand: a dexterous robot hand for space. *IEEE International Conference on Robotics and Automation, 1999. Proceedings* (Vol.2). IEEE.

[88] Ghafoor, A., Dai, J. S., & Duffy, J. (2004). Stiffness modeling of the soft-finger contact in robotic grasping. *Journal of Mechanical Design, 126*(4), 646-656.

[89] http://www.barrett.com/robot/products-hand.htm.

[90] Aminzadeh, V., Walker, R., Cupcic, U., Hugo, E., & Dai, J. S. (2012).*Friction Compensation and Control Strategy for the Dexterous Robotic Hands*. *Advances in Reconfigurable Mechanisms and Robots I*. Springer London.

[91] Emmanouil, E., Wei, G., & Dai, J. S. (2015). Spherical trigonometry constrained kinematics for a dexterous robotic hand with an articulated palm. *Robotica, -1*, 1-18.

[92] Dai, J. S., & Wang, D. (2007). Geometric analysis and synthesis of the metamorphic robotic hand. *Journal of Mechanical Design, 129*(11), 1191-1197.

[93] Dai, J. S., Wang, D., & Cui, L. (2009). Orientation and workspace analysis of themultifingered metamorphic hand-metahand. *IEEE Transactions on Robotics, 25*(4), 942-947.

[94] Cui, L., & Dai, J. S. (2012). Reciprocity-based singular value decomposition for inverse kinematic analysis of the metamorphic multifingered hand. *Journal of Mechanisms & Robotics, 4*(3), 034502-6.

[95] Dai, J. S., & Jones, J. R. (1999). Mobility in metamorphic mechanisms of foldable/erectable kinds. *Journal of Mechanical Design, 121*(3), 375-382.

[96] Murray, R. M., Li, Z., and Sastry, S. S., 1994. *A methematical introduction to robotic manipulation*. CRC Press.

[97] Wei, G., Emmanouil, E., Aminzadeh, V., & Dai, J. S. (2013). Structure Design, Kinematics and Grasp Constraint of a Metamorphic Robotic Hand for Meat Deboning Operation. *ASME 2013 International Design Engineering Technical Conferences and Computers and Information in Engineering Conference* (pp.V06BT07A019-V06BT07A019).

[98] Ahin, E., Akmak, M., Ar, M. R., Ur, E., & oluk, G&#. (2007). To afford or not to afford: a new formalization of affordances toward affordance-based robot control. *Adaptive Behavior, 15*(4), 447-472.

[99] Detry, R., Kraft, D., Kroemer, O., Bodenhagen, L., Peters, J., & Krüger, N., et al. (2011). Learning grasp affordance densities. *Paladyn Journal of Behavioral Robotics, 2*(1), 1-17.

[100] Song, H. O., Fritz, M., Gu, C., & Darrell, T. (2011). Visual grasp affordances from appearance-based cues. *IEEE International Conference on Computer Vision Workshops, ICCV 2011 Workshops, Barcelona, Spain, November* (pp.998-1005).

[101] Detry, R., Baseski, E., Popovic, M., Touati, Y., Kruger, N., & Kroemer, O., et al. (2009). Learning object-specific grasp affordance densities.*IEEE, International Conference on Development and Learning* (pp.1-7). IEEE.

[102] Denavit, J., & Hartenberg, R. S. (1955). A kinematic notation for lower-pair mechanisms based on matrices. *Trans.of the Asme.journal of Applied Mechanics, 22*, 215-221.

[103] Siciliano, B., Sciavicco, L., Villani, L., & Oriolo, G. (2010). *Robotics: modelling, planning and control*. Springer Science & Business Media.

[104] http://www.neobotix-robots.com/

[105] Bischoff, R. (2011, May). KUKA youBot–a milestone for education and research in mobile manipulation. In *IEEE ICRA Workshop–A New Generation of Educational Robots. KUKA Laboratories GmbH, Shanghai International Convention Center, Augsburg, China* (Vol. 76).

[106] Srinivasa, S. S., Ferguson, D., Helfrich, C. J., Berenson, D., Collet, A., Diankov, R., ... & Weghe, M. V. (2010). HERB: a home exploring robotic butler. *Autonomous Robots*, *28*(1), 5-20.

[107] Liu, Y. W., & Ting, K. L. (1994). On the rotatability of spherical N-bar chains.*Journal of Mechanical Design*, *116*(3), 920-923.

[108] Brockett, R. W. (1984). Robotic manipulators and the product of exponentials formula. In *Mathematical theory of networks and systems* (pp. 120-129). Springer Berlin Heidelberg.

[109] Gan, D., Liao, Q., Wei, S., Dai, J. S., & Qiao, S. (2008). Dual quaternion-based inverse kinematics of the general spatial 7R mechanism. *Proceedings of the Institution of Mechanical Engineers, Part C: Journal of Mechanical Engineering Science*, *222*(8), 1593-1598.

[110] Gao, Z., Wei, G., & Dai, J. S. (2015). Inverse kinematics and workspace analysis of the metamorphic hand. *Proceedings of the Institution of Mechanical Engineers, Part C: Journal of Mechanical Engineering Science*,*229*(5), 965-975.

[111] Gibson, J. J. (2014). *The ecological approach to visual perception: classic edition*. Psychology Press.

[112] Borràs J, Dollar AM (2013) A parallel robots framework to study precision grasping and dexterous manipulation. In: Robotics and Automation (ICRA), 2013 IEEE International Conference on pp 1595–1601. IEEE.

[113] Tu, L., 2008. An introduction to manifolds. Vol. 200. No. 8. Springer New York.

[114] Warner, F. W., 1971. Foundations of differentiable manifolds and Lie groups. Vol. 94. Springer.

[115] Hervé, J. M., 1999. "The Lie group of rigid body displacements, a fundamental tool for mechanism design". Mechanism and Machine theory, 34(5), pp. 719-730.

[116] Hervé, J.M., 1978. "Analyze structurelle des mécanismes par groupe des déplacements (in French)", Mech. Mach. Theory, 13, pp. 437□450.

[117] Meng, J., Liu, G., and Li, Z., 2007. "A geometric theory for analysis and synthesis of sub-6 DoF parallel manipulators". Robotics, IEEE Transactions on, 23(4), pp. 625□649.

[118] Thomas, F., & Torras, C. (1988). A group-theoretic approach to the computation of symbolic part relations. *IEEE Journal on Robotics & Automation, 4*(6), 622-634.

[119] Feix, T., Romero, J., Ek, C. H., & Schmiedmayer, H. B. (2013). A metric for comparing the anthropomorphic motion capability of artificial hands.*IEEE Transactions on Robotics, 29*(1), 82-93.

[120] Gelberman, R. H., Panagis, J. S., Taleisnik, J., & Baumgaertner, M. (1983). The arterial anatomy of the human carpus. part i: the extraosseous vascularity. *Journal of Hand Surgery, 8*(4), 367-75.

[121] Sangole, A. P., & Levin, M. F. (2008). Arches of the hand in reach to grasp. *Journal of Biomechanics, 41*(4), 829-37.

[122] Kuo, L. C., Chiu, H. Y., Chang, C. W., Hsu, H. Y., & Sun, Y. N. (2008). Functional workspace for precision manipulation between thumb and fingers in normal hands. *Journal of Electromyography & Kinesiology Official Journal of the International Society of Electrophysiological Kinesiology, 19*(5), 829-39.

[123] Wang, X., Liu, Y., Yang, D., & Li, N. (2010). Progress in the biomechatronic design and control of a hand prosthesis. 5880-5885.

[124] O. Bock. (2011). SensorHand speed. [Online]. Available: http://www.ottobock.com/cps /rde/xchg/ob_com_en/hs.xsl/3652.html

[125] O. Bock. (2011). Otto Bock at the trade fair 2010 Leipzig. [Online]. Available: http://www leipzig.ottobock.de/index.php?id=161&no_cache=1&L=1

[126] Gaiser, Immanuel, et al. "A new anthropomorphic robotic hand." *Humanoid Robots, 2008. Humanoids 2008. 8th IEEE-RAS International Conference on*. IEEE, 2008.

Appendix A

Suppose a rigid body rotates about an arbitrary joint O with an angular velocity $\boldsymbol{\omega}$, shown in Fig. A.1. The linear velocities of two distinct points A and B can be expressed as,

$$\boldsymbol{v}_{\mathrm{A}} = \boldsymbol{\omega} \times \boldsymbol{r}_{\mathrm{OA}}\,,\ \boldsymbol{v}_{\mathrm{B}} = \boldsymbol{\omega} \times \boldsymbol{r}_{\mathrm{OB}} \quad . \tag{A.1}$$

The relation between $\boldsymbol{v}_{\mathrm{A}}$ and $\boldsymbol{v}_{\mathrm{B}}$ is given by,

$$\boldsymbol{v}_{\mathrm{B}} = \boldsymbol{\omega} \times \boldsymbol{r}_{\mathrm{OB}} = \boldsymbol{\omega} \times \left(\boldsymbol{r}_{\mathrm{OA}} + \boldsymbol{r}_{\mathrm{AB}}\right) = \boldsymbol{v}_{\mathrm{A}} + \boldsymbol{\omega} \times \boldsymbol{r}_{\mathrm{AB}}\,. \tag{A.2}$$

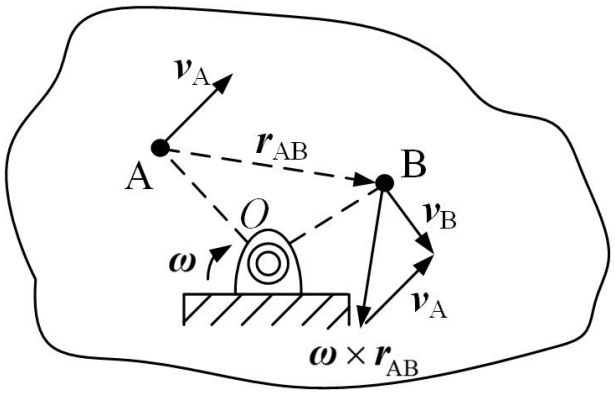

Figure A.1.Relationship of linear velocities of two distinct points in a rigid body

Appendix B

$$E_1 = e_1 u_1^2 u_3^2 + e_2 u_1^2 + e_3 u_3^2 + e_6 u_1 u_3 + e_9$$
$$E_2 = e_5 u_1^2 u_3 + e_7 u_1 u_3^2 + e_{11} u_1 + e_{13} u_3$$
$$E_3 = e_4 u_1^2 u_3^2 + e_8 u_1^2 + e_{10} u_3^2 + e_{12} u_1 u_3 + e_{14}$$

$$F_1 = f_1 u_1^2 u_3^2 + f_2 u_3^2 u_1 + f_4 u_1^2 u_3 + f_5 u_1^2 + f_6 u_3^2 + f_{11} u_3 + f_{12} u_1 + f_{16}$$
$$F_2 = \left(f_3 u_1^2 u_3^2 + f_8 u_1^2 + f_9 u_3^2 + f_{14} u_1 u_3 + f_{18} \right)$$
$$F_3 = f_7 u_1^2 u_3^2 + f_{10} u_1^2 u_3 + f_{13} u_3^2 u_1 + f_{15} u_1^2 + f_{17} u_3^2 + f_{19} u_3 + f_{20} u_1 + f_{21}$$

$$G_1 = g_1 u_1^2 + g_3$$
$$G_2 = g_4 u_1$$
$$G_3 = g_2 u_1^2 + g_5$$

$$e_1 = s\delta_3 c\varphi_4 - c\delta_3 s\varphi_4 - x_{C_3'}$$
$$e_2 = -s\delta_3 c\varphi_4 + c\delta_3 s\varphi_4 - x_{C_3'}$$
$$e_3 = -s\delta_3 c\varphi_4 + c\delta_3 s\varphi_4 - x_{C_3'}$$
$$e_4 = -s\delta_3 c\varphi_4 - c\delta_3 s\varphi_4 - x_{C_3'}$$
$$e_5 = -4 s\delta_3$$
$$e_6 = -2$$
$$e_7 = -4 c\varphi_4$$
$$e_8 = s\delta_3 c\varphi_4 + c\delta_3 s\varphi_4 - x_{C_3'}$$
$$e_9 = s\delta_3 c\varphi_4 - c\delta_3 s\varphi_4 - x_{C_3'}$$
$$e_{10} = s\delta_3 c\varphi_4 + c\delta_3 s\varphi_4 - x_{C_3'}$$
$$e_{11} = 4 c\varphi_4$$
$$e_{12} = 4$$
$$e_{13} = 4 s\delta_3$$
$$e_{14} = -s\delta_3 c\varphi_4 - c\delta_3 s\varphi_4 - x_{C_3'}$$

$$f_2 = 2$$
$$f_3 = 2s\delta_3$$
$$f_4 = 2s\delta_3 c\varphi_4 - 2c\delta_3 s\varphi_4$$
$$f_5 = -y_{C_3'}$$
$$f_6 = -y_{C_3'}$$
$$f_7 = -y_{C_3'}$$
$$f_8 = -2s\delta_3$$
$$f_9 = -2s\delta_3$$
$$f_{10} = -2s\delta_3 c\varphi_4 - 2c\delta_3 s\varphi_4$$
$$f_{11} = -2s\delta_3 c\varphi_4 + 2c\delta_3 s\varphi_4$$
$$f_{12} = -2$$
$$f_{13} = -2$$
$$f_{14} = -8c\varphi_4$$
$$f_{15} = -y_{C_3'}$$
$$f_{16} = -y_{C_3'}$$
$$f_{17} = -y_{C_3'}$$
$$f_{18} = 2s\delta_3$$
$$f_{19} = 2s\delta_3 c\varphi_4 + 2c\delta_3 s\varphi_4$$
$$f_{20} = 2$$
$$f_{21} = -y_{C_3'}$$

$$g_1 = -c\delta_3 c\varphi_4 - s\delta_3 s\varphi_4 - z_{C_3'}$$
$$g_2 = -c\delta_3 c\varphi_4 + s\delta_3 s\varphi_4 - z_{C_3'}$$
$$g_3 = c\delta_3 c\varphi_4 + s\delta_3 s\varphi_4 - z_{C_3'}$$
$$g_4 = 4s\varphi_4$$
$$g_5 = c\delta_3 c\varphi_4 - s\delta_3 s\varphi_4 - z_{C_3'}$$

Appendix C

Elements in $\mathbf{R}_{OmOp}$ and $\boldsymbol{p}_{O_mO_p}$.

$$r_{11} = c_7\left(c_3c_5 - s_3c_4s_5\right) - s_7\left[s_6\left(c_3s_5 + s_3c_4c_5\right) + c_6s_3s_4\right]$$

$$r_{12} = -s_7\left(c_3c_5 - c_4s_3s_5\right) + c_7\left[s_6(c_3s_5 + c_4c_5s_3) + c_6s_3s_4\right]$$

$$r_{13} = c_6\left(c_3s_5 + c_4c_5s_3\right) - s_3s_4s_6$$

$$\begin{aligned} r_{21} = &-c_7\left(s_{12}c_5s_3 + c_{12}s_4s_5 + s_{12}c_3c_4s_5\right) + \\ &s_7[c_6\left(c_{12}c_4 - s_{12}c_3s_4\right) - s_6(c_{12}c_5s_4 - s_{12}s_3s_5 + s_{12}c_3c_4c_5)] \end{aligned}$$

$$\begin{aligned} r_{22} = &s_7\left(s_{12}c_5s_3 + c_{12}s_4s_5 + s_{12}c_3c_4s_5\right) + \\ &c_7[c_6(c_{12}c_4 - s_{12}c_3s_4) - s_6(c_{12}c_5s_4 - s_{12}s_3s_5 + s_{12}c_3c_4c_5)] \end{aligned}$$

$$r_{23} = c_6(c_{12}c_5s_4 - s_{12}s_3s_5 + s_{12}c_3c_4c_5) + s_6(c_{12}c_4 - s_{12}c_3s_4)$$

$$\begin{aligned} r_{31} = &-c_7(c_{12}c_5s_3 - s_{12}s_4s_5 + c_{12}c_3c_4s_5) - \\ &s_7[c_6(s_{12}c_4 + c_{12}c_3s_4) - s_6(c_{12}s_3s_5 + s_{12}c_5s_4 - c_{12}c_3c_4c_5)] \end{aligned}$$

$$\begin{aligned} r_{32} = &s_7(c_{12}c_5s_3 - s_{12}s_4s_5 + c_{12}c_3c_4s_5) - \\ &c_7[c_6(s_{12}c_4 + c_{12}c_3s_4) - s_6(c_{12}s_3s_5 + s_{12}c_5s_4 - c_{12}c_3c_4c_5)] \end{aligned}$$

$$r_{33} = -s_6(s_{12}c_4 + c_{12}c_3s_4) - c_6(c_{12}s_3s_5 + s_{12}c_5s_4 - c_{12}c_3c_4c_5)$$

$$p_1 = -a_5s_3s_4 - a_6[s_7(c_3c_5 - s_3c_4s_5) + c_7(c_3s_5s_6 + s_3s_4c_6 + s_3c_4c_5s_6)]$$

$$\begin{aligned} p_2 = &a_1 + a_2c_1 + (a_3 + a_4)c_{12} + a_5(c_{12}c_4 - s_{12}c_3s_4) + \\ &a_6\{c_7[s_6(s_{12}s_3s_5 - s_{12}c_3c_4c_5 - c_{12}c_5s_4) - \\ &c_6(s_{12}c_3s_4 + c_{12}c_4)] + s_7(c_{12}s_4s_5 + s_{12}c_3c_4c_5 + s_{12}s_3c_5)\} \end{aligned}$$

$$\begin{aligned} p_3 = &-a_2s_1 - (a_3 + a_4)s_{12} - a_5(c_{12}c_3s_4 + s_{12}c_4) + \\ &a_6\{c_7[s_6(-c_{12}c_3c_4c_5 + s_{12}c_5s_4 + c_{12}s_3s_5) - \\ &c_6(c_{12}c_3s_4 + s_{12}c_4)] - s_7(s_{12}s_4s_5 - c_{12}c_5s_3 - c_{12}c_3c_4s_5)\} \end{aligned}$$